



Memo version 2.3

BESIII Analysis Memo

BAM-766

August 5, 2025

Precise measurement of CP asymmetry $\Sigma^+ \rightarrow p\pi^0$ in J/ψ and $\psi(3686) \rightarrow \Sigma^+\bar{\Sigma}^-$ processes

Yunlong Xiao^{*a}, Xiao Chu^a, Liang Yan^{†1a}, Patrik Adlarson^b, Andrzej Kupsc^b, and Haibo Li^c

^a*Fudan University, People's Republic of China*

^b*Uppsala University, Sweden*

^c*Institute of High Energy Physics, People's Republic of China*

Referee Committee

Karin Schoenning (Chair)¹, Jianyu Zhang², Wenjing Zheng³

¹*Uppsala University, Sweden*

²*University of Chinese Academy of Sciences, People's Republic of China*

³*Institute of High Energy Physics, People's Republic of China*

Pubcomm Editors

Varvara Batozskaya^g, Guy Wilkinson^h

^g*Institute of High Energy Physics*

^h*University of Oxford*

HN : <http://hnb3.ihep.ac.cn/HyperNews/get/paper766.html>

Abstract

Using the data samples of $(10087 \pm 44) \times 10^6$ J/ψ and $(2712.4 \pm 14.3) \times 10^6$ $\psi(3686)$ taken with the Beijing Spectrometer (BESIII) at the Beijing Electron-Positron Collider(BEPCII), the decay processes $J/\psi \rightarrow \Sigma^+\bar{\Sigma}^-$ ($\Sigma^+ \rightarrow p\pi^0$, $\bar{\Sigma}^- \rightarrow \bar{p}\pi^0$) and $\psi(3686) \rightarrow \Sigma^+\bar{\Sigma}^-$ ($\Sigma^+ \rightarrow p\pi^0$, $\bar{\Sigma}^- \rightarrow \bar{p}\pi^0$) have been measured exclusively. The branching fractions of $J/\psi \rightarrow \Sigma^+\bar{\Sigma}^-$ and $\psi(3686) \rightarrow \Sigma^+\bar{\Sigma}^-$ are measured to be $(10.94 \pm 0.02 \pm 0.19) \times 10^{-4}$ and $(2.57 \pm 0.01 \pm 0.12) \times 10^{-4}$, with an improved precision compared to previous measurements, and the parameters $\alpha_{J/\psi}$, $\Delta\Phi_{J/\psi}$, $\alpha_{\psi(3686)}$, and $\Delta\Phi_{\psi(3686)}$ are improved, as listed below:

- 25 • $\alpha_{J/\psi} = -0.5047 \pm 0.0018 \pm 0.0010$
26 • $\Delta\Phi_{J/\psi} = -0.2744 \pm 0.0033 \pm 0.0010$
27 • $\alpha_{\psi(3686)} = 0.7133 \pm 0.0094 \pm 0.0065$
28 • $\Delta\Phi_{\psi(3686)} = 0.427 \pm 0.022 \pm 0.003$

29 The parameter $\alpha_{(\Sigma^+ \rightarrow p\pi^0)}$ and $\alpha_{(\bar{\Sigma}^- \rightarrow \bar{p}\pi^0)}$ are improved significantly, as listed below:

- 30 • $\alpha_{(\Sigma^+ \rightarrow p\pi^0)} = -0.975 \pm 0.011 \pm 0.002$
31 • $\alpha_{(\bar{\Sigma}^- \rightarrow \bar{p}\pi^0)} = 0.999 \pm 0.011 \pm 0.004$

32 The CP asymmetry is extracted, as listed below:

- 33 • $A_{CP} = -0.0118 \pm 0.0083 \pm 0.0028$

*xiaoyl20@fudan.edu.cn
†yanl@fudan.edu.cn

34 **Contents**

35	1 Introduction	4
36	1.1 Polarization and CP violation	4
37	1.2 Angular parameter and branching fraction	8
38	2 Detector	10
39	3 Data and Monte Carlo	11
40	3.1 Data	11
41	3.2 Monte Carlo Simulation	11
42	4 Event Selection of $\Psi \rightarrow \Sigma^+ \bar{\Sigma}^-$, $\Sigma^+ \rightarrow p\pi^0$, $\bar{\Sigma}^- \rightarrow \bar{p}\pi^0$	12
43	4.1 Good Track Selection	12
44	4.2 Particle identification	12
45	4.3 Good photon selection	12
46	4.4 π^0 reconstruction	13
47	4.5 kinematic fit	13
48	4.6 R_{xy} requirement	14
49	4.7 mass window	15
50	4.8 Background analysis	16
51	5 Measurement Method	18
52	5.1 Likelihood function construction	18
53	5.2 Function Minimization	19
54	5.3 Input/output check	19
55	6 MC Efficiency Difference	21
56	6.1 MC efficiency	21
57	7 Decay Parameter Measurement	25
58	7.1 Simultaneous fit by using two decay channels	25
59	8 Branching Results	28
60	8.1 Branching fractions of $J/\psi \rightarrow \Sigma^+ \bar{\Sigma}^-$ and $\psi(3686) \rightarrow \Sigma^+ \bar{\Sigma}^-$	28

61	9 Systematic uncertainty	30
62	9.1 Systematic uncertainties of decay parameters	30
63	9.1.1 MC efficiency correction	30
64	9.1.2 Kinematic fitting	31
65	9.1.3 Fitting method	33
66	9.1.4 Signal mass window	34
67	9.1.5 Background estimation	36
68	9.1.6 Summary of decay parameter uncertainties	38
69	9.2 Systematic uncertainties of branching fraction measurement	38
70	9.2.1 MC efficiency correction for charged tracks and π^0	38
71	9.2.2 Decay parameters	39
72	9.2.3 Fitting function	39
73	9.2.4 Background estimation	40
74	9.2.5 Kinematic fitting	40
75	9.2.6 Branching fraction of $\Sigma^+ \rightarrow p\pi^0$	41
76	9.2.7 Impact of the interference between the $\psi(3686)$ and continuum contribution	41
77	9.2.8 Total number of J/ψ and $\psi(3686)$	41
78	9.2.9 Summary of branching fraction uncertainties	41
79	10 Summary	42
80	11 Some comparisons and checks	44
81	11.1 The definition of moments	44
82	11.2 comparison of the different moments related to θ_{Σ^+} for $J/\psi \rightarrow \Sigma^+\bar{\Sigma}^-$ decay channel	46
83	11.3 comparison of the different moments related to θ_{Σ^+} for $\psi(3686) \rightarrow \Sigma^+\bar{\Sigma}^-$ decay channel	48
84	A π^0 control sample	56
85	A.1 Particle identification	56
86	A.2 Good shower	56
87	A.3 π^0 reconstruction	57
88	A.4 Σ^+ reconstruction	57
89	A.5 π^0 reconstruction efficiency	57
90	A.5.1 Found π^0	58
91	A.5.2 Not found π^0	62

92	B p (\bar{p}) control sample	66
93	B.1 Particle identification	66
94	B.2 Good shower	66
95	B.3 π^0 reconstruction	67
96	B.4 kinematic fit	67
97	B.5 selection of p (\bar{p})	67
98	B.6 p (\bar{p}) reconstruction efficiency	68
99	B.7 p reconstruction efficiency	69
100	B.7.1 Found p	69
101	B.7.2 Not found p	74
102	B.8 \bar{p} reconstruction efficiency	79
103	B.8.1 Found \bar{p}	79
104	B.8.2 Not found \bar{p}	84
105	C The ratio of selection efficiency between data and MC	89
106	C.1 from our results	89
107	C.2 from other results	90

108 1 Introduction

109 1.1 Polarization and CP violation

110 In the field of high energy particle and nuclear physics, the study of hyperon polarization can be
 111 used to understand the spin structure of hyperon, the vortical structure, magnetic field distribution in
 112 quark gluon plasma, and measure the decay parameter of hyperon [1–4]. In theory, the production of
 113 Σ^+ hyperon transverse polarization from unpolarized quarks could be described using fragmentation
 114 function, which is denoted by $D_{1T}^{\perp\Sigma^+/q}(z, q_\perp^2)$ [2–5]. Experimentally, non-leptonic Σ^+ hyperon decay,
 115 exacting the angular distribution of daughter baryon, the polarization could be described as:

$$116 \frac{dN}{d\Omega} = \frac{1}{4\pi} (1 + \alpha_h \cdot |\vec{P}_h| \cdot \cos \theta_P), \quad (1)$$

116 where α_h is decay parameter, \vec{P}_h is hyperon polarization, and θ_P is angle between polarization direction
 117 and direction in the hyperon rest frame. Correspondingly, the decay asymmetry parameter of the anti-
 118 hyperon is denoted as $\bar{\alpha}_h$. The P and CP asymmetries could be determined according to α_h ($\bar{\alpha}_h$) [6]
 119 and $A_{CP} = (\alpha_h + \bar{\alpha}_h)/(\alpha_h - \bar{\alpha}_h)$ [7, 8], which means non-zero α_h ($\bar{\alpha}_h$) and A_{CP} indicate P and CP
 120 violation. If the \vec{P}_h is known, the P and CP violation can be measured [9–14]. Correspondingly, if
 121 the asymmetric parameter of hyperons has been measured, the polarization property of hyperons can
 122 be studied in detail, including baryon spectroscopy, heavy ion physics and the hyperon related research
 123 of the Large Hadron Collider [15–19]. Recently, the global polarization of Ξ^- and Ω^- hyperons has
 124 been measured in the STAR Collaboration at the center-of-mass (CM) energy $\sqrt{s} = 200$ GeV [20]. Λ
 125 is the lightest hyperon, and its global polarization has been observed in ALICE Collaboration [21] at
 126 the $\sqrt{s} = 2.76$ and 5.02 TeV, also in the STAR Collaboration at the $\sqrt{s} < 200$ GeV [18], and also
 127 in the ATLAS Collaboration at the $\sqrt{s} = 7$ TeV [16]. Its transverse polarization has been observed
 128 in the Belle Collaboration at the $\sqrt{s} = 10.58$ GeV [22]. However, It is hardly measured in the non-
 129 perturbation QCD region, such as $J/\psi \rightarrow \Sigma^+ \bar{\Sigma}^-$ and $\psi(3686) \rightarrow \Sigma^+ \bar{\Sigma}^-$ decay process at the $\sqrt{s} = 3.097$
 130 and 3.686 GeV. In the past, the decay parameters of Σ^+ were measured through this target experiment
 131 process $\pi^+ + p \rightarrow K^+ + \Sigma^+$ using the transverse polarization properties of Σ^+ [23]. Similarly, The
 132 transverse polarization phenomenon can also be observed in electron and positron annihilation reaction
 133 processes $e^+ e^- \rightarrow BX$ and $e^+ e^- \rightarrow \Psi \rightarrow BX$, where B represents baryon and Ψ denotes both J/ψ and
 134 $\psi(3686)$ [10–14, 22, 24]. Here, the electron and positron beams are unpolarized.

135 Charge-parity (CP) violation, the breaking of the combination of charge-conjugation symmetry and
 136 parity symmetry is one of the least understood aspects of high-energy physics. It is the research frontier
 137 in particle and nuclear physics with significant implications for understanding matter-antimatter asym-
 138 metry in the universe [25]. However, the Cabibbo-Kobayashi-Maskawa mechanism for CP violation is

insufficient to generate the matter-dominated universe [26]. Therefore, it is of great importance to search for new sources of CP violation, especially in the hyperon sector, after the CP violations have been observed successively in the K , B , and D mesons decays [27–32]. In the beginning, two-body hyperon weak decays were used to establish parity violation [6], while it has attracted considerable interest research in the CP violation test recently. Hyperon non-leptonic decays have played a vital role in studying CP violation in particle physics [33]. As an ideal probe, it can be used to study strong interaction region from non-perturbation to perturbation. Besides, it can use to test standard model by the production and decay of the hyperon. Historically, the HyperCP collaboration has measured the CP violation of charged Ξ and Λ particles, but no evidence of CP violation has been found [34] [35]. In 2019, the BESIII collaboration have reported $\alpha_{(\Lambda \rightarrow p\pi^-)} = 0.750 \pm 0.009 \pm 0.004$ [13], which is significantly different compared to the value of 0.642 ± 0.013 [36] from older measurement in 1975 year. In 2022, the BESIII collaboration have also reported the most precise value $\alpha_{(\Lambda \rightarrow p\pi^-)} = 0.7519 \pm 0.0036 \pm 0.0024$ [14], which means that the differences are more significant. So far, the parameters $\alpha_{(\Sigma^+ \rightarrow p\pi^0)}$ and $\alpha_{(\bar{\Sigma}^- \rightarrow \bar{p}\pi^0)}$ have been precise measured by the BESIII collaboration [12], which are consistent with previous results. The decay parameters of some hyperons are listed in the Table 1. In this work, we want to improve previous measurements (red words).

Tab. 1: The decay parameters of hyperon(All information is from PDG [37])

parameters	value	parameters	value
$\alpha_{(\Sigma^+ \rightarrow p\pi^0)}$	-0.982 ± 0.014	$\alpha_{(\Lambda \rightarrow p\pi^-)}$	0.748 ± 0.007
$\alpha_{(\bar{\Sigma}^- \rightarrow \bar{p}\pi^0)}$	0.99 ± 0.04	$\alpha_{(\bar{\Lambda} \rightarrow \bar{p}\pi^-)}$	-0.757 ± 0.004
$\frac{\alpha_{(\Sigma^+ \rightarrow p\pi^0)} + \alpha_{(\bar{\Sigma}^- \rightarrow \bar{p}\pi^0)}}{\alpha_{(\Sigma^+ \rightarrow p\pi^0)} - \alpha_{(\bar{\Sigma}^- \rightarrow \bar{p}\pi^0)}}$	0.00 ± 0.04	$\frac{\alpha_{(\Lambda \rightarrow p\pi^-)} + \alpha_{(\bar{\Lambda} \rightarrow \bar{p}\pi^+)}}{\alpha_{(\Lambda \rightarrow p\pi^-)} - \alpha_{(\bar{\Lambda} \rightarrow \bar{p}\pi^+)}}$	-0.002 ± 0.004

In the above formula 1 we notice that α (decay parameter) and P (polarization) appear as a product in the angular momentum distribution, which means that we cannot derive the decay parameter from the angular distribution of a single final state particle if we do not know the polarization of this particle. However, in the BESIII experiment, Σ^+ and the $\bar{\Sigma}^-$ hyperon are produced by electron-positron annihilation. It provides a unique environment to study the production and decay of hyperons. Recently, the J/ψ data of 10 billion and $\psi(3686)$ data of 2.7 billion taken with the Beijing Spectrometer at the Beijing Electron-Positron Collider. It's good for measuring the decay parameters that are about Σ decays into proton and anti-proton and the conservation of CP in baryon region will be tested with high accuracy.

To describe the reaction $e^+e^- \rightarrow \Psi \rightarrow \Sigma^+\bar{\Sigma}^- \rightarrow p\pi^0\bar{p}\pi^0$ (Ψ represent J/ψ and $\psi(3686)$), the theoret-

¹⁶⁴ ical formula of differential cross-section [38] we used is

$$\begin{aligned} W(\xi) = & t_0(\xi) + \alpha_\psi t_5(\xi) \\ & + \alpha_{\Sigma^+} \alpha_{\bar{\Sigma}^-} (t_1(\xi) + \sqrt{1 - \alpha_\psi^2} \cos(\Delta\Phi) t_2(\xi) + \alpha_\psi t_6(\xi)) \\ & + \sqrt{1 - \alpha_\psi^2} \sin(\Delta\Phi) (\alpha_{\Sigma^+} t_3(\xi) - \alpha_{\bar{\Sigma}^-} t_4(\xi)). \end{aligned} \quad (2)$$

¹⁶⁵ The arguments to the function are

$$\begin{aligned} t_0(\xi) &= 1 \\ t_1(\xi) &= \sin^2 \theta_\Sigma \sin \theta_p \sin \theta_{\bar{p}} \cos \phi_p \cos \phi_{\bar{p}} + \cos^2 \theta_\Sigma \cos \theta_p \cos \theta_{\bar{p}} \\ t_2(\xi) &= \sin \theta_\Sigma \cos \theta_\Sigma (\sin \theta_p \cos \theta_{\bar{p}} \cos \phi_p + \cos \theta_p \sin \theta_{\bar{p}} \cos \phi_{\bar{p}}) \\ t_3(\xi) &= \sin \theta_\Sigma \cos \theta_\Sigma \sin \theta_p \sin \phi_p \\ t_4(\xi) &= \sin \theta_\Sigma \cos \theta_\Sigma \sin \theta_{\bar{p}} \sin \phi_{\bar{p}} \\ t_5(\xi) &= \cos^2 \theta_\Sigma \\ t_6(\xi) &= \cos \theta_p \cos \theta_{\bar{p}} - \sin^2 \theta_\Sigma \sin \theta_p \sin \theta_{\bar{p}} \sin \phi_p \sin \phi_{\bar{p}} \end{aligned} \quad (3)$$

¹⁶⁶ The formula 3 consists of three parts: the first term ($t_0(\xi) + \alpha_\psi t_5(\xi)$) represents the scattering angle
¹⁶⁷ θ_{Σ^+} of the Σ^+ particle, the second term ($\alpha_{\Sigma^+} \alpha_{\bar{\Sigma}^-} (t_1(\xi) + \sqrt{1 - \alpha_\psi^2} \cos(\Delta\Phi) t_2(\xi) + \alpha_\psi t_6(\xi))$) represents the
¹⁶⁸ correlation of the spins between Σ^+ and $\bar{\Sigma}^-$, and the third term ($\sqrt{1 - \alpha_\psi^2} \sin(\Delta\Phi) (\alpha_{\Sigma^+} t_3(\xi) - \alpha_{\bar{\Sigma}^-} t_4(\xi))$) is
¹⁶⁹ the independent hyperon polarization term. The $\Delta\Phi$ represents the magnitude of hyperonic polarization.
¹⁷⁰ It can be seen from the third term that if $\Delta\Phi$ is not equal to 0, then we can obtain the decay parameters
¹⁷¹ α_{Σ^+} and $\alpha_{\bar{\Sigma}^-}$ of both Sigma hyperon and anti-Sigma hyperon, and further test the conserved quantity of
¹⁷² CP. The corresponding parameters in the formula can be obtained by analyzing and fitting the angular
¹⁷³ distribution information of the data.

¹⁷⁴ The full differential cross-section can be described by the five measured angles $\xi = (\theta_\Sigma, \theta_p, \phi_p, \theta_{\bar{p}}, \phi_{\bar{p}})$.
¹⁷⁵ Here θ_Σ is the angle between Σ^+ and the electron (e^-) beam in the reaction center-of-mass frame. The
¹⁷⁶ other four angles are the polar and azimuthal angles of the proton and anti-proton in the helicity frame,
¹⁷⁷ respectively [39] [40]. To obtain the helicity angles, one begins from the production scattering plane of
¹⁷⁸ $e^+ e^- \rightarrow J/\psi(\psi(3686)) \rightarrow \Sigma^+ \bar{\Sigma}^- \rightarrow p \pi^0 \bar{p} \pi^0$ the system. This is obtained by considering the centre-of-
¹⁷⁹ mass (CM) system where the four-momenta of the electron-positron and $\Sigma^+ \bar{\Sigma}^-$ are given by

$$\begin{aligned} \vec{p}_{\Sigma^+} &= -\vec{p}_{\bar{\Sigma}^-} = \vec{p} \\ \frac{\vec{k}_{e^-}}{|\vec{k}_{e^-}|} &= -\frac{\vec{k}_{e^+}}{|\vec{k}_{e^+}|} = \vec{k}. \end{aligned} \quad (4)$$

¹⁸⁰ The xz-scattering plane is defined by the \vec{p} and \vec{k} vectors, while the y-axis is the normal to the plane.

181 From a right-handed coordinate system with the basis vectors

$$\begin{aligned}\vec{e}_x &= \frac{1}{\sin\theta_\Sigma}(\vec{p} \times \vec{k}) \times \vec{p} \\ \vec{e}_y &= \frac{1}{\sin\theta_\Sigma}(\vec{p} \times \vec{k}) \\ \vec{e}_z &= \vec{p},\end{aligned}\tag{5}$$

182 the helicity angles are obtained, where \vec{p} and \vec{k} are the unit vectors of \vec{p}_Σ and \vec{k}_e , respectively. As
 183 seen from the basis vector definitions in Figure 1, the helicity angles are defined with respect to the
 184 direction of the outgoing hyperon in the CM frame (\vec{e}_z). Technically the helicity angles are obtained by
 185 (i) boosting the hyperon(anti-hyperon) in the CM frame and obtain the polar, $\theta_\Sigma^+(\theta_{\bar{\Sigma}^-})$ and $\phi_{\Sigma^+}(\phi_{\bar{\Sigma}^-})$, (ii)
 186 by boosting the proton(antiproton) first in the CM frame and then into the hyperon(anti-hyperon) rest
 187 frame, (iii) and then by rotating the proton(antiproton) with respect to the boosted z-axis and y-axis with
 188 an angle $-\phi_{\Sigma^+}(\phi_{\bar{\Sigma}^-})$ and $-\theta_\Sigma^+(\theta_{\bar{\Sigma}^-})$, respectively. All corresponding symbols are listed in the Table 2.

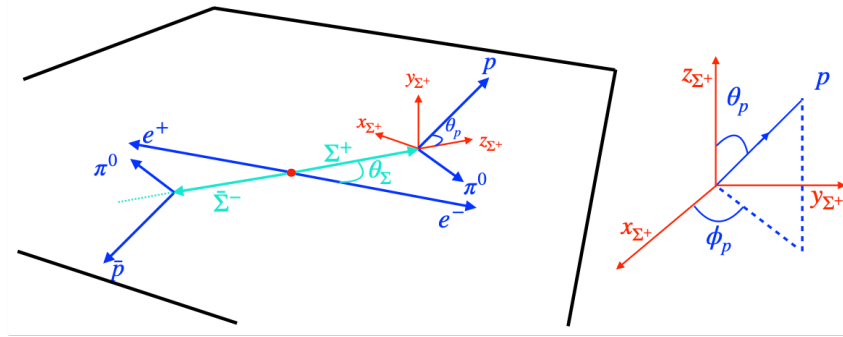


Fig. 1: The helicity frame we used in the $e^+e^- \rightarrow J/\psi(\psi(3686) \rightarrow \Sigma^+\bar{\Sigma}^-, \Sigma^+ \rightarrow p\pi^0, \bar{\Sigma}^- \rightarrow \bar{p}\pi^0)$.

Tab. 2: Meaning of symbol

Symbol	Meaning
α_ψ	Angle distribution parameter
$\Delta\Phi$	Polarization parameter
α_{Σ^+}	Decay parameter
$\alpha_{\bar{\Sigma}^-}$	Decay parameter
θ_Σ	Angle between the electron and the hyperon
θ_p	Polar angle between the p and the Σ^+ in Σ^+ system
$\theta_{\bar{p}}$	Polar angle between the \bar{p} and the $\bar{\Sigma}^-$ in $\bar{\Sigma}^-$ system
ϕ_p	Azimuth angle between the p and the Σ^+ in Σ^+ system
$\phi_{\bar{p}}$	Azimuth angle between the \bar{p} and the $\bar{\Sigma}^-$ in $\bar{\Sigma}^-$ system

189 **1.2 Angular parameter and branching fraction**

190 Secondly, the angular distribution of the baryon states is also very interesting topic. In general, the
 191 angular distribution of a neutral vector resonance $J/\psi, \psi(3686)$ decay into a hadron anti-hadron pair can
 192 be described as: $1 + \alpha_\psi \cos^2 \theta$, where α_ψ is the angular distribution parameter of the baryon, θ is a polar
 193 angle between the baryon and the positron beam in the centre-of-mass (c.m.) system. In the limit of
 194 infinitely heavy charm mass, the hadron helicity conservation rule implies angular distribution parameter
 195 $\alpha_\psi = 1$ [41]. The values of angular distribution of $J/\psi \rightarrow \Sigma^+ \bar{\Sigma}^-$ and $\psi(3686) \rightarrow \Sigma^+ \bar{\Sigma}^-$ have been
 196 predicted theoretically based on first order perturbative QCD. In the prediction of Claudson, Glashow
 197 and Wise [42], the mass of the final baryon is taken into account as a whole, while the constituent
 198 quarks inside the baryon are taken as massless when calculating the decay amplitude. In the prediction
 199 of Carimalo [43], mass effects at the quark level are taken into consideration. Experimentally, the related
 200 measurements are needed for the test. With the above Eq. 2 and 3, we could measure parameters($\alpha_{J/\psi}$,
 201 $\Delta\Phi_{J/\psi}, \alpha_{\psi(3686)}, \Delta\Phi_{\psi(3686)}, \alpha_{(\Sigma^+ \rightarrow p\pi^0)}, \alpha_{(\bar{\Sigma}^- \rightarrow \bar{p}\pi^0)}$) by fitting the five-dimensional distributions.

202 Lastly, the amplitudes of J/ψ and $\psi(3686)$ decay to different baryon octet pairs are supposed to be
 203 the same under the assumption of flavour-SU(3) symmetry. However, branching fractions are not only
 204 determined by strong interaction amplitudes, but also by electromagnetic interactions and interference
 205 between the two amplitudes, although these contributions are much smaller than the expected flavour-
 206 SU(3) breaking effects. Perturbative QCD [44] [45] predicts that the partial widths for J/ψ decays
 207 into an exclusive hadronic state h are proportional to the squares of the wave-function, which are well
 208 determined from the leptonic widths. And it is also related to the strong coupling constant, which is
 209 expected to behave in the same way for the two resonances J/ψ and $\psi(3686)$. From this assumption
 210 $J/\psi \rightarrow h$ and $\psi(3686) \rightarrow h$ can be related via

$$\frac{B(\psi(3686) \rightarrow h)}{B(J/\psi \rightarrow h)} \approx \frac{B(\psi(3686) \rightarrow e^+ e^-)}{B(J/\psi \rightarrow e^+ e^-)} \approx 12\%.$$

211 This relation defines the "12% rule", which works reasonably well for many specific decay modes.
 212 A large violation of this rule was observed by later experiments [46] [47] [48], particularly in $\rho \pi$
 213 decay. Recent reviews [49] [50] of relevant theories and experiments conclude that current theoret-
 214 ical explanations are unsatisfactory. Many explanations [51] of the $\rho\pi$ puzzle have been proposed,
 215 including the J/ψ -glueball admixture scheme [52], the intrinsic-charm-component scheme [53], the
 216 sequential-fragmentation model [54], the exponential form-factor model [55], the S - D wave-mixing
 217 scheme [56, 57], the final-state interaction scheme and others [58]. However, none of these explana-
 218 tions can account for all existing experimental results. Clearly, more experimental results are desirable
 219 and tests of the 12% rule using the baryonic decay modes are helpful in understanding the $\rho\pi$ puzzle. The

220 study of baryon spectroscopy plays an important role in the development of the quark model and in the
221 understanding of QCD [59]. However, our knowledge of baryon is limited. The study of $J/\psi \rightarrow \Sigma^+ \bar{\Sigma}^-$
222 and $\psi(3686) \rightarrow \Sigma^+ \bar{\Sigma}^-$ in BESIII and new method application supply a good opportunity to further study
223 the baryon behaviors.

224 **2 Detector**

225 The BESIII detector [60] records symmetric e^+e^- collisions provided by the BEPCII storage ring [61],
226 which operates with a peak luminosity of $1 \times 10^{33} \text{ cm}^{-2}\text{s}^{-1}$ in the center of mass energy range from 2.0
227 to 4.94 GeV. BESIII has collected large data samples in this energy region [62]. The cylindrical core
228 of the BESIII detector covers 93% of the full solid angle and consists of a helium-based multilayer
229 drift chamber (MDC), a plastic scintillator time-of-flight system (TOF), and a CsI(Tl) electromagnetic
230 calorimeter (EMC), which are all enclosed in a superconducting solenoidal magnet providing a 1.0 T (0.9
231 T in 2012) magnetic field. The solenoid is supported by an octagonal flux-return yoke with resistive plate
232 counter muon identification modules interleaved with steel. The charged-particle momentum resolution
233 at 1 GeV/c is 0.5%, and the dE/dx resolution is 6% for electrons from Bhabha scattering. The EMC
234 measures photon energies with a resolution of 2.5% (5%) at 1 GeV in the barrel (end cap) region. The
235 time resolution in the TOF barrel region is 68 ps, while that in the end cap region is 110 ps. The end cap
236 TOF system was upgraded in 2015 using multi-gap resistive plate chamber technology, providing a time
237 resolution of 60 ps [63].

238 3 Data and Monte Carlo

239 3.1 Data

240 The data samples of $(10087 \pm 44) \times 10^6 J/\psi$ and $(2712.4 \pm 14.3) \times 10^6 \psi(3686)$ events [64, 65] have
 241 been collected with the BESIII detector at the BEPCII collider during 2009, 2012, 2017, 2018, and 2021
 242 year.

243 3.2 Monte Carlo Simulation

244 Simulated samples produced with the GEANT4-based [66] Monte Carlo (MC) package which in-
 245 cludes the geometric description of the BESIII detector and the detector response, are used to determine
 246 the detection efficiency and to estimate the backgrounds. The J/ψ and $\psi(3686)$ resonances are simu-
 247 lated with the KKMC generator [67], which is an event generator based on precise predictions of the
 248 Electroweak Standard Model for the process. The beam energy spread and initial state radiation (ISR)
 249 are taken into account in the simulation. The software framework used for the data analysis is BESIII
 250 Offline Software System (BOSS), which is developed from Gaudi. **This work is under BOSS version**
 251 **7.0.8 and 7.0.9 for $J/\psi \rightarrow \Sigma^+ \bar{\Sigma}^-$ and $\psi(3686) \rightarrow \Sigma^+ \bar{\Sigma}^-$ decay channels, which are shown Table 3.** About
 252 $10000 \times 10^6 J/\psi$ and $400 \times 10^6 \psi(3686)$ MC inclusive events are used to investigate possible back-
 253 grounds. The known decay modes are modelled with EVTGEN [68] using branching fractions taken
 254 from the Particle Data Group [37], and the remaining unknown charmonium decays are modelled with
 255 LUNDCHARM [69]. Final state radiation (FSR) from charged final state particles is incorporated using
 256 the PHOTOS package.

257 Besides, The Signal MC samples used in this analysis are listed: About 1000 million and 10 million
 258 PHSP MC samples of $J/\psi \rightarrow \Sigma^+ \bar{\Sigma}^-$ and $\psi(3686) \rightarrow \Sigma^+ \bar{\Sigma}^-$ are used to get the normalization factor. About
 259 100 million and 20 million DIY MC samples of $J/\psi \rightarrow \Sigma^+ \bar{\Sigma}^-$ and $\psi(3686) \rightarrow \Sigma^+ \bar{\Sigma}^-$ are used to perform
 260 the input/output check.

Tab. 3: Collected Ψ data sets at BESIII

Collected Ψ in different years	Number of events	Boss Version
J/ψ (2009)	224.0 ± 1.3 M	7.0.8
J/ψ (2012)	1088.5 ± 4.4 M	7.0.8
J/ψ (2017 – 2019)	8774.0 ± 39.4 M	7.0.8
$\psi(3686)$ (2009)	107.0 ± 0.8 M	7.0.9
$\psi(3686)$ (2012)	341.1 ± 2.1 M	7.0.9
$\psi(3686)$ (2021)	2264.2 ± 9.5 M	7.0.9

261 **4 Event Selection of $\Psi \rightarrow \Sigma^+ \bar{\Sigma}^-$, $\Sigma^+ \rightarrow p\pi^0$, $\bar{\Sigma}^- \rightarrow \bar{p}\pi^0$**

262 **4.1 Good Track Selection**

263 Charged tracks reconstructed by main drift chamber(MDC) hit information must be fitted by Kalman
264 method successfully and come from the interaction region in three dimensions. Due to changing beam
265 conditions, the interaction point (IP) moves. Thus, a separate average IP (beam position) is determined
266 for each run using the VertexDbSvc package since it can read the vertex information of each run in the
267 database. So, we can use it to select point tracks. The Σ^+ particle has a longer life time, so it requires a
268 wider distance and the reference we refer to is [70]. Relative to this run-dependent IP, each charged track
269 must satisfy the following requirements:

- 270 • $V_{xy} < 2$ cm,
- 271 • $|V_z| < 10$ cm,
- 272 • $|\cos\theta| < 0.93$.
- 273 • Good tracks is required $N = 2$

274 Here, θ is the polar angle of the charged track with respect to the beam axis, V_{xy} and $|V_z|$ are the closest
275 approaches of a charged track to the interaction point in the Oxy plane and in the z position.

276 **4.2 Particle identification**

277 The charged p and \bar{p} are identified via ParticleID package by using the TOF and dE/dx measure-
278 ments with which the combined confidence levels $\mathcal{L}(p)$ and $\mathcal{L}(\bar{p})$ for proton and anti-proton hypotheses
279 are calculated, respectively. The particle is taken as $p(\bar{p})$ if the $Prob_{PID}$ more than any other particle hy-
280 pothesis. We require the proton and anti-proton candidates satisfy the following criteria:

- 281 • p : $\mathcal{L}(p) > \mathcal{L}(\pi)$ and $\mathcal{L}(p) > \mathcal{L}(K)$,
- 282 • \bar{p} : $\mathcal{L}(\bar{p}) > \mathcal{L}(\pi)$ and $\mathcal{L}(\bar{p}) > \mathcal{L}(K)$,

283 **4.3 Good photon selection**

- 284 • Photon candidates are identified using showers in the EMC. The deposited energy of each shower
285 must be more than 25 MeV in the barrel region ($|\cos\theta| < 0.80$) and more than 50 MeV in the end
286 cap region ($0.86 < |\cos\theta| < 0.92$).
- 287 • To suppress electronic noise and showers unrelated to the event, the difference between the EMC
288 time and the event start time is required to be within (0, 700) ns.

- 289 • To exclude showers that originate from charged tracks, the angle between the position of each
 290 shower in the EMC and the closest extrapolated charged track must be greater than 10 degrees.

 291 • The number of good showers $N_\gamma \geq 2$.

292 **4.4 π^0 reconstruction**

293 The π^0 mesons are reconstructed by the decays $\pi^0 \rightarrow \gamma\gamma$. To reconstruct π^0 meson, we perform a
 294 kinematic fit on $\pi^0 \rightarrow \gamma\gamma$ and require that the χ^2 of the kinematic fit is less than 100. π^0 candidates
 295 are reconstructed from pairs of photons whose invariant mass satisfies $[M_{\pi^0} - 60] < M_{\gamma\gamma} < [M_{\pi^0} + 40]$
 296 MeV/c², where M_{π^0} is the nominal mass of π^0 taken from the PDG. Besides, the number of candidates
 297 is larger than or equal 1.

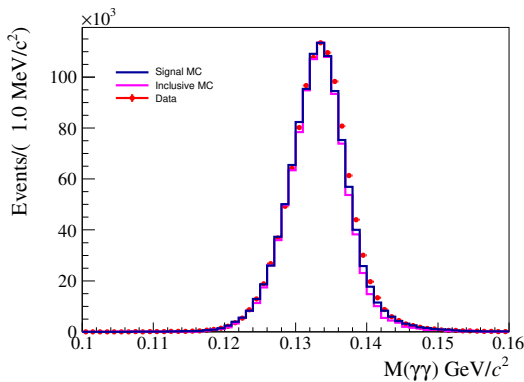


Fig. 2: The invariant mass distribution for π^0 .

298 **4.5 kinematic fit**

299 In our analysis, the π^0 reconstruction of $\bar{\Sigma}^-$ decay will be affected by anti-protons, since anti-protons
 300 can annihilate with materials in EMC and generate a large number of secondary showers. For the analysis
 301 of precise measurement of CP asymmetry $\Sigma^+ \rightarrow p\pi^0$, the requirement of the angle between the position
 302 of each shower in the EMC and the charged track(anti-proton) greater than 20 degrees is ineffective. So,
 303 π^0 of $\bar{\Sigma}^-$ decay is missing in the kinematic fit method, and an additional advantage is that the selection
 304 efficiency will also increased. π^0 invariant mass of Σ^+ decay is constrained in the known π^0 mass (PDG).
 305 Therefore, the constraint of kinematic fit is equal to be (4-3+1) = 2. This figures of χ^2_{2C} distributions are
 306 shown Figure 3.

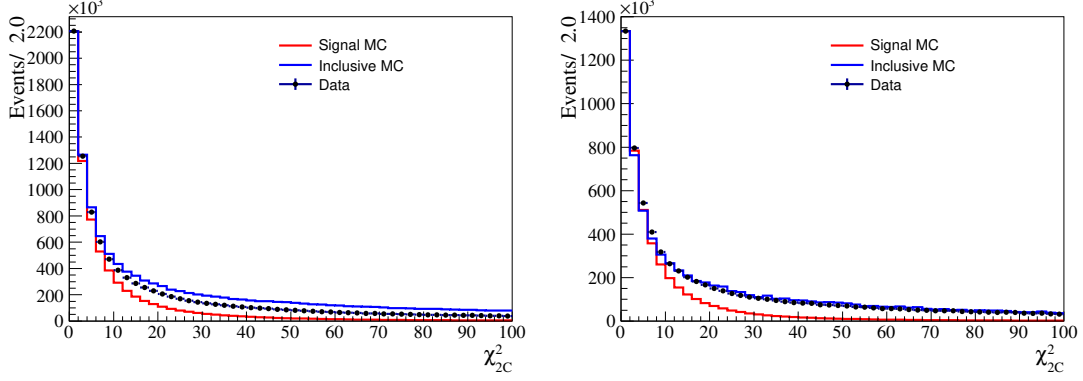


Fig. 3: The χ^2_{2C} distribution for $J/\psi \rightarrow \Sigma^+\bar{\Sigma}^-$, $\Sigma^+ \rightarrow p\pi^0$, $\bar{\Sigma}^- \rightarrow \bar{p}\pi^0$ and $\psi(3686) \rightarrow \Sigma^+\bar{\Sigma}^-$, $\Sigma^+ \rightarrow p\pi^0$, $\bar{\Sigma}^- \rightarrow \bar{p}\pi^0$.

307 A requirement on the quality of the 2C kinematic fit $\chi^2_{2C} \leq 30$ is imposed. If the number of π^0
 308 candidates in an event is more than one, the combination with the lowest χ^2_{2C} is selected as the final event
 309 candidate. This χ^2_{2C} value is optimized based on the figure of merit as the Figure 4 shown. In the plot, S
 310 is signal MC, and B is the backgrounds from the inclusive MC. Besides, the signal MC has been scaled
 311 to luminosity of data via our measurement of branching fraction.

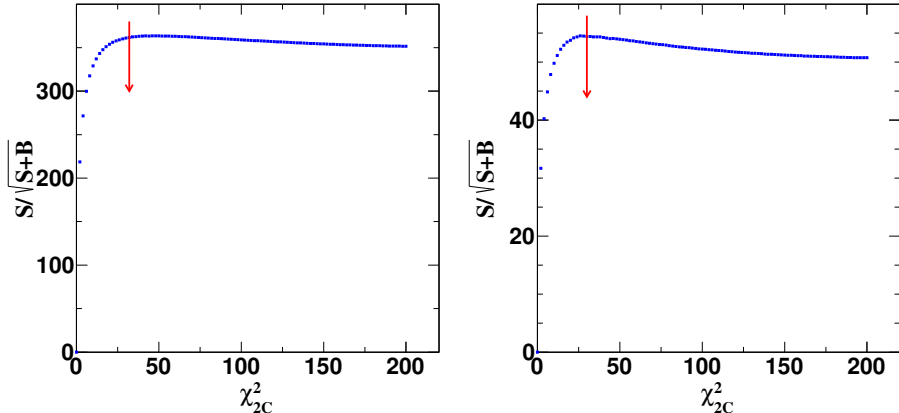


Fig. 4: Figure of merit for the χ^2_{4C} , the figures are for $J/\psi \rightarrow \Sigma^+\bar{\Sigma}^-$, $\Sigma^+ \rightarrow p\pi^0$, $\bar{\Sigma}^- \rightarrow \bar{p}\pi^0$ (left) and $\psi(3686) \rightarrow \Sigma^+\bar{\Sigma}^-$, $\Sigma^+ \rightarrow p\pi^0$, $\bar{\Sigma}^- \rightarrow \bar{p}\pi^0$ (right), where S is signal MC, and B is the backgrounds from the inclusive MC.

312 4.6 R_{xy} requirement

313 R_{xy} , the closest approaches of the track to the interaction point are shown Figure 5. Compared with
 314 $\Delta^+\bar{\Delta}^-$ particles, $\Sigma^+\bar{\Sigma}^-$ particles have a longer lifetime, which means $\Sigma^+\bar{\Sigma}^-$ particles have larger R_{xy} value.
 315 Using $R_{xy} > 0.34$ requirement, 64% of background contribution $J/\psi \rightarrow \Delta^+\bar{\Delta}^-$, $\Delta^+ \rightarrow p\pi^0$, $\bar{\Delta}^- \rightarrow \bar{p}\pi^0$
 316 and $\psi(3686) \rightarrow \Delta^+\bar{\Delta}^-$, $\Delta^+ \rightarrow p\pi^0$, $\bar{\Delta}^- \rightarrow \bar{p}\pi^0$ can be removed. This R_{xy} value is optimized based on

317 the figure of merit as shown the Figure 6. In the plot, S is signal MC, and B is the backgrounds from
 318 the inclusive MC. Besides, the signal MC has been scaled to luminosity of data via our measurement
 319 of branching fraction. The influence of R_{xy} requirement has been included and studied by using control
 320 sample in the appendix.

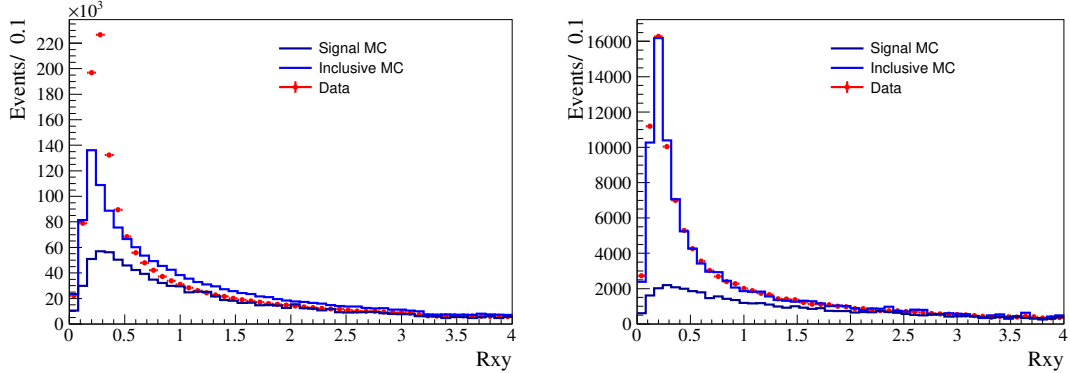


Fig. 5: The R_{xy} distribution for $J/\psi \rightarrow \Sigma^+\bar{\Sigma}^-$, $\Sigma^+ \rightarrow p\pi^0$, $\bar{\Sigma}^- \rightarrow \bar{p}\pi^0$ and $\psi(3686) \rightarrow \Sigma^+\bar{\Sigma}^-$, $\Sigma^+ \rightarrow p\pi^0$, $\bar{\Sigma}^- \rightarrow \bar{p}\pi^0$.

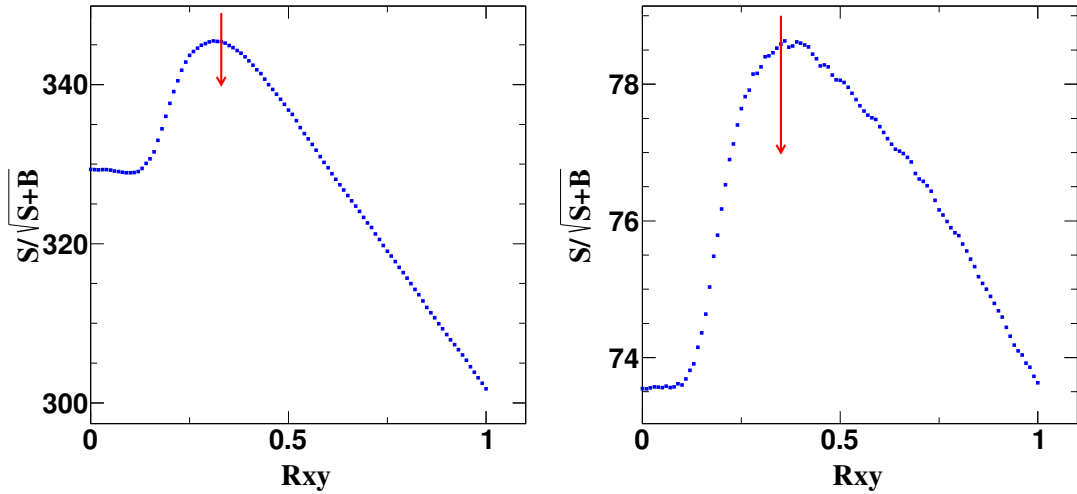


Fig. 6: Figure of R_{xy} , the closest approaches of vertex point to the interaction point. Here, vertex point can be obtained by performing vertex fit for p and \bar{p} . The figures are for $J/\psi \rightarrow \Sigma^+\bar{\Sigma}^-$, $\Sigma^+ \rightarrow p\pi^0$, $\bar{\Sigma}^- \rightarrow \bar{p}\pi^0$ (left) and $\psi(3686) \rightarrow \Sigma^+\bar{\Sigma}^-$, $\Sigma^+ \rightarrow p\pi^0$, $\bar{\Sigma}^- \rightarrow \bar{p}\pi^0$ (right), where S is signal MC, and B is the backgrounds from the inclusive MC.

321 4.7 mass window

322 The requirements of $p\pi^0$ and $\bar{p}\pi^0$ mass windows are set to be [1.172, 1.200] and [1.167, 1.212]
 323 GeV/ c^2 and are determined by the fitting of invariant mass of $p\pi^0$ and $\bar{p}\pi^0$ as the Figure 8. The double

324 Gaussian plus Johnson functions are used to describe the signals, and the mass window is defined as a
 325 range of approximately 3σ .

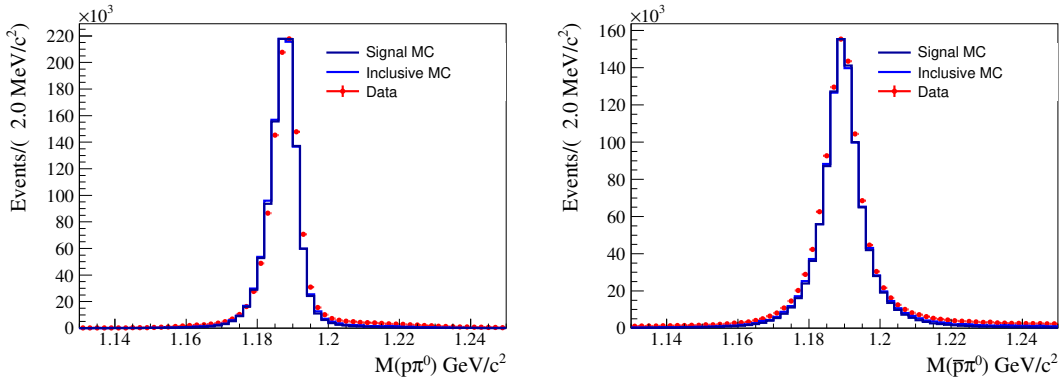


Fig. 7: Figure of invariant mass, the left figure is for Σ^+ , and the right is for $\bar{\Sigma}^-$.

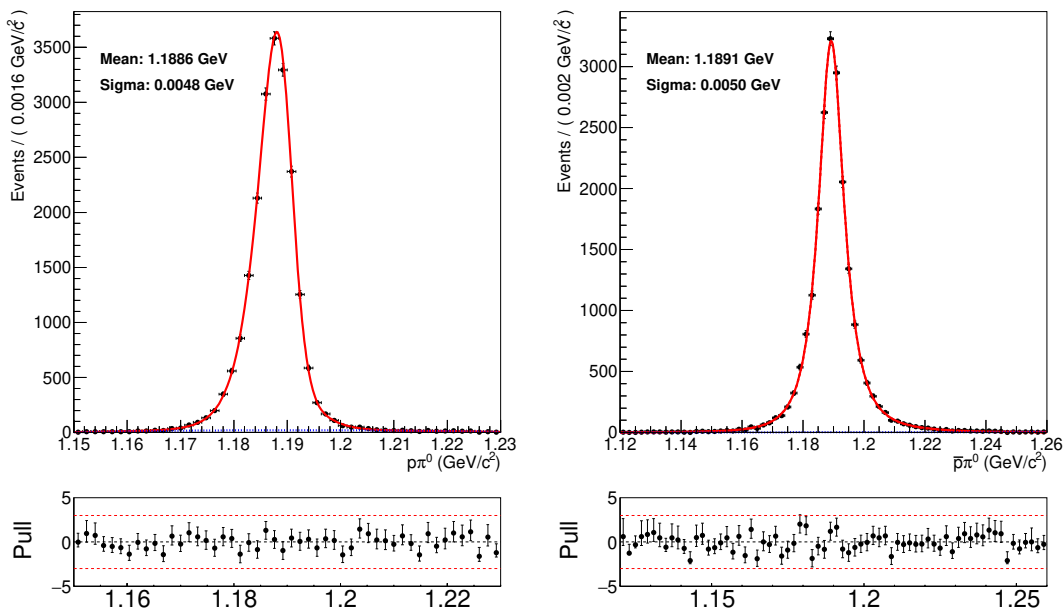


Fig. 8: The left and right figures are $p\pi^0$ and $\bar{p}\pi^0$ invariant masses for the signal MC. The black dots with error bars are the signal MC, the red solid lines are the total fitting function.

326 4.8 Background analysis

327 The background level in this channels is studied based on the J/ψ and $\psi(3686)$ inclusive samples.
 328 There are 140228 events which pass the event selections, and the number of background events is 1324,
 329 which means that the background level is 0.9% for $J/\psi \rightarrow \Sigma^+\bar{\Sigma}^-$ ($\Sigma^+ \rightarrow p\pi^0$, $\bar{\Sigma}^- \rightarrow \bar{p}\pi^0$) decay process.

330 There are 6258 events which pass the event selections, and the number of background events is 45,
 331 which means that the background level is 0.7% for $\psi(3686) \rightarrow \Sigma^+ \bar{\Sigma}^- (\Sigma^+ \rightarrow p\pi^0, \bar{\Sigma}^- \rightarrow \bar{p}\pi^0)$ decay
 332 process. The background contributions are also estimated to be 3.4% and 1.3% for J/ψ and $\psi(3686)$
 333 decay processes by fitting data samples, as Figure 19. Besides, the possible background have been
 334 studied in this MEMO [73] and it is quite small. The detail background channels could be found in
 335 Table 4 and Table 5.

Tab. 4: Topology of $J/\psi \rightarrow \Sigma^+ \bar{\Sigma}^-$ in generic J/ψ inclusive MC sample.

rowNo	decay tree	decay final state	iDcyTr	nEtr	nCEtr
1	$J/\psi \rightarrow \Sigma^+ \bar{\Sigma}^-, \Sigma^+ \rightarrow \pi^0 p, \bar{\Sigma}^- \rightarrow \pi^0 \bar{p}$	$\pi^0 \pi^0 p \bar{p}$	0	137961	137961
2	$J/\psi \rightarrow \Delta^+ \bar{\Delta}^+, \Delta^+ \rightarrow \pi^0 p, \bar{\Delta}^+ \rightarrow \pi^0 \bar{p}$	$\pi^0 \pi^0 p \bar{p}$	1	741	138702
3	$J/\psi \rightarrow \Sigma^+ \bar{\Sigma}^-, \Sigma^+ \rightarrow \pi^0 p, \bar{\Sigma}^- \rightarrow \pi^0 \bar{p}, \pi^0 \rightarrow e^+ e^- \gamma$	$e^+ e^- \pi^0 p \bar{p} \gamma$	7	566	139268
4	$J/\psi \rightarrow \Sigma^+ \bar{\Sigma}^- \gamma^f, \Sigma^+ \rightarrow \pi^0 p, \bar{\Sigma}^- \rightarrow \pi^0 \bar{p}$	$\pi^0 \pi^0 p \bar{p} \gamma^f$	4	298	139566
5	$J/\psi \rightarrow \pi^0 \pi^0 p \bar{p}$	$\pi^0 \pi^0 p \bar{p}$	6	120	139686
6	$J/\psi \rightarrow \eta_c \gamma, \eta_c \rightarrow \Sigma^+ \bar{\Sigma}^-, \Sigma^+ \rightarrow \pi^0 p, \bar{\Sigma}^- \rightarrow \pi^0 \bar{p}$	$\pi^0 \pi^0 p \bar{p} \gamma$	5	120	139806
7	$J/\psi \rightarrow \Lambda \bar{\Lambda}, \Lambda \rightarrow \pi^- p, \bar{\Lambda} \rightarrow \pi^+ \bar{p}$	$\pi^+ \pi^- p \bar{p}$	2	71	139877
8	$J/\psi \rightarrow \eta p \bar{p}, \eta \rightarrow \gamma \gamma$	$p \bar{p} \gamma \gamma$	3	69	139946
9	$J/\psi \rightarrow \Sigma^+ \bar{\Sigma}^- \gamma, \Sigma^+ \rightarrow \pi^0 p, \bar{\Sigma}^- \rightarrow \pi^0 \bar{p}$	$\pi^0 \pi^0 p \bar{p} \gamma$	10	58	140004
10	$J/\psi \rightarrow \Sigma^+ \bar{\Sigma}^-, \Sigma^+ \rightarrow \pi^0 p, \bar{\Sigma}^- \rightarrow \bar{p} \gamma$	$\pi^0 p \bar{p} \gamma$	14	55	140059
11	$J/\psi \rightarrow \eta p \bar{p}, \eta \rightarrow \pi^0 \pi^0 \pi^0$	$\pi^0 \pi^0 \pi^0 p \bar{p}$	16	54	140113

Tab. 5: Topology of $\psi(3686) \rightarrow \Sigma^+ \bar{\Sigma}^-$ in generic $\psi(3686)$ inclusive MC sample.

rowNo	decay tree	decay final state	iDcyTr	nEtr	nCEtr
1	$\psi' \rightarrow \Sigma^+ \bar{\Sigma}^-, \Sigma^+ \rightarrow \pi^0 p, \bar{\Sigma}^- \rightarrow \pi^0 \bar{p}$	$\pi^0 \pi^0 p \bar{p}$	0	6141	6141
2	$\psi' \rightarrow \Sigma^+ \bar{\Sigma}^- \gamma^f, \Sigma^+ \rightarrow \pi^0 p, \bar{\Sigma}^- \rightarrow \pi^0 \bar{p}$	$\pi^0 \pi^0 p \bar{p} \gamma^f$	1	42	6183
3	$\psi' \rightarrow \Sigma^+ \bar{\Sigma}^-, \Sigma^+ \rightarrow \pi^0 p, \bar{\Sigma}^- \rightarrow \pi^0 \bar{p}, \pi^0 \rightarrow e^+ e^- \gamma$	$e^+ e^- \pi^0 p \bar{p} \gamma$	10	26	6209
4	$\psi' \rightarrow \Delta^+ \bar{\Delta}^+, \Delta^+ \rightarrow \pi^0 p, \bar{\Delta}^+ \rightarrow \pi^0 \bar{p}$	$\pi^0 \pi^0 p \bar{p}$	3	13	6222
5	$\psi' \rightarrow \chi_{c0} \gamma, \chi_{c0} \rightarrow \Sigma^+ \bar{\Sigma}^-, \Sigma^+ \rightarrow \pi^0 p, \bar{\Sigma}^- \rightarrow \pi^0 \bar{p}$	$\pi^0 \pi^0 p \bar{p} \gamma$	8	7	6229
6	$\psi' \rightarrow \chi_{c0} \gamma, \chi_{c0} \rightarrow \pi^0 p \bar{p}$	$\pi^0 p \bar{p} \gamma$	2	5	6234
7	$\psi' \rightarrow \pi^0 \pi^0 J/\psi, J/\psi \rightarrow p \bar{p}$	$\pi^0 \pi^0 p \bar{p}$	14	5	6239
8	$\psi' \rightarrow \chi_{c2} \gamma, \chi_{c2} \rightarrow \pi^0 p \bar{p}$	$\pi^0 p \bar{p} \gamma$	7	3	6242
9	$\psi' \rightarrow \Sigma^+ \bar{\Sigma}^-, \Sigma^+ \rightarrow \pi^0 p, \bar{\Sigma}^- \rightarrow \pi^0 \bar{p}, \pi^0 \rightarrow e^+ e^- \gamma \gamma^f$	$e^+ e^- \pi^0 p \bar{p} \gamma \gamma^f$	21	3	6245
10	$\psi' \rightarrow \pi^0 \pi^0 J/\psi, J/\psi \rightarrow p \bar{p} \gamma$	$\pi^0 \pi^0 p \bar{p} \gamma$	4	2	6247
11	$\psi' \rightarrow \pi^0 \pi^0 J/\psi, J/\psi \rightarrow e^+ e^- \gamma^f$	$e^+ e^- \pi^0 \pi^0 \gamma^f$	13	2	6249
12	$\psi' \rightarrow \pi^0 \pi^0 J/\psi, J/\psi \rightarrow \pi^0 p \bar{p}$	$\pi^0 \pi^0 \pi^0 p \bar{p}$	6	2	6251

336 5 Measurement Method

337 In the introduction part, the differential cross section could be described by the function of angular distributions including decay parameters θ_{Σ^+} , θ_p , ϕ_p , $\theta_{\bar{p}}$, and $\phi_{\bar{p}}$. The definitions of these helicity parameters could be found in the introduction. The $\alpha_{J/\psi}$, $\alpha_{\psi(3686)}$, $\Delta\Phi_{J/\psi}$, $\Delta\Phi_{\psi(3686)}$, α_{Σ^+} , and α_{Σ^-} are decay parameters, which are need to be extracted from those angular distribution in the decay channels of $J/\psi \rightarrow \Sigma^+ \bar{\Sigma}^- \rightarrow p\pi^0 \bar{p}\pi^0$ and $\psi(3686) \rightarrow \Sigma^+ \bar{\Sigma}^- \rightarrow p\pi^0 \bar{p}\pi^0$.

342 5.1 Likelihood function construction

343 The maximum likelihood method is used to fit data to yield the decay parameters. The joint likelihood function is define by

$$\mathcal{L} = \prod_{i=1}^N \text{Prob}(p_i) = \prod_{i=1}^N \frac{W_i}{C},$$

$$C = \frac{1}{N_{mc}} \sum_{j=1}^{N_{mc}} W_j^{mc},$$

345 where $\text{Prob}(P_i)$ is the probability of event i characterized by the measurements P_i (the θ_{Σ^+} , θ_p , ϕ_p , $\theta_{\bar{p}}$, and $\phi_{\bar{p}}$ are helix angles), W is the differential cross section, and C is the the normalization factor for the cross section. We generate a large phase space MC samples to estimate the normalization factor, as the above equation shows, N_{mc} is the number of events generated in phase space MC. Here the detector efficiency is included in the W . Instead of working with the likelihood function \mathcal{L} , it is more convenient to work with the logarithm of \mathcal{L} ,

$$S = -\ln \mathcal{L} = -\ln \sum_{i=1}^N W_i + \ln C$$

351 After the background events are substracted, the objective function is modified to:

$$S = -\ln \mathcal{L}_{data}^{J/\psi} - \ln \mathcal{L}_{data}^{\psi(3686)} + \ln \mathcal{L}_{bg}^{J/\psi} + \ln \mathcal{L}_{bg}^{\psi(3686)},$$

352 where $\mathcal{L}_{data}^{J/\psi}$ and $\mathcal{L}_{data}^{\psi(3686)}$ are the likelihood functions of events for J/ψ and $\psi(3686)$ decay channels, 353 and $\mathcal{L}_{bg}^{J/\psi}$ and $\mathcal{L}_{bg}^{\psi(3686)}$ are the likelihood functions of background events for J/ψ and $\psi(3686)$ decay 354 channels. By minimize the S , which equals to maximize \mathcal{L} , the decay parameters of θ_{Σ^+} , θ_p , ϕ_p , $\theta_{\bar{p}}$, and 355 $\phi_{\bar{p}}$ could be extracted.

356 5.2 Function Minimization

357 The package MINUIT available in the CERN library is famous in the field of high energy physics,
358 which is widely used to minimize the objective function in the data analysis to extract the parameters in
359 questions. There are two methods to calculate the extremum: one is the chi-square(binned fit), another
360 one is the log-likelihood (un-binned fit), which is used in this analysis. In the final output of MINUIT
361 package, we could get the parameter values and error matrix.

362 5.3 Input/output check

363 To validate the reliability of the fitting results, 100 times DIY Monte Carlo samples are generated and
364 have been applied the same selection criteria, as Figure 9. In these samples, the amplitude information
365 is based on differential cross section based on the Eq. 2 and 3. And the inputs of decay parameters are
366 from the real data fitting results, which are listed in the Table 10. Here, the output values are consistent
367 with input parameters within 1σ of Gaussian function, and the difference between output and input is
368 taken as systematic uncertainty in the chapter of systematic uncertainty estimation.

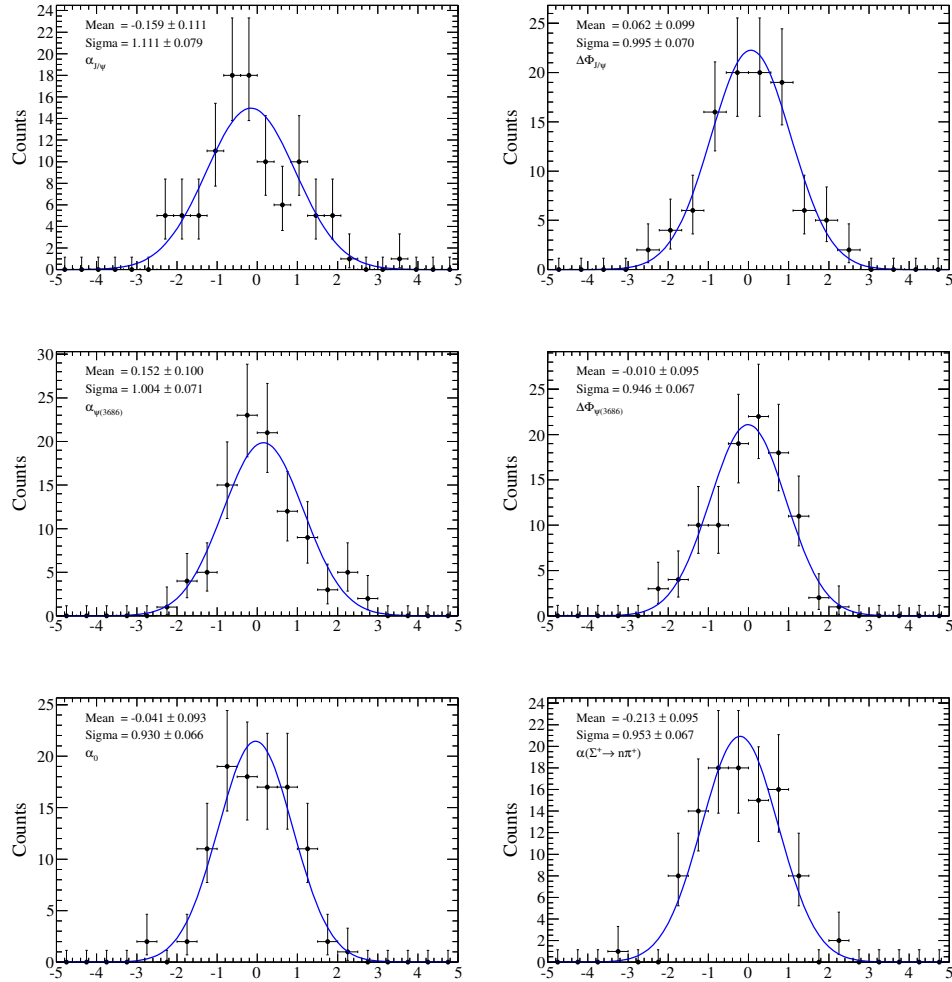


Fig. 9: The pull distributions for fitted parameters for $J/\psi \rightarrow \Sigma^+\bar{\Sigma}^-$ ($\Sigma^+ \rightarrow p\pi^0, \bar{\Sigma}^- \rightarrow \bar{p}\pi^0$) and $\psi(3686) \rightarrow \Sigma^+\bar{\Sigma}^-$ ($\Sigma^+ \rightarrow p\pi^0, \bar{\Sigma}^- \rightarrow \bar{p}\pi^0$).

369 6 MC Efficiency Difference

370 6.1 MC efficiency

371 To precisely extract decay parameters from the decay channels of $J/\psi \rightarrow \Sigma^+ \bar{\Sigma}^-$ ($\Sigma^+ \rightarrow p\pi^0, \bar{\Sigma}^- \rightarrow$
 372 $\bar{p}\pi^0$) and $\psi(3686) \rightarrow \Sigma^+ \bar{\Sigma}^-$ ($\Sigma^+ \rightarrow p\pi^0, \bar{\Sigma}^- \rightarrow \bar{p}\pi^0$), the difference of detection efficiency between MC
 373 and data should be considered. In our fitting method, the efficiency is considered in the phase space
 374 MC sample which is used to calculate the normalization factors. When we generate the phase space
 375 MC sample, we take the detection efficiency difference between data and MC into account. By selecting
 376 the control sample $J/\psi \rightarrow \Sigma^+ \bar{\Sigma}^- \rightarrow p\bar{p}\pi^0\pi^0$, the selection efficiencies of proton, anti-proton, and π^0
 377 are compared in different transverse momenta and polar angles, as shown in the Appendix C and the
 378 Figure 14. Besides, the control sample $J/\psi \rightarrow p\bar{p}\pi^+\pi^-$ is also used to study selection efficiencies of
 379 proton [75], anti-proton [75], as shown in Figure 10-13. The results of decay parameters are consistent
 380 whether we use control sample $J/\psi \rightarrow \Sigma^+ \bar{\Sigma}^- \rightarrow p\bar{p}\pi^0\pi^0$ or $J/\psi \rightarrow p\bar{p}\pi^+\pi^-$.

In order to correct the detection efficiency to real data, we did in the following steps. Firstly, for each event, the efficiency ratio between data and MC could be calculated by:

$$r_\epsilon = \frac{\epsilon_p^{data} \times \epsilon_{\bar{p}}^{data} \times \epsilon_{\pi^0}^{data}}{\epsilon_p^{MC} \times \epsilon_{\bar{p}}^{MC} \times \epsilon_{\pi^0}^{MC}}.$$

381 For the case $r_\epsilon < 1$, a random number η within (0,1) is generated, if $\eta < r_\epsilon$, this event is accepted.
 382 If not, this event is rejected. For another case $r_\epsilon > 1$, this event is accepted. To increase the correction
 383 procedure, when $r_\epsilon > 1$, we also generate a random number η within (0,1). If $r_\epsilon - 1 > \eta$, this event
 384 is accepted twice. By looping all phase space MC events, we could get a new MC sample which the
 385 efficiency is corrected to the real data, as Figure 15.

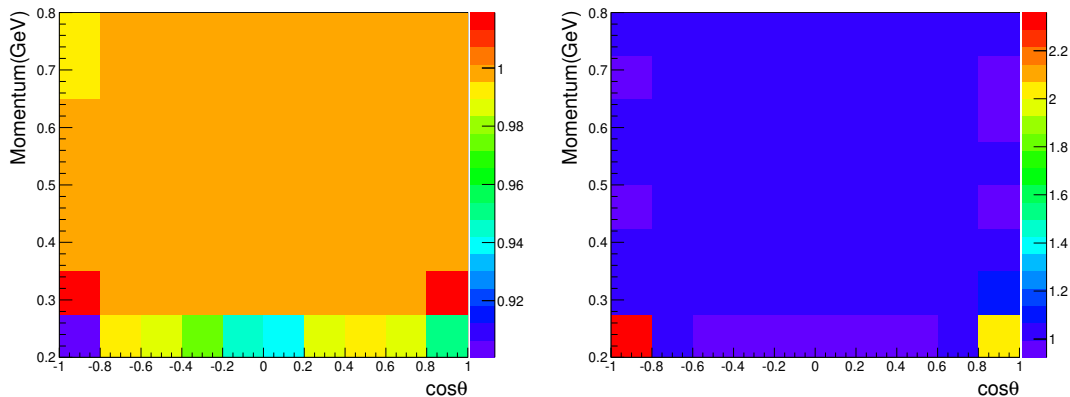


Fig. 10: The correction factor $\epsilon_{\bar{p}}^{data} / \epsilon_{\bar{p}}^{MC}$ in terms of $\cos\theta$ in different momentum range by using control sample $J/\psi \rightarrow p\bar{p}\pi^+\pi^-$ (left: 2009 year, right: 2012 year).

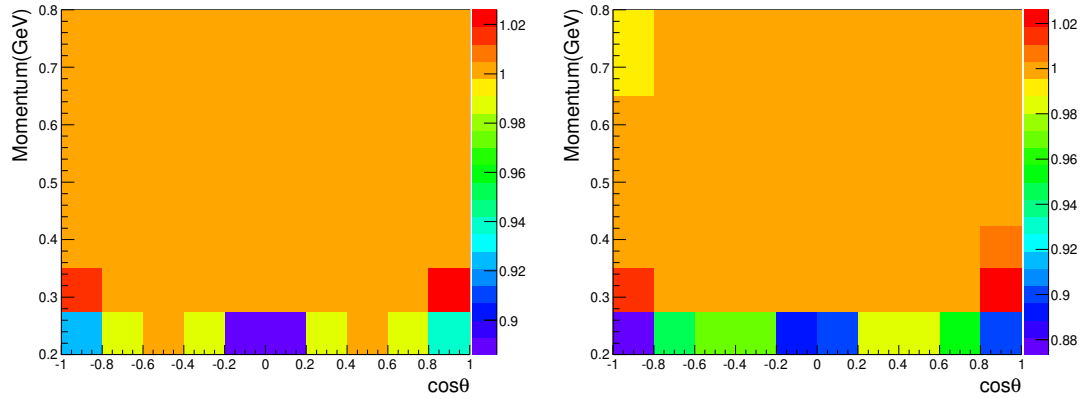


Fig. 11: The correction factor $\epsilon_{\bar{p}}^{data}/\epsilon_{\bar{p}}^{MC}$ in terms of $\cos\theta$ in different momentum range by using control sample $J/\psi \rightarrow p\bar{p}\pi^+\pi^-$ (left: 2018 year, right: 2019 year).

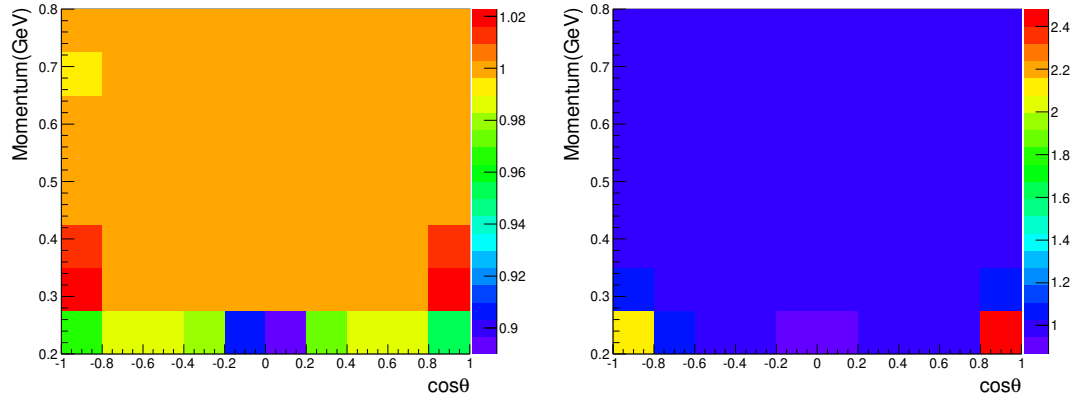


Fig. 12: The correction factor $\epsilon_p^{data}/\epsilon_p^{MC}$ in terms of $\cos\theta$ in different momentum range by using control sample $J/\psi \rightarrow p\bar{p}\pi^+\pi^-$ (left: 2009 year, right: 2012 year).

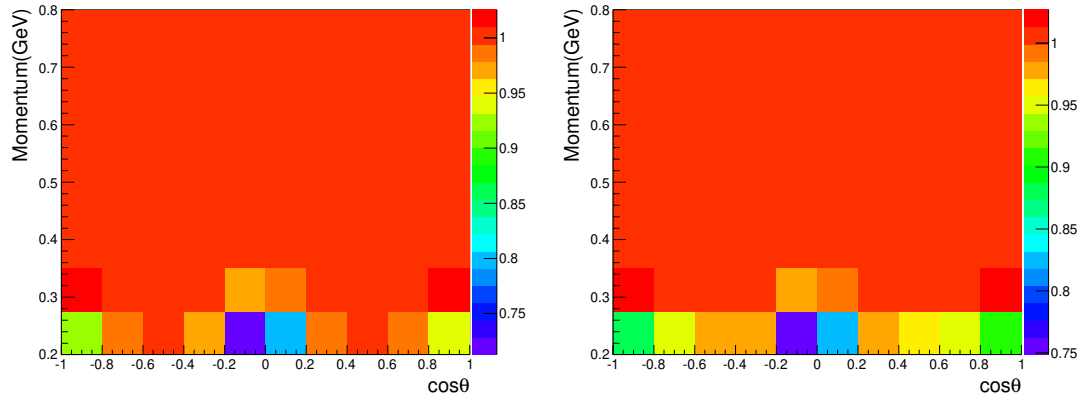


Fig. 13: The correction factor $\epsilon_p^{data}/\epsilon_p^{MC}$ in terms of $\cos\theta$ in different momentum range by using control sample $J/\psi \rightarrow p\bar{p}\pi^+\pi^-$ (left: 2018 year, right: 2019 year).

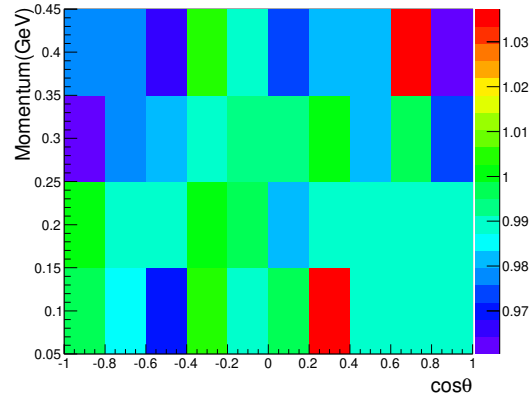


Fig. 14: The π^0 selection efficiency in terms of $\cos\theta$ in different momentum range.

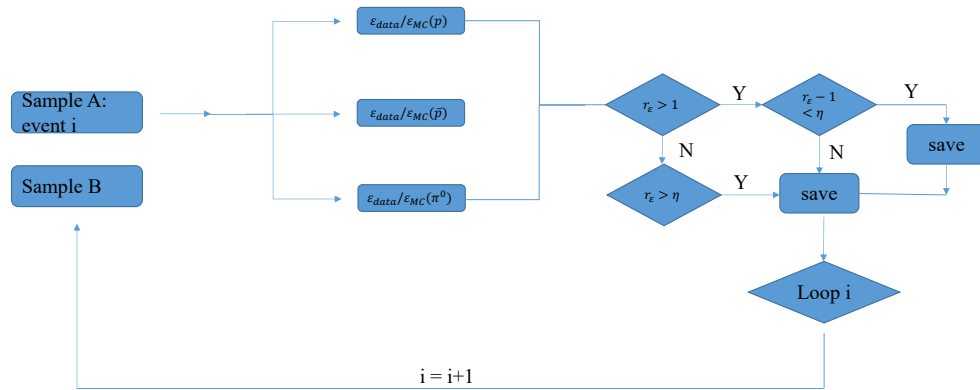


Fig. 15: PHSP MC correction flow

386 7 Decay Parameter Measurement

387 7.1 Simultaneous fit by using two decay channels

388 The mass window of signal is defined as in [1.167, 1.212] GeV/c² for $\bar{\Sigma}^-$. The background contri-
 389 bution in signal region is estimated by $N_{tot} - 1.1 \times N_{sideband}$, where $N_{sideband}$ is number of events in the
 390 sideband regions [1.12, 1.14] and [1.24, 1.26] GeV/c² for $\bar{\Sigma}^-$. Comparing the integral of background in
 391 signal region and sideband region, the scale factor of 1.1 is determined by fitting invariant mass of $\bar{p}\pi^0$,
 392 as shown Figure 19, and N_{tot} represents total number of events in signal region. The simultaneous fit is
 393 performed in the real data by:

$$S = -\ln \mathcal{L}_{data}^{J/\psi} - \ln \mathcal{L}_{data}^{\psi(3686)} + 1.1 \times \ln \mathcal{L}_{bg}^{J/\psi} + 1.1 \times \ln \mathcal{L}_{bg}^{\psi(3686)}. \quad (6)$$

394 By minimize the S , which equals to maximize \mathcal{L} , the decay parameters of θ_{Σ^+} , θ_p , ϕ_p , $\theta_{\bar{p}}$, and $\phi_{\bar{p}}$ could
 395 be extracted, as shown Figure 16.

396 For $J/\psi \rightarrow \Sigma^+ \bar{\Sigma}^-$ ($\Sigma^+ \rightarrow p\pi^0$, $\bar{\Sigma}^- \rightarrow \bar{p}\pi^0$) and $\psi(3686) \rightarrow \Sigma^+ \bar{\Sigma}^-$ ($\Sigma^+ \rightarrow p\pi^0$, $\bar{\Sigma}^- \rightarrow \bar{p}\pi^0$) de-
 397 cay processes, as we know that the term of $\sqrt{1 - \alpha_\psi^2} \sin(\Delta\Phi)(\alpha_{\Sigma^+} t_3(\xi) - \alpha_{\bar{\Sigma}^-} t_4(\xi))$ represents the po-
 398 larization contribution(it come from formula 2). Hence, if we did the integration to $\sin \theta_p \sin \phi_p$ and
 399 $\sin \theta_{\bar{p}} \sin \phi_{\bar{p}}$, we could observed the polarization behavior dependence on $\cos \theta_{\Sigma^+}$ which is proportional
 400 to $M(\cos \theta_{\Sigma^+}) = (\alpha_{\Sigma^+} - \bar{\alpha}_{\bar{\Sigma}^-}) \sqrt{1 - \alpha_{J/\psi}^2} \sin(\Delta\Phi) \sin \theta_{\Sigma^+} \cos \theta_{\Sigma^+}$. The variable $M(\cos \theta_{\Sigma^+})$ is calculated by
 401 $\frac{m}{N} \sum_i^{N(m)} (\sin \theta_p \sin \phi_p^{(i)} - \sin \theta_{\bar{p}} \sin \phi_{\bar{p}}^{(i)})$, where m equals to 32 (32 bins in $\cos \theta_{\Sigma^+}$), N is the total number
 402 of events in the data sample, $N(m)$ is the number of events in the $\cos \theta_{\Sigma^+}$ bin, and $\theta_p, \phi_p, \theta_{\bar{p}}, \phi_{\bar{p}}$ are the
 403 polar and azimuthal angles of proton and anti-proton. The distributions of $J/\psi \rightarrow \Sigma^+ \bar{\Sigma}^-$ ($\Sigma^+ \rightarrow p\pi^0$,
 404 $\bar{\Sigma}^- \rightarrow \bar{p}\pi^0$) and $\psi(3686) \rightarrow \Sigma^+ \bar{\Sigma}^-$ ($\Sigma^+ \rightarrow p\pi^0$, $\bar{\Sigma}^- \rightarrow \bar{p}\pi^0$) processes are shown in Figure 17. Comparing
 405 with the phase space distributions(green ones in the plots) and the real data(black dots), respectively,
 406 which mean the $\Delta\Phi$ is not zero and there are polarization existence.

```

FCN=-88684.2 FROM MINOS      STATUS=SUCCESSFUL    337 CALLS      509 TOTAL
                           EDM=1.11726e-07   STRATEGY= 1   ERROR MATRIX ACCURATE
EXT PARAMETER          PARABOLIC     MINOS ERRORS
NO.  NAME        VALUE       ERROR      NEGATIVE      POSITIVE
 1  alpha_jpsi -5.04191e-01  1.74945e-03 -1.74981e-03  1.74976e-03
 2  dphi_jpsi -2.74336e-01  3.25701e-03 -3.25849e-03  3.25582e-03
 3  S->p     -9.75306e-01  1.05640e-02 -1.06281e-02  1.05056e-02
 4  Sbar->pbar 9.98590e-01  1.08275e-02 -1.07762e-02  1.08771e-02
 5  alpha_psip  7.13349e-01  9.35717e-03 -9.37766e-03  9.32902e-03
 6  dphi_psip  4.26655e-01  2.17455e-02 -2.16426e-02  2.18383e-02
                           ERR DEF= 0.5
EXTERNAL ERROR MATRIX.  NDIM= 25   NPAR= 6   ERR DEF=0.5
 3.061e-06  3.977e-07 -7.386e-07  8.894e-07 -8.975e-07 -7.993e-07
 3.977e-07  1.061e-05 -1.449e-06 -1.024e-06 -2.524e-07 -2.029e-07
-7.386e-07 -1.449e-06  1.116e-04  1.119e-04  1.430e-06 -6.642e-07
 8.894e-07 -1.024e-06  1.119e-04  1.172e-04 -1.344e-06 -3.180e-06
-8.975e-07 -2.524e-07  1.430e-06 -1.344e-06  8.756e-05  3.702e-05
-7.993e-07 -2.029e-07 -6.642e-07 -3.180e-06  3.702e-05  4.729e-04
PARAMETER CORRELATION COEFFICIENTS
NO. GLOBAL   1   2   3   4   5   6
 1  0.41688  1.000  0.070 -0.040  0.047 -0.055 -0.021
 2  0.08672  0.070  1.000 -0.042 -0.029 -0.008 -0.003
 3  0.98209 -0.040 -0.042  1.000  0.978  0.014 -0.003
 4  0.98209  0.047 -0.029  0.978  1.000 -0.013 -0.014
 5  0.21974 -0.055 -0.008  0.014 -0.013  1.000  0.182
 6  0.18408 -0.021 -0.003 -0.003 -0.014  0.182  1.000
START MNCONTOUR CALCULATION OF 10 POINTS ON CONTOUR.

```

Fig. 16: The fitting results status for $J/\psi \rightarrow \Sigma^+ \bar{\Sigma}^-$ ($\Sigma^+ \rightarrow p\pi^0$, $\bar{\Sigma}^- \rightarrow \bar{p}\pi^0$) and $\psi(3686) \rightarrow \Sigma^+ \bar{\Sigma}^-$ ($\Sigma^+ \rightarrow p\pi^0$, $\bar{\Sigma}^- \rightarrow \bar{p}\pi^0$).

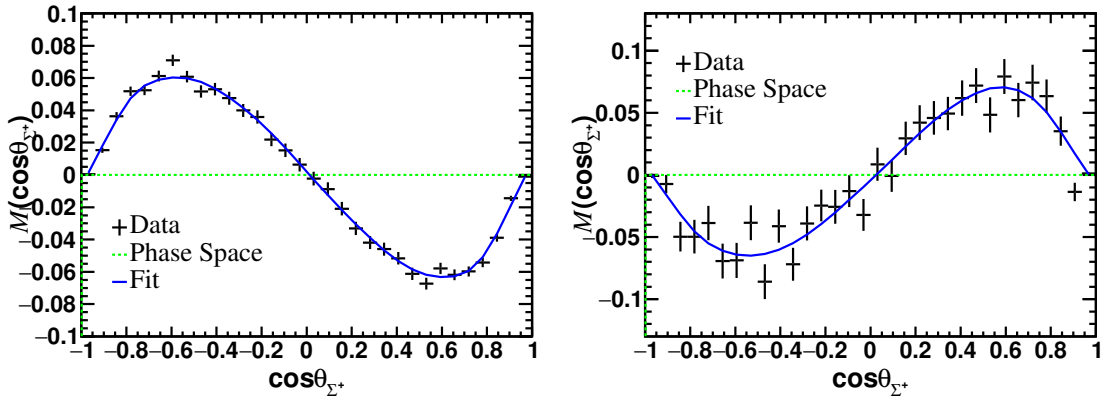


Fig. 17: The fitting results for moment of $\sin \theta \sin \phi$ for $J/\psi \rightarrow \Sigma^+ \bar{\Sigma}^-$ (Left) and $\psi(3686) \rightarrow \Sigma^+ \bar{\Sigma}^-$ (Right). The black dots are real data, the blue solid lines are fitting results, and the green dashed lines are phase space contributions.

407 The spin polarization is governed by the psionic form factor phase $\Delta\Phi$ and depends on the Σ^+ scat-
408 tering angle via:

$$\vec{P}_h(\cos \theta_{\Sigma^+}) = \frac{\sqrt{1 - \alpha_\Psi^2} \sin(\Delta\Phi) \cos \theta_{\Sigma^+} \sin \theta_{\Sigma^+}}{1 + \alpha_\Psi \cos^2 \theta_{\Sigma^+}}. \quad (7)$$

409 The Σ^+ polarization from J/ψ and $\psi(3686)$ decays, $\vec{P}_h(\cos \theta_{\Sigma^+})$, are independently measured in ten equal-
410 ly sized intervals of $\cos \theta_{\Sigma^+}$ with the same method, as Tab. 6. The $R(\cos \theta_{\Sigma^+})$ denotes the magnitude ratio

of $\vec{P}_h(\cos \theta_{\Sigma^+})$ between processes $\psi(3686)$ and J/ψ via the Eq. 7. The angular distribution of $R(\cos \theta_{\Sigma^+})$ is shown in Fig. 18. The fitting function of $R(\cos \theta_{\Sigma^+})$ is constructed via ratio between J/ψ and $\psi(3686)$ of Eq. 7. $R(\cos \theta_{\Sigma^+})$ values smaller than zero imply that the polarization of Σ^+ is opposite in same angular bins. The value of $\cos \theta_{\Sigma^+}$ approaches 1 or -1, indicating that the direction of the Σ^+ momentum is close to the beam direction. The absolute value of the ratio $R(\cos \theta_{\Sigma^+})$ is less than 1 in the beam direction, which means that compared to the Σ^+ from the decay of J/ψ , the polarization of Σ^+ from the decay of $\psi(3686)$ is firstly observed to decrease along the electron beam direction. Based on our first study of the magnitude of R in the decay of charmonium into hyperon-antihyperon pairs, we observe an increase in the difference at larger angles and the maximum in the direction perpendicular to the beam axis.

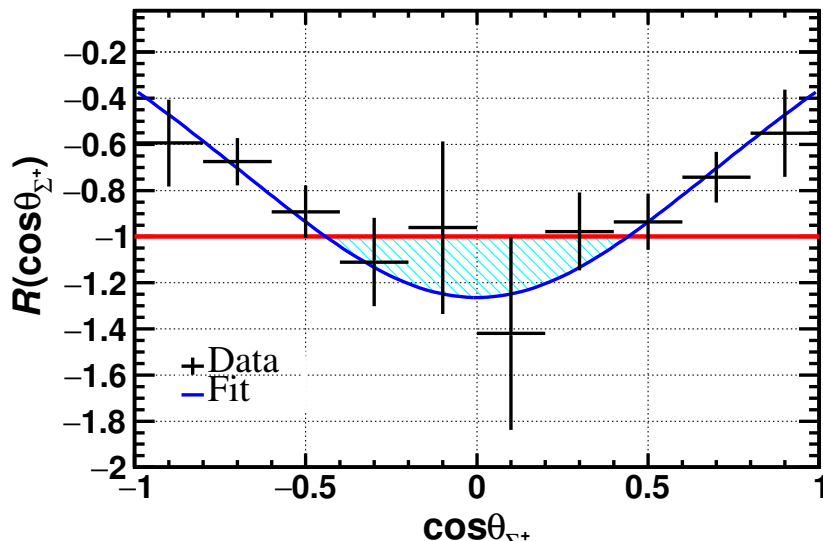


Fig. 18: The angular distribution of the magnitude ratio of polarization between $\psi(3686)$ and J/ψ decays. The black dots with error bars are the data, the blue solid line is the fitting results, the red line represents a ratio of -1. Comparing the Σ^+ from the J/ψ decay, the range of $\cos \theta_{\Sigma^+}$ in the shaded area (perpendicular to the electron beam direction) indicates the enhanced polarization of Σ^+ in the $\psi(3686)$ decay.

Tab. 6: The number of events and $R(\cos \theta_{\Sigma^+})$ for $\Psi \rightarrow \Sigma^+ \bar{\Sigma}^-, \Sigma^+ \rightarrow p\pi^0, \bar{\Sigma}^- \rightarrow \bar{p}\pi^0$

Bin	J/ψ events	$\psi(3686)$ events	$R(\cos \theta_{\Sigma^+})$
[-1.0, -0.8]	24761	2319	-0.594 ± 0.189
[-0.8, -0.6]	86955	6176	-0.675 ± 0.103
[-0.6, -0.4]	117707	6558	-0.892 ± 0.114
[-0.4, -0.2]	140071	6451	-1.110 ± 0.192
[-0.2, 0.0]	150884	6538	-0.961 ± 0.374
[0.0, 0.2]	152243	6455	-1.420 ± 0.418
[0.2, 0.4]	139611	6730	-0.978 ± 0.169
[0.4, 0.6]	117836	6638	-0.936 ± 0.112
[0.6, 0.8]	87180	6349	-0.742 ± 0.110
[0.8, 1.0]	24727	2186	-0.552 ± 0.189

420 8 Branching Results

421 The branch fraction of each channels is calculated according to

$$Br = \frac{N_{sig}(X)}{\varepsilon \times \prod Br_i \times N_{tot}}, \quad (8)$$

422 where X represents each decay channel, $N_{sig}(X)$ is the signal events by fitting method, ε is the detection
 423 efficiency determined by MC which is generated according to the decay parameters measured in the real
 424 data, $\prod Br_i$ is the product branching fractions of all the intermediate states in each channel, N_{tot} is the
 425 total number of J/ψ events or $\psi(3686)$ events.

426 For the subsections 8.1, the fit function PDFs(probability density function) in the fit code are de-
 427 scribed as: $N_{sig} \times PDF_{Signal} \otimes Gauss(Mean, \sigma) + N_{bkg} \times PDF_{2nd-OrderPolynomialFunction}$, where N_{sig} rep-
 428 resents signal events and N_{bkg} represents background events. For the $J/\psi \rightarrow \Sigma^+ \bar{\Sigma}^-$ process, in order to
 429 better describe the background contribution, an additional PDF is provided from the background shape
 430 of inclusive MC.

431 8.1 Branching fractions of $J/\psi \rightarrow \Sigma^+ \bar{\Sigma}^-$ and $\psi(3686) \rightarrow \Sigma^+ \bar{\Sigma}^-$

432 To yield the signal events, the fitting of the invariant mass of $\bar{p}\pi^0$ is performed in the region of [1.11,
 433 1.27] GeV/c^2 . The signal is described by double Gaussian plus Johnson functions, whose parameters
 434 are same as signal MC. The difference between data and MC in the resolution is described by the signal
 435 model convoluted with Gaussian function. The background is described with 2nd order polynomial
 436 function. Figure 19 shows the fittings of the $\bar{p}\pi^0$ invariant mass for $J/\psi \rightarrow \Sigma^+ \bar{\Sigma}^-$ and $\psi(3686) \rightarrow \Sigma^+ \bar{\Sigma}^-$
 437 process, where the red solid lines are the total fitting function, the red dash lines are signal function, and
 438 blue lines are the background function. The fitting results are listed in the Tabbe 7, and the branching
 439 fractions of $J/\psi \rightarrow \Sigma^+ \bar{\Sigma}^-$ and $\psi(3686) \rightarrow \Sigma^+ \bar{\Sigma}^-$ are measured to be $(10.94 \pm 0.02) \times 10^{-4}$ and $(2.57 \pm$
 440 $0.01) \times 10^{-4}$, respectively.

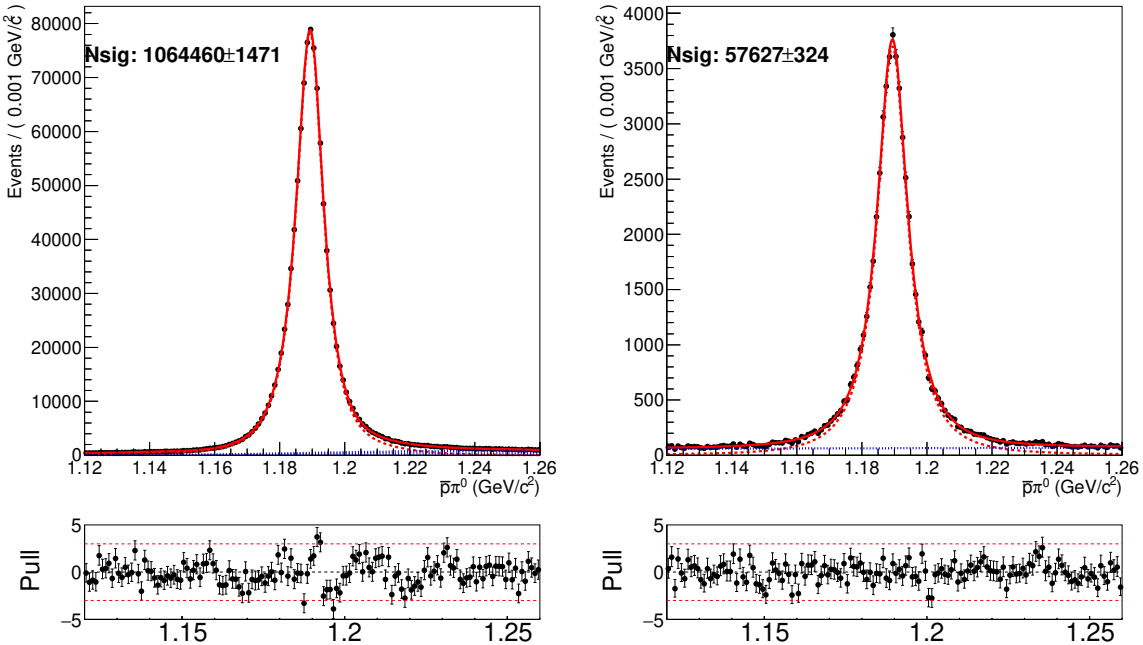


Fig. 19: The fittings of $p\pi^0$ invariant mass for $J/\psi \rightarrow \Sigma^+ \bar{\Sigma}^-$, $\Sigma^+ \rightarrow p\pi^0$, $\bar{\Sigma}^- \rightarrow \bar{p}\pi^0$ (Left) and $\psi(3686) \rightarrow \Sigma^+ \bar{\Sigma}^-$, $\Sigma^+ \rightarrow p\pi^0$, $\bar{\Sigma}^- \rightarrow \bar{p}\pi^0$ (Right).

Tab. 7: The number of events for $J/\psi \rightarrow \Sigma^+ \bar{\Sigma}^-$, $\Sigma^+ \rightarrow p\pi^0$, $\bar{\Sigma}^- \rightarrow \bar{p}\pi^0$

Channel	N_{sig}	$\varepsilon\%$	$Br(\times 10^{-4})$
$J/\psi \rightarrow \Sigma^+ \bar{\Sigma}^-$	1064460 ± 1471	36.7	(10.94 ± 0.02)
$\psi(3686) \rightarrow \Sigma^+ \bar{\Sigma}^-$	57627 ± 324	31.4	(2.54 ± 0.01)

441 9 Systematic uncertainty

442 The systematic uncertainties of the decay parameters and branching fractions are studied separately.

443 9.1 Systematic uncertainties of decay parameters

444 The systematic uncertainties of decay parameters consist of MC efficiency correction uncertainties,
 445 fitting method, kinematic fitting, signal mass window, and the background estimation. They are listed in
 446 the Table 15.

447 9.1.1 MC efficiency correction

448 The differences of selection efficiency have been studied and corrected using control samples in the
 449 Section 6.1. We found that the difference is quite small for proton, anti-proton, and π^0 . For the nominal
 450 values of the decay parameters, we take these corrections of selection efficiency into account. We use
 451 the correlation factor and the statistical error of the correction factor to generate Gaussian distribution of
 452 correlation factor. Then, 100 times different corrections are used in PHSP MC, and results of parameters
 453 are shown in Figure 20. The widths of Gaussian are taken as the systematic uncertainty, which are listed
 454 in the Table 8.

Tab. 8: The uncertainties of MC efficiency correction

Decay Parameters	difference
$\alpha_{J/\psi}$	0.0001
$\Delta\Phi_{J/\psi}$	0.0003
$\alpha_{(\Sigma^+ \rightarrow p\pi^0)}$	0.0007
$\alpha_{(\bar{\Sigma}^- \rightarrow \bar{p}\pi^0)}$	0.0009
$\alpha_{\psi(3686)}$	0.0002
$\Delta\Phi_{\psi(3686)}$	0.0003
A_{CP}	0.0008
$\alpha_{(\Sigma^+ \rightarrow p\pi^0)} \text{ average}$	0.00007

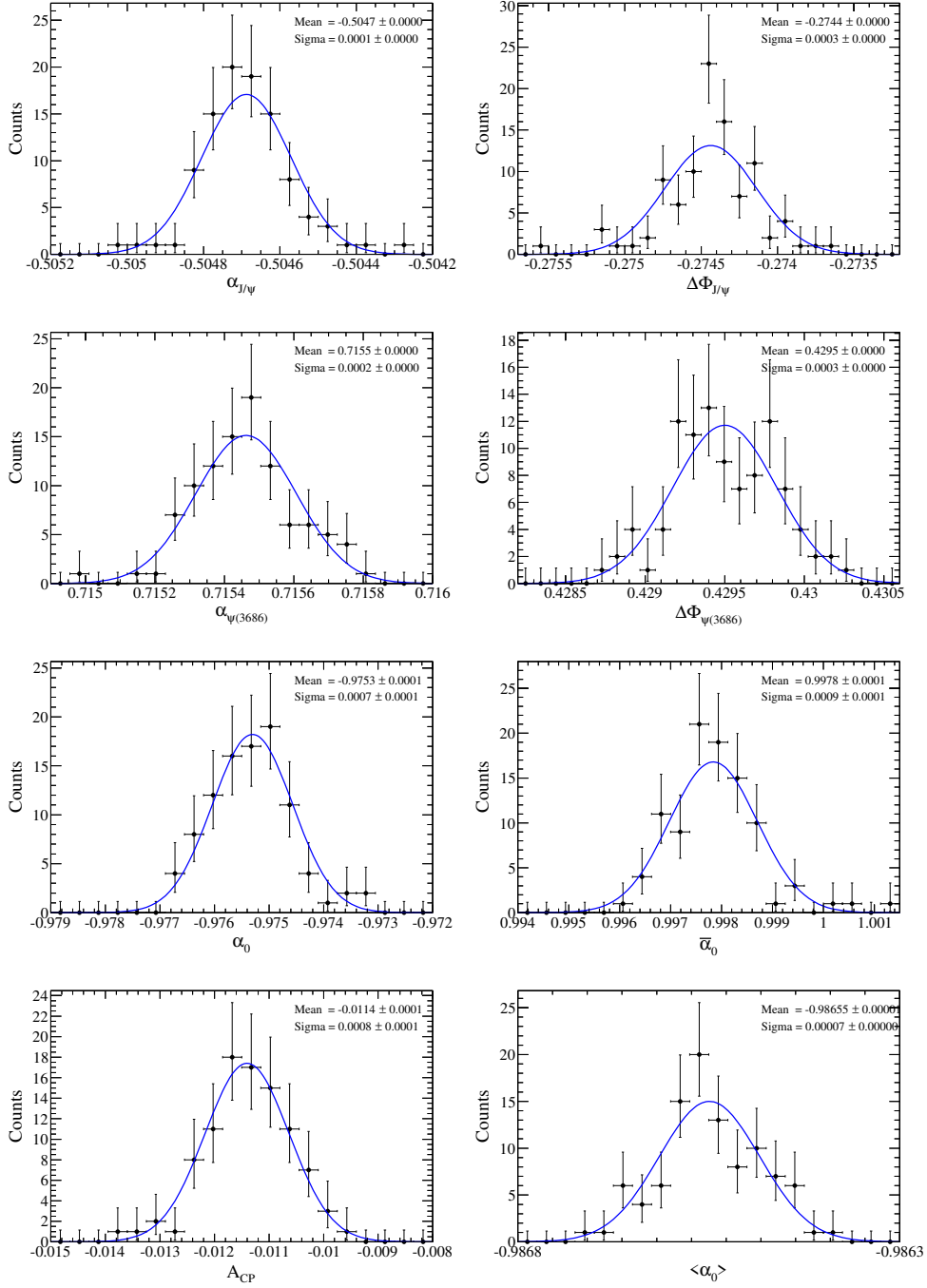


Fig. 20: The distributions for fitted parameters for $J/\psi \rightarrow \Sigma^+ \bar{\Sigma}^-$ ($\Sigma^+ \rightarrow p\pi^0, \bar{\Sigma}^- \rightarrow \bar{p}\pi^0$) and $\psi(3686) \rightarrow \Sigma^+ \bar{\Sigma}^-$ ($\Sigma^+ \rightarrow p\pi^0, \bar{\Sigma}^- \rightarrow \bar{p}\pi^0$).

455 9.1.2 Kinematic fitting

456 In our analysis, we apply the requirement of $\chi^2_{2C} \leq 30$, then take the measurements of parameters
 457 under this requirement as nominal values. In order to consider systematic uncertainty from kinematic

458 fitting, we change the value of requirement of $\chi^2_{2C} \leq 30$ from 30 to 22, 24, 26, 28, 32, 34, 36, 38, and
 459 compare different results of parameters, which are shown in Figure 21. In addition, we use the Barlow test
 460 method to determine whether the systematic uncertainty of this requirement should be taken into account.
 461 As long as there is a Barlow test value greater than 2 in this test, we will consider systematic uncertainty.
 462 For example, the Barlow test ξ of the α is calculated by $\xi = \frac{|\alpha_{\text{nominal}} - \alpha_{\text{test}}|}{\sqrt{\sigma_{\text{nominal}}^2 - \sigma_{\text{test}}^2}}$, where α_{test} represents the
 463 different parameters after applying different requirements of χ^2_{2C} , α_{nominal} represents nominal value, and
 464 σ_{nominal} and σ_{test} represent their uncertainties. The distributions of Barlow tests of decay parameters are
 465 shown in Figure 22. Here, the value of Barlow test is larger than to be 2, which means that the systematic
 466 uncertainty of differences between MC simulation and data need to be considered. For different results,
 467 they are described by using the first order polynomial, and we take the maximum difference between the
 468 results of first order polynomial fitting and the nominal value as the systematic uncertainties, as shown
 469 in Table 9.

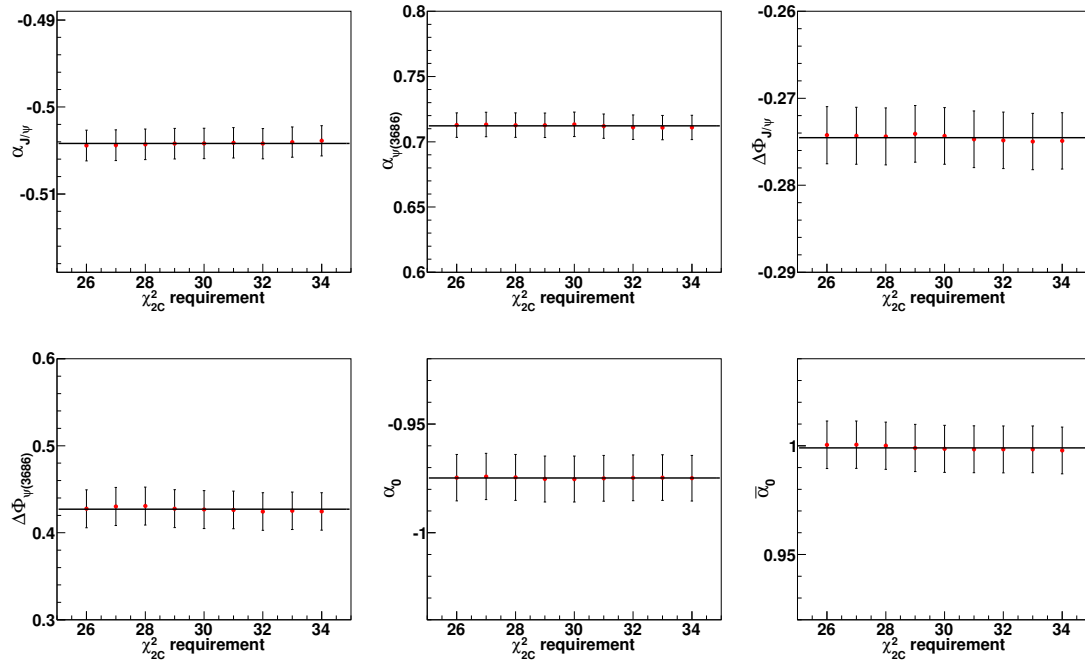


Fig. 21: Red data points and black error bars give different values of decay parameters in different χ^2_{2C} requirements.

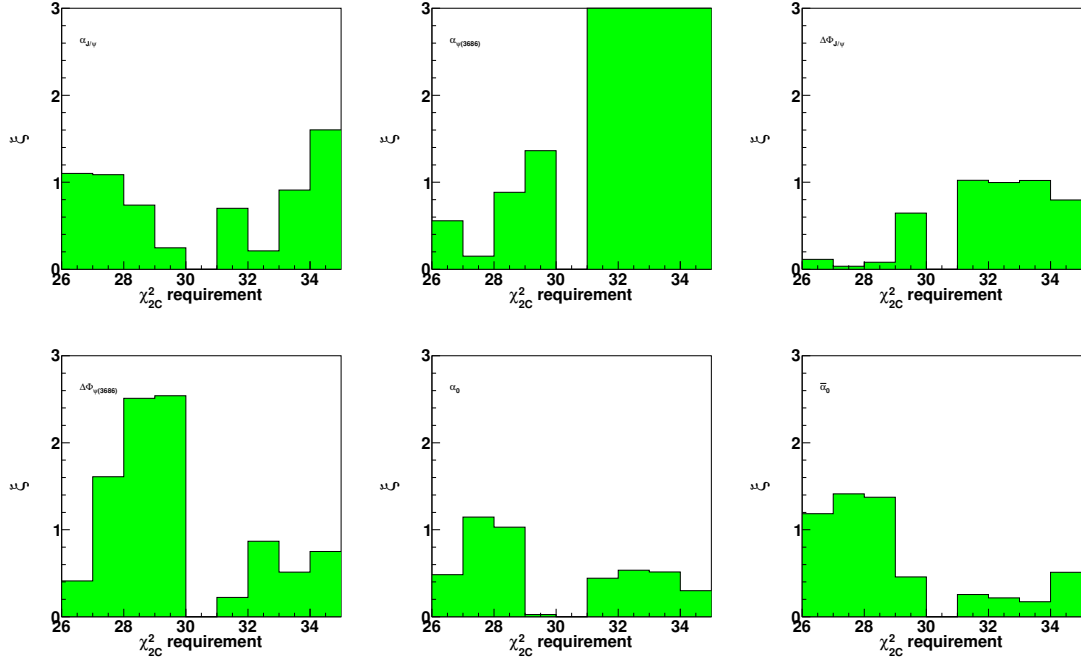


Fig. 22: The Barlow test of different χ^2_{2C} requirements for decay parameters. The green histogram represent the values of Barlow test in different requirements.

Tab. 9: The uncertainties of kinematic fitting for the decay parameters ($\Sigma^+ \rightarrow p\pi^0$, $\bar{\Sigma}^- \rightarrow \bar{p}\pi^0$)

Decay Parameters	nominal results	new results with barlow test method	difference
$\alpha_{J/\psi}$	-0.5047 ± 0.0018	—	—
$\Delta\Phi_{J/\psi}$	-0.2744 ± 0.0033	—	—
$\alpha_{(\Sigma^+ \rightarrow p\pi^0)}$	-0.9753 ± 0.0106	—	—
$\alpha_{(\bar{\Sigma}^- \rightarrow \bar{p}\pi^0)}$	0.9978 ± 0.0108	—	—
$\alpha_{(\Sigma^+ \rightarrow p\pi^0)}$ average	-0.9869 ± 0.0011	—	—
A_{CP}	-0.0118 ± 0.0083	—	—
$\alpha_{\psi(3686)}$	0.7155 ± 0.0094	0.7131	0.0024
$\Delta\Phi_{\psi(3686)}$	0.4295 ± 0.0217	0.4273	0.0021

470 9.1.3 Fitting method

471 We compared the input values and output values which are listed in the Table 10. The output values
 472 are consistent with input parameters within 1σ of Gaussian function, and the difference between out-
 473 put and input is taken as systematic uncertainty of the fitting method. The pull distributions for fitted
 474 parameter can be found in the Figure 9.

Tab. 10: Fitting method for the decay parameters ($\Sigma^+ \rightarrow p\pi^0$, $\bar{\Sigma}^- \rightarrow \bar{p}\pi^0$)

Decay Parameters	input	output	difference
$\alpha_{J/\psi}$	-0.510	-0.5094	0.0006
$\Delta\Phi_{J/\psi}$	-0.276	-0.2757	0.0003
$\alpha_{(\Sigma^+ \rightarrow p\pi^0)}$	-0.982	-0.9826	0.0006
$\alpha_{(\bar{\Sigma}^- \rightarrow \bar{p}\pi^0)}$	0.982	0.9784	0.0036
$\alpha_{(\Sigma^+ \rightarrow p\pi^0)} \text{ average}$	-0.982	-0.9805	0.0015
A_{CP}	0.000	0.0021	0.0021
$\alpha_{\psi(3686)}$	0.717	0.7184	0.0014
$\Delta\Phi_{\psi(3686)}$	0.486	0.4859	0.0001

475 **9.1.4 Signal mass window**

476 In our analysis, the requirement of mass box $28\text{MeV}/c^2$ ($1.172 - 1.200 \text{ GeV}/c^2$) and $45 \text{ MeV}/c^2$
 477 ($1.167 - 1.212 \text{ GeV}/c^2$) for $p\pi^0$ and $\bar{p}\pi^0$ mass windows is used to extract signal and measure decay
 478 parameters. In order to consider systematic uncertainty from signal mass window, we change the value
 479 of requirements of $28 \times 45 \text{ MeV}/c^2$ from 28×45 to 24×41 , 25×42 , 26×43 , 27×44 , 29×46 , 30×47 , 31×48 ,
 480 30×49 (Reduce or expand mass box by 4 MeV, with each change of 1 MeV), and compare different results
 481 of parameters, which are shown in Figure 23. In addition, we use the Barlow test method to determine
 482 whether the systematic uncertainty of this requirement should be taken into account. The distributions of
 483 Barlow tests of decay parameters are shown in Figure 24. Here, the value of Barlow test is larger than to
 484 be 2, which means that the systematic uncertainty of differences between MC simulation and data need
 485 to be considered. For different results, they are described by using the first order polynomial, and we
 486 take the maximum difference between the results of first order polynomial fitting and the nominal value
 487 as the systematic uncertainties, as shown in Table 11.

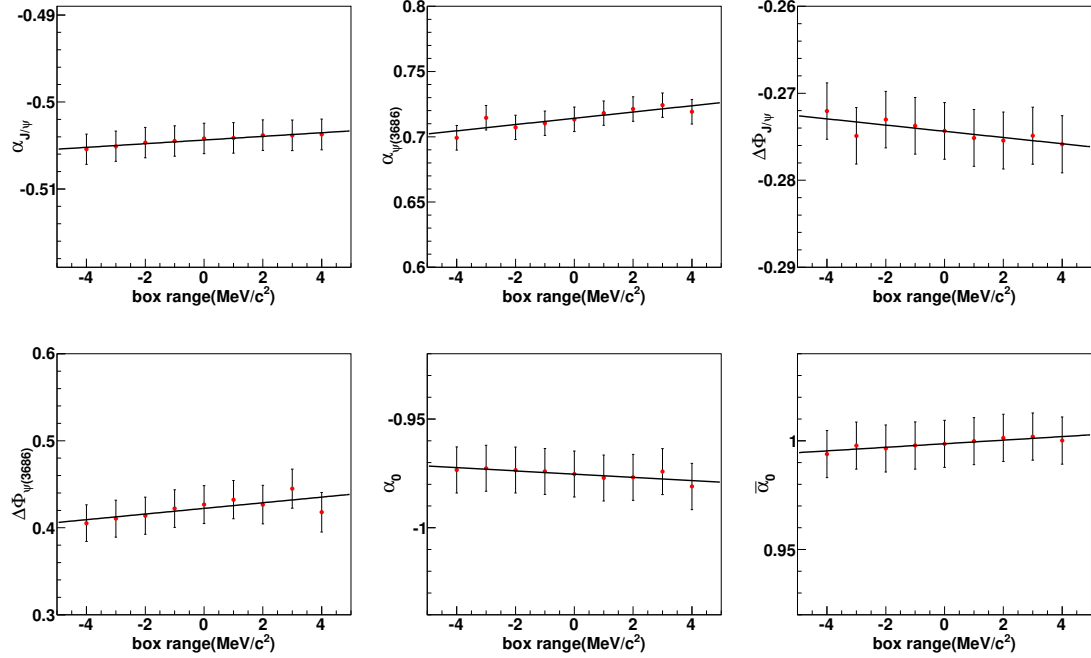


Fig. 23: Red data points and black error bars give different values of decay parameters in different signal mass windows.

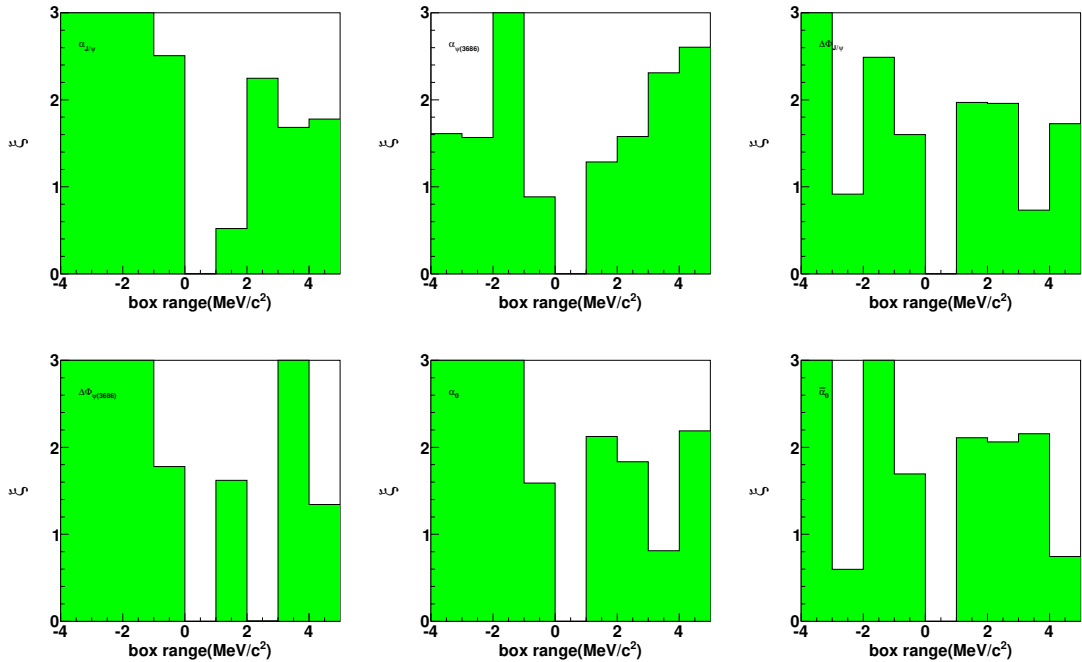


Fig. 24: The Barlow test of different signal mass windows for decay parameters. The green histogram represent the values of Barlow test in different requirements.

Tab. 11: Signal mass window for the decay parameters ($\Sigma^+ \rightarrow p\pi^0$, $\bar{\Sigma}^- \rightarrow \bar{p}\pi^0$)

Decay Parameters	nominal results	new results with barlow test method	difference
$\alpha_{J/\psi}$	-0.5047 ± 0.0018	-0.5042	0.0005
$\Delta\Phi_{J/\psi}$	-0.2744 ± 0.0033	-0.2752	0.0008
$\alpha_{(\Sigma^+ \rightarrow p\pi^0)}$	-0.9753 ± 0.0106	-0.9768	0.0015
$\alpha_{(\bar{\Sigma}^- \rightarrow \bar{p}\pi^0)}$	0.9978 ± 0.0108	0.9962	0.0016
$\alpha_{(\Sigma^+ \rightarrow p\pi^0)} \text{ average}$	-0.98655 ± 0.0011	-0.9865	0.00005
A_{CP}	-0.0114 ± 0.0083	-0.0098	0.0016
$\alpha_{\psi(3686)}$	0.7155 ± 0.0094	0.7211	0.0056
$\Delta\Phi_{\psi(3686)}$	0.4295 ± 0.0217	0.4315	0.0020

488 9.1.5 Background estimation

489 The signal yields are extracted based on the sideband subtraction. The uncertainty due to the effect of
 490 sideband subtraction are estimated by changing sideband regions of $\bar{p}\pi^0$ from [1.120, 1.140] & [1.240,
 491 1.260] GeV/c^2 to [1.116, 1.136] & [1.236, 1.256] GeV/c^2 , [1.117, 1.137] & [1.237, 1.257] GeV/c^2 ,
 492 [1.118, 1.138] & [1.238, 1.258] GeV/c^2 , [1.119, 1.139] & [1.239, 1.259] GeV/c^2 , [1.121, 1.141] &
 493 [1.241, 1.261] GeV/c^2 , [1.122, 1.142] & [1.242, 1.262] GeV/c^2 , [1.123, 1.143] & [1.243, 1.263] GeV/c^2 ,
 494 [1.124, 1.144] & [1.244, 1.264] GeV/c^2 (Move 4 MeV to the left or right, with each change of 1 MeV),
 495 and compare different results of parameters, which are shown in Figure 25. In addition, we use the
 496 Barlow test method to determine whether the systematic uncertainty of this requirement should be taken
 497 into account. The distributions of Barlow tests of decay parameters are shown in Figure 26. For different
 498 results, they are described by using the first order polynomial, and we take the maximum difference
 499 between the results of first order polynomial fitting and the nominal value as the systematic uncertainties,
 500 as shown in Table 12.

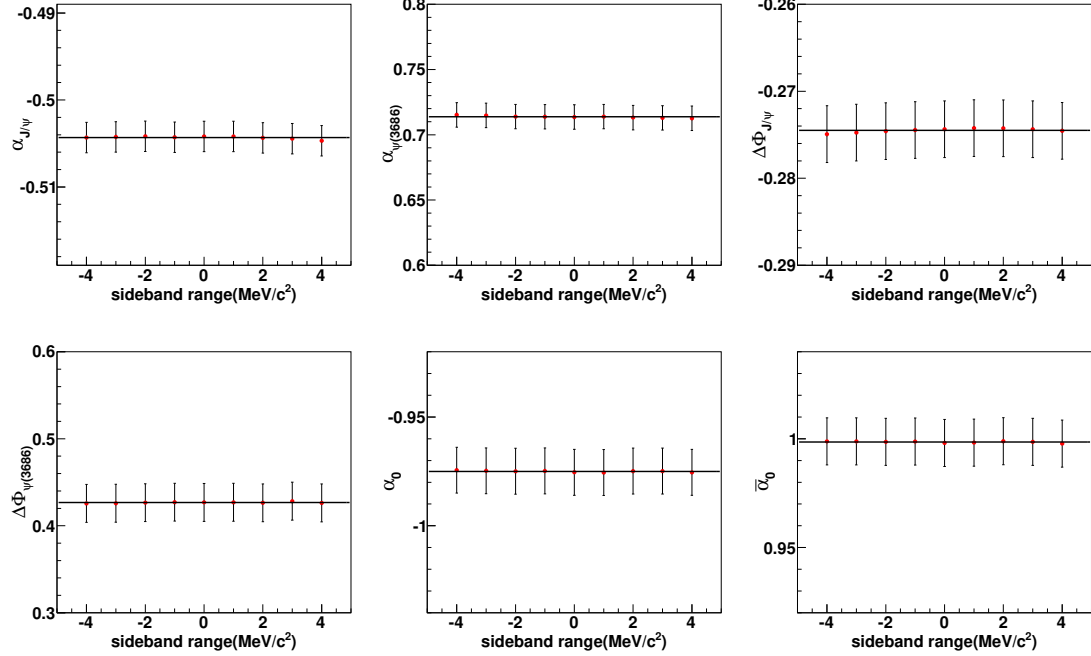


Fig. 25: Red data points and black error bars give different values of decay parameters in different sideband windows.

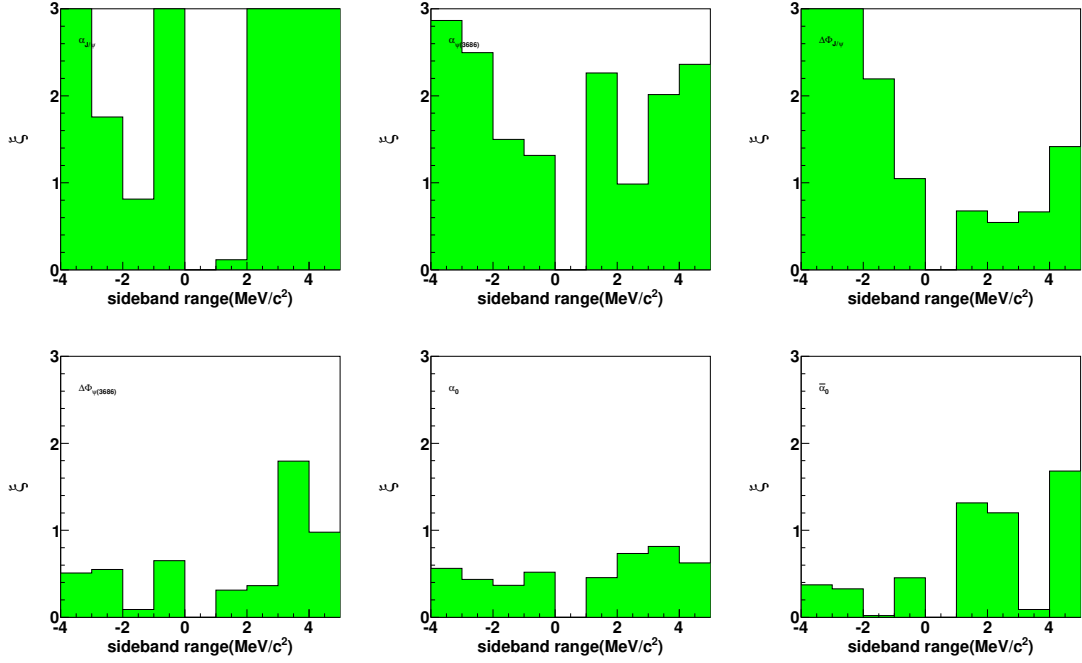


Fig. 26: The Barlow test of different signal mass windows for decay parameters. The green histogram represent the values of Barlow test in different sideband windows.

Tab. 12: Background uncertainties for the decay parameters ($\Sigma^+ \rightarrow p\pi^0$, $\bar{\Sigma}^- \rightarrow \bar{p}\pi^0$)

Decay Parameters	nominal	new bkg consideration(larger difference)	difference
$\alpha_{J/\psi}$	-0.5047 ± 0.0018	-0.5044	0.0003
$\Delta\Phi_{J/\psi}$	-0.2744 ± 0.0033	-0.2747	0.0003
$\alpha_{(\Sigma^+ \rightarrow p\pi^0)}$	-0.9753 ± 0.0106	–	–
$\alpha_{(\bar{\Sigma}^- \rightarrow \bar{p}\pi^0)}$	0.9986 ± 0.0108	–	–
$\alpha_{(\Sigma^+ \rightarrow p\pi^0)} \text{ average}$	-0.98655 ± 0.0011	–	–
A_{CP}	-0.0114 ± 0.0083	–	–
$\alpha_{\psi(3686)}$	0.7155 ± 0.0094	0.7131	0.0024
$\Delta\Phi_{\psi(3686)}$	0.4295 ± 0.0217	–	–

501 9.1.6 Summary of decay parameter uncertainties

502 All the sources of systematic uncertainties are treated as uncorrelated and summed in quadrature,
 503 listed in Table 13.

Tab. 13: The total uncertainties of decay parameters

Systematic error	$\alpha_{J/\psi}$	$\Delta\Phi_{J/\psi}$	$\alpha_{(\Sigma^+ \rightarrow p\pi^0)}$	$\alpha_{(\bar{\Sigma}^- \rightarrow \bar{p}\pi^0)}$	$\alpha_{(\Sigma^+ \rightarrow p\pi^0)} \text{ avg}$	A_{CP}	$\alpha_{\psi(3686)}$	$\Delta\Phi_{\psi(3686)}$
MC efficiency correction	0.0001	0.0003	0.0007	0.0009	0.00007	0.0008	0.0002	0.0003
Kinematic fitting	0.0006	–	–	–	–	–	0.0019	0.0021
Fitting method	0.0006	0.0003	0.0006	0.0036	0.0015	0.0021	0.0014	0.0001
Signal mass window	0.0005	0.0008	0.0015	0.0016	0.00005	0.0016	0.0056	0.0020
Background	0.0003	0.0003	–	–	–	–	0.0024	–
Total	0.0009	0.0010	0.0018	0.0040	0.0016	0.0028	0.0065	0.0030

504 9.2 Systematic uncertainties of branching fraction measurement

505 9.2.1 MC efficiency correction for charged tracks and π^0

We use 1,000,000 J/ψ MC DIY event to estimate the event selection efficiencies. The differences of detection efficiencies for proton, anti-proton, and π^0 between data and MC have been corrected according to momentums and polar angles. The uncertainties for these correction are estimated by the following formula:

$$\Delta^2 = \sum_{i=0}^n \left(\frac{\epsilon_i - \epsilon_0}{\epsilon_0} \right)^2$$

506 where n denotes the number of bins of two dimensional histograms, as shown in in Figure 10-14, ϵ_0 is
 507 the nominal value of efficiency, and ϵ_i is the efficiency when we change the correction factor in 1σ range
 508 for i bin. The uncertainties of charged tracking and PID efficiencies are estimated to 0.18% and 0.14%
 509 for $J/\psi \rightarrow \Sigma^+\bar{\Sigma}^-$ and $\psi(3686) \rightarrow \Sigma^+\bar{\Sigma}^-$. The uncertainties of π^0 reconstruction efficiencies are estimated
 510 to 0.41% and 0.40% for $J/\psi \rightarrow \Sigma^+\bar{\Sigma}^-$ and $\psi(3686) \rightarrow \Sigma^+\bar{\Sigma}^-$.

511 **9.2.2 Decay parameters**

512 The efficiency is calculated based on the MC sample which is generated with decay parameters
 513 measured by ourselves. We use the correlation matrix in a multivariate Gaussian to randomly generate
 514 100 sets of parameters (taking correlation into account) to generate 200 sets DIY MC samples. Then,
 515 the selection efficiencies can be obtained and are shown Figure 27. We take the width of Gaussian as the
 516 systematic uncertainty, which are 0.33% for $J/\psi \rightarrow \Sigma^+ \bar{\Sigma}^-$ and 0.30% for $\psi(3686) \rightarrow \Sigma^+ \bar{\Sigma}^-$, respectively.

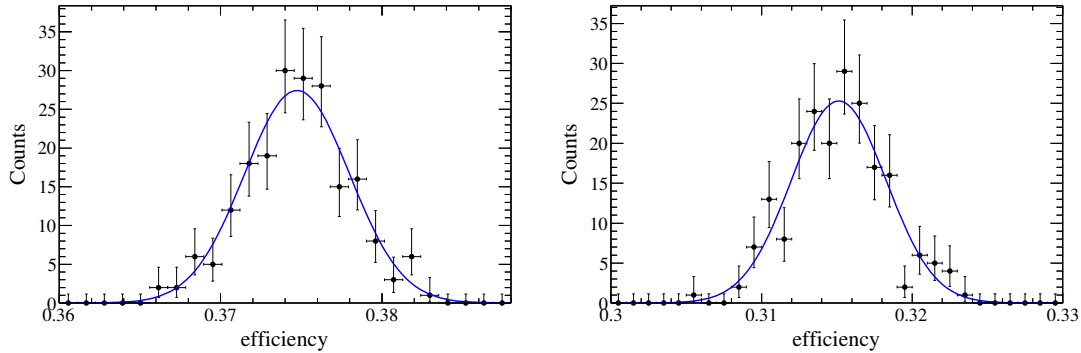


Fig. 27: The distribution of selection efficiency for $J/\psi \rightarrow \Sigma^+ \bar{\Sigma}^-$, $\Sigma^+ \rightarrow p\pi^0$, $\bar{\Sigma}^- \rightarrow \bar{p}\pi^0$ (Left). The distribution of selection efficiency for $\psi(3686) \rightarrow \Sigma^+ \bar{\Sigma}^-$, $\Sigma^+ \rightarrow p\pi^0$, $\bar{\Sigma}^- \rightarrow \bar{p}\pi^0$ (Right).

517 **9.2.3 Fitting function**

518 To estimate the uncertainties of fitting function, we use the double Gaussian function to describe the
 519 signal instead of signal shape in the Figure 28. To compare the branching fractions with the nominal
 520 values, the differences are taken as the systematic uncertainties, 0.7% for $J/\psi \rightarrow \Sigma^+ \bar{\Sigma}^-$ and 0.2% for
 521 $\psi(3686) \rightarrow \Sigma^+ \bar{\Sigma}^-$.

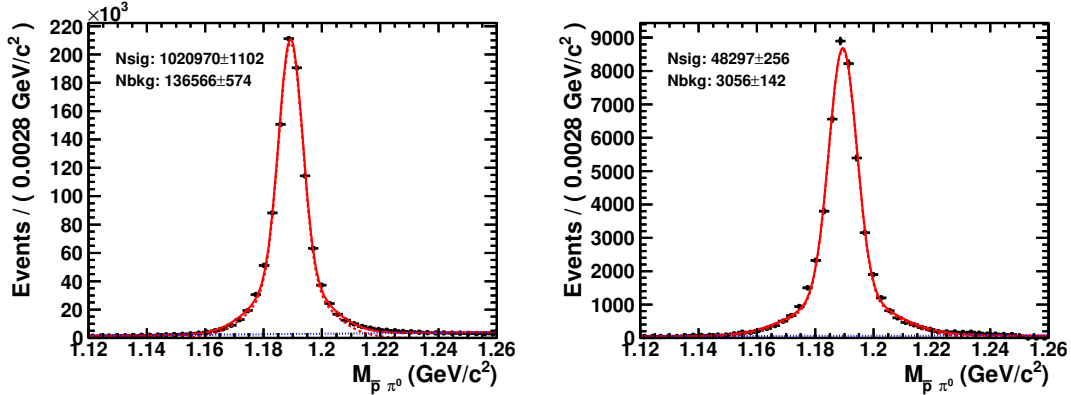


Fig. 28: The fitting result of $p\pi^0$ invariant mass for $J/\psi \rightarrow \Sigma^+\bar{\Sigma}^-$, $\Sigma^+ \rightarrow p\pi^0$, $\bar{\Sigma}^- \rightarrow \bar{p}\pi^0$ (Left). The fitting result of $p\pi^0$ invariant mass for $\psi(3686) \rightarrow \Sigma^+\bar{\Sigma}^-$, $\Sigma^+ \rightarrow p\pi^0$, $\bar{\Sigma}^- \rightarrow \bar{p}\pi^0$ (Right).

522 9.2.4 Background estimation

523 To estimate the uncertainties of background events, we changed the order of polynomial functions
 524 for background descriptions. The differences are taken as the systematic uncertainties comparing the
 525 nominal values, 1.3% for $J/\psi \rightarrow \Sigma^+\bar{\Sigma}^-$ and 1.0% for $\psi(3686) \rightarrow \Sigma^+\bar{\Sigma}^-$.

526 9.2.5 Kinematic fitting

527 The χ^2_{2C} distribution is consistent between MC and data, whether we use the track correction for the
 528 helix parameters or not, as shown Figure 29. Then we could use the difference between before correction
 529 and after correction as the systematic uncertainties, and take the value with correction as the nominal
 530 one. The differences are taken as the systematic uncertainties, 0.1% for $J/\psi \rightarrow \Sigma^+\bar{\Sigma}^-$ and 0.1% for
 531 $\psi(3686) \rightarrow \Sigma^+\bar{\Sigma}^-$.

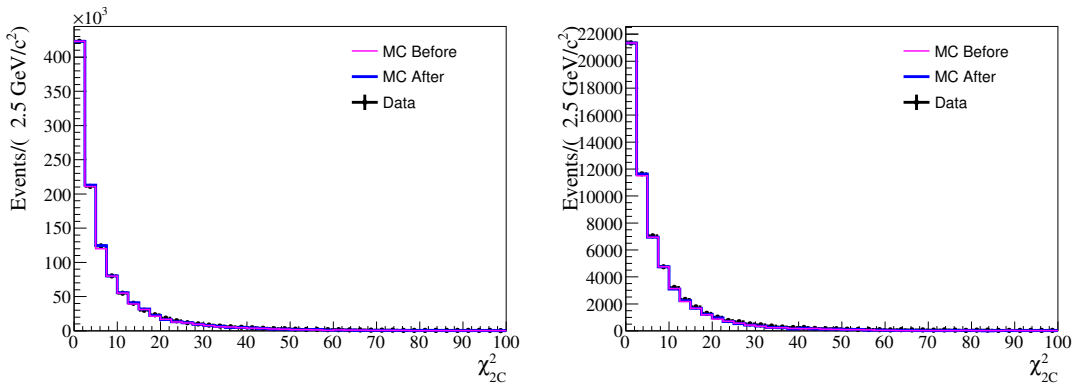


Fig. 29: The χ^2_{2C} distribution for $J/\psi \rightarrow \Sigma^+\bar{\Sigma}^-$, $\Sigma^+ \rightarrow p\pi^0$, $\bar{\Sigma}^- \rightarrow \bar{p}\pi^0$ (Left) and $\psi(3686) \rightarrow \Sigma^+\bar{\Sigma}^-$, $\Sigma^+ \rightarrow p\pi^0$, $\bar{\Sigma}^- \rightarrow \bar{p}\pi^0$ (Right).

532 **9.2.6 Branching fraction of $\Sigma^+ \rightarrow p\pi^0$**

533 Based on the PDG table, the branching fraction of $\Sigma^+ \rightarrow p\pi^0$ is $(51.57 \pm 0.30)\%$. We take 0.6% as
 534 the systematic uncertainty of intermediate state branching fraction.

535 **9.2.7 Impact of the interference between the $\psi(3686)$ and continuum contribution**

The impact of the interference between the $\psi(3686)$ and continuum has been considered by referring to this article [78]). The ratio of cross section from the interference term with respect to the resonance and continuum is defined as:

$$r_R^f = \frac{\sigma_{int}^f(s)}{\sigma_R^f(s)} = \frac{2}{\hbar c} \sqrt{\frac{\sigma_c^f(s)}{B_f}} \frac{M}{\sqrt{12\pi B_{ee}}} \sin \phi$$

536 (Formula.5 in this article [78]), where $\sigma_c^f(s) \approx 1 \times 10^{-3}$ nb [79], $B_f = 2.57 \times 10^{-4}$, $M = 3.686$ GeV,
 537 and the magnitudes of the ratios reach maxima when the relative phase $\phi = 90^\circ$. Therefore, the value
 538 $r_R^{(f,max)} = 4.3\%$, is taken as systematic uncertainty from impact of interference.

539 **9.2.8 Total number of J/ψ and $\psi(3686)$**

540 The total number of J/ψ mesons are based on inclusive hadronic events, as described in [64, 65].
 541 The uncertainties of the total number are determined to be 0.39% for J/ψ events and 0.53% for $\psi(3686)$
 542 events.

543 **9.2.9 Summary of branching fraction uncertainties**

544 The branching fraction of $J/\psi \rightarrow \Sigma^+ \bar{\Sigma}^-$ and $\psi(3686) \rightarrow \Sigma^+ \bar{\Sigma}^-$ are determined by fitting invariant
 545 mass $\bar{p}\pi^0$. The uncertainties of the branching fraction measurement include the uncertainties of MC effi-
 546 ciency correction, uncertainties of decay parameters, fitting function, background estimation, kinematic
 547 fitting, branching fraction of $\Sigma^+ \rightarrow p\pi^0$, interference between the $\psi(3686)$ and continuum, and total
 548 number of J/ψ and $\psi(3686)$ events, which are listed in the Table 14.

Tab. 14: Summary of branching fraction uncertainties (%)

Source	$J/\psi \rightarrow \Sigma^+ \bar{\Sigma}^-$	$\psi(3686) \rightarrow \Sigma^+ \bar{\Sigma}^-$
MC efficiency correction (p , \bar{p} , and π^0)	0.5	0.5
Decay parameters	0.3	0.3
Fitting function	0.7	0.2
Background estimation	1.3	1.0
Kinematic fitting	0.1	0.1
Branching fraction	0.6	0.6
Continuum contribution	–	4.3
Total number	0.4	0.5
Total	1.8	4.6

549 10 Summary

550 In summary, based on the $(10087 \pm 44) \times 10^6 J/\psi$ and $(2712.4 \pm 14.3) \times 10^6 \psi(3686)$ events collected at
 551 BESIII detector, the branching fractions and decay parameters of $J/\psi \rightarrow \Sigma^+ \bar{\Sigma}^-$ ($\Sigma^+ \rightarrow p\pi^0$, $\bar{\Sigma}^- \rightarrow \bar{p}\pi^0$)
 552 and $\psi(3686) \rightarrow \Sigma^+ \bar{\Sigma}^-$ ($\Sigma^+ \rightarrow p\pi^0$, $\bar{\Sigma}^- \rightarrow \bar{p}\pi^0$) are measured which are listed in Table 15 and Table 16.

553 And by comparison the branching fractions of $J/\psi \rightarrow \Sigma^+ \bar{\Sigma}^-$ and $\psi(3686) \rightarrow \Sigma^+ \bar{\Sigma}^-$, the Q value of
 554 "12%" is tested to be $Q = \frac{P_{J/\psi}}{P_{\psi(3686)}} \times \frac{Br(\psi(3686) \rightarrow \Sigma^+ \bar{\Sigma}^-)}{Br(J/\psi \rightarrow \Sigma^+ \bar{\Sigma}^-)} = \frac{1}{1.4194} \times \frac{2.57 \pm 0.12}{10.94 \pm 0.19} = 16.6\% \pm 0.7\%$, (The $\frac{P_{J/\psi}}{P_{\psi(3686)}}$ is
 555 correction factor of the phase space, where $P_{J/\psi}$ or $P_{\psi(3686)}$ is the Σ^+ momentum in the J/ψ or $\psi(3686)$
 556 decay process). The polarization is well consistent with previous measurement, and the $\alpha_{(\Sigma^+ \rightarrow p\pi^0)}$ and
 557 $\alpha_{(\bar{\Sigma}^- \rightarrow \bar{p}\pi^0)}$ values are improved by a factor of four compared to the previous results. The branching
 558 fractions of $J/\psi \rightarrow \Sigma^+ \bar{\Sigma}^- = (10.94 \pm 0.02 \pm 0.19) \times 10^{-4}$ and $\psi(3686) \rightarrow \Sigma^+ \bar{\Sigma}^- = (2.57 \pm 0.01 \pm 0.12) \times 10^{-4}$
 559 are measured independently. We considered systematic and statistical uncertainties, the CP asymmetry
 560 $A_{CP} = -0.0118 \pm 0.0083 \pm 0.0028$ is extracted with the highest accuracy.

Tab. 15: The decay parameters of $J/\psi \rightarrow \Sigma^+ \bar{\Sigma}^-$ ($\Sigma^+ \rightarrow p\pi^0$, $\bar{\Sigma}^- \rightarrow \bar{p}\pi^0$) and $\psi(3686) \rightarrow \Sigma^+ \bar{\Sigma}^-$ ($\Sigma^+ \rightarrow p\pi^0$, $\bar{\Sigma}^- \rightarrow \bar{p}\pi^0$)

Decay parameters	Our measurements	Previous measurements	Difference
$\alpha_{J/\psi}$	$-0.5047 \pm 0.0018 \pm 0.0010$	$-0.508 \pm 0.006 \pm 0.004$ [12]	$<1\sigma$
$\Delta\Phi_{J/\psi}$	$-0.2744 \pm 0.0033 \pm 0.0010$	$-0.270 \pm 0.012 \pm 0.009$ [12]	$<1\sigma$
$\alpha_{(\Sigma^+ \rightarrow p\pi^0)}$	$-0.975 \pm 0.011 \pm 0.002$	$-0.998 \pm 0.037 \pm 0.009$ [12]	$<1\sigma$
$\alpha_{(\bar{\Sigma}^- \rightarrow \bar{p}\pi^0)}$	$0.999 \pm 0.011 \pm 0.004$	$0.990 \pm 0.037 \pm 0.011$ [12]	$<1\sigma$
A_{CP}	$-0.0118 \pm 0.0083 \pm 0.0028$	$-0.004 \pm 0.037 \pm 0.010$ [12]	$<1\sigma$
$\alpha_{\psi(3686)}$	$0.7133 \pm 0.0094 \pm 0.0065$	$0.682 \pm 0.030 \pm 0.011$ [12]	$<1\sigma$
$\Delta\Phi_{\psi(3686)}$	$0.427 \pm 0.022 \pm 0.003$	$0.379 \pm 0.070 \pm 0.014$ [12]	$<1\sigma$

Tab. 16: The branching ratios of $J/\psi \rightarrow \Sigma^+ \bar{\Sigma}^-$ and $\psi(3686) \rightarrow \Sigma^+ \bar{\Sigma}^-$

Memo	$Br(J/\psi \rightarrow \Sigma^+ \bar{\Sigma}^-) \times 10^{-4}$	$Br(\psi(3686) \rightarrow \Sigma^+ \bar{\Sigma}^-) \times 10^{-4}$
Our measurement	$10.94 \pm 0.02 \pm 0.19$	$2.57 \pm 0.01 \pm 0.12$
PDG	10.7 ± 0.4	2.43 ± 0.1
Memo (BAM-00272)	$10.61 \pm 0.04 \pm 0.38$	$2.52 \pm 0.04 \pm 0.10$
Memo (BAM-00559)	10.78 ± 0.01 or 10.62 ± 0.01	–
Memo (BAM-00552)	$10.85 \pm 0.01 \pm 0.31$	–

561 11 Some comparisons and checks**562 11.1 The definition of moments**

563 The formulas of $n1_x$, $n1_y$, $n1_z$, $n2_x$, $n2_y$, and $n2_z$ are defined as below:

$$\begin{aligned} n1_x &= \sin \theta_p \cos \phi_p, \\ n1_y &= \sin \theta_p \sin \phi_p, \\ n1_z &= \cos \theta_p, \\ n2_x &= \sin \theta_{\bar{p}} \cos \phi_{\bar{p}}, \\ n2_y &= \sin \theta_{\bar{p}} \sin \phi_{\bar{p}}, \\ n1_z &= \cos \theta_{\bar{p}}, \end{aligned} \tag{9}$$

564 where $\theta_p, \phi_p, \theta_{\bar{p}}, \phi_{\bar{p}}$ are the polar and azimuthal angles of proton and anti-proton.

565 Therefore, the formulas of $n1_x$, $n1_y$, $n1_z$, $n2_x$, $n2_y$, and $n2_z$ can be determined as below:

$$\begin{aligned}
 T_1(\theta_{\Sigma^+}) &= \sum_i^{N(m)} n1_x, \\
 T_2(\theta_{\Sigma^+}) &= \sum_i^{N(m)} n1_y, \\
 T_3(\theta_{\Sigma^+}) &= \sum_i^{N(m)} n1_z, \\
 T_4(\theta_{\Sigma^+}) &= \sum_i^{N(m)} n2_x, \\
 T_5(\theta_{\Sigma^+}) &= \sum_i^{N(m)} n2_y, \\
 T_6(\theta_{\Sigma^+}) &= \sum_i^{N(m)} n2_z, \\
 T_7(\theta_{\Sigma^+}) &= \sum_i^{N(m)} n1_x \times n2_x, \\
 T_8(\theta_{\Sigma^+}) &= \sum_i^{N(m)} n1_x \times n2_y, \\
 T_9(\theta_{\Sigma^+}) &= \sum_i^{N(m)} n1_x \times n2_z, \\
 T_{10}(\theta_{\Sigma^+}) &= \sum_i^{N(m)} n1_y \times n2_x, \\
 T_{11}(\theta_{\Sigma^+}) &= \sum_i^{N(m)} n1_y \times n2_y, \\
 T_{12}(\theta_{\Sigma^+}) &= \sum_i^{N(m)} n1_y \times n2_z, \\
 T_{13}(\theta_{\Sigma^+}) &= \sum_i^{N(m)} n1_z \times n2_x, \\
 T_{14}(\theta_{\Sigma^+}) &= \sum_i^{N(m)} n1_z \times n2_y, \\
 T_{15}(\theta_{\Sigma^+}) &= \sum_i^{N(m)} n1_z \times n2_z,
 \end{aligned} \tag{10}$$

566 where, $N(m)$ is the number of events in the i_{th} $\cos\theta_{\Sigma^+}$ bin.

567 **11.2 comparison of the different moments related to θ_{Σ^+} for $J/\psi \rightarrow \Sigma^+\bar{\Sigma}^-$ decay channel**

568 The distributions of the different moments are shown in the Fig. 30 for J/ψ samples in 2009 and 2012
 569 years.

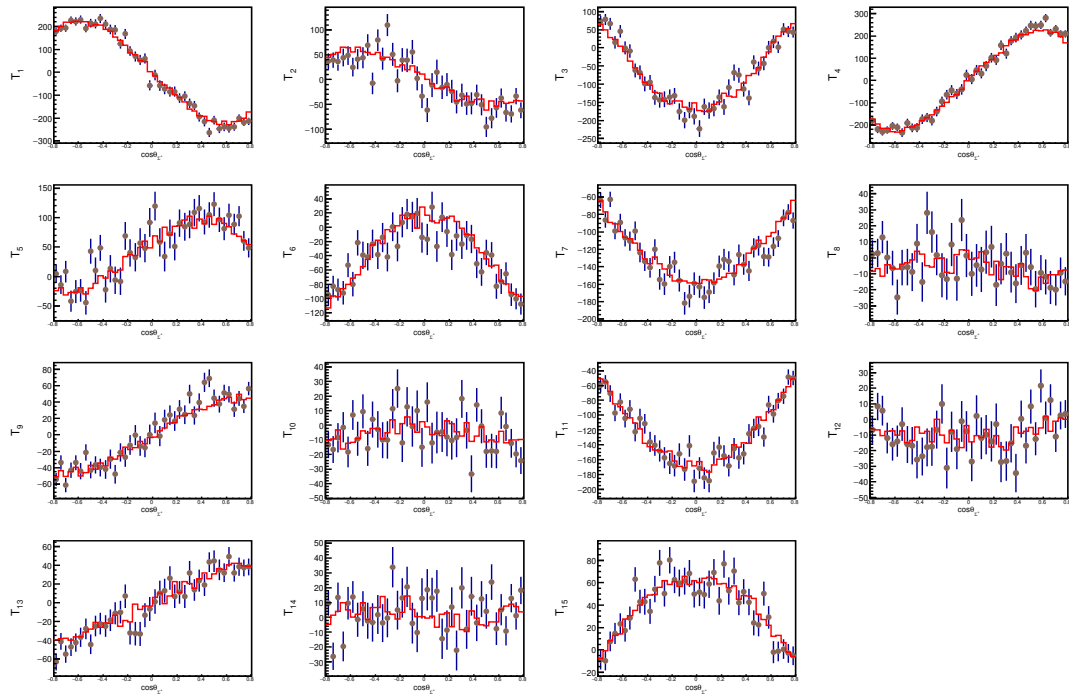


Fig. 30: The fitting results of different moments for $J/\psi \rightarrow \Sigma^+\bar{\Sigma}^-$ in 2009 and 2012 years.

570 The distributions of the different moments are shown in the Fig. 31 for J/ψ samples in 2017 year.

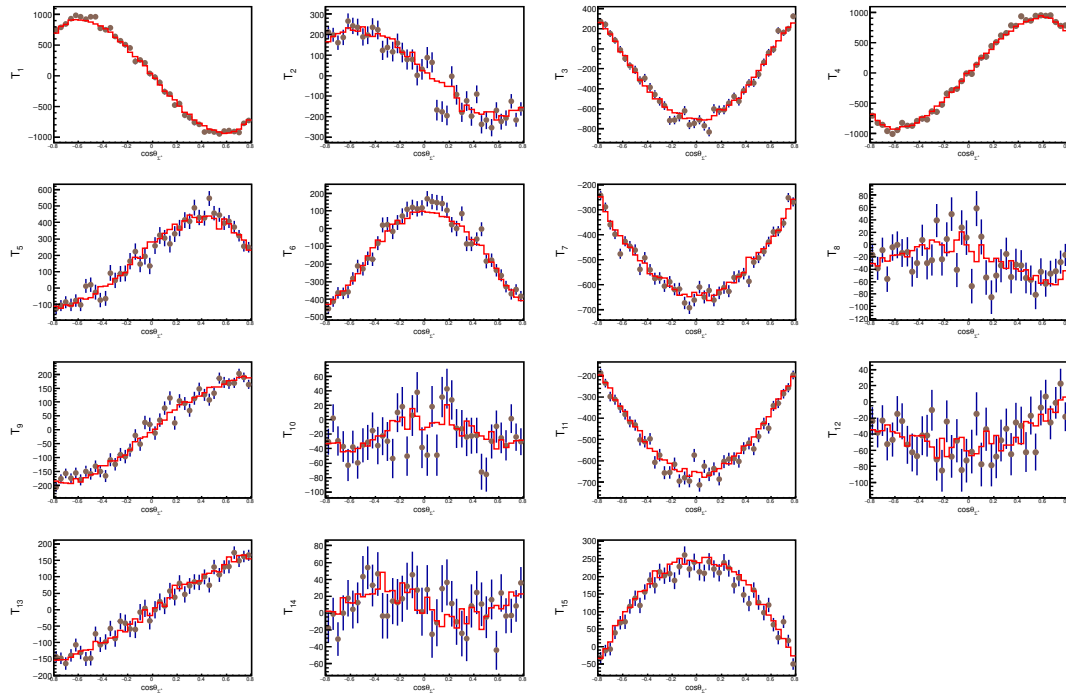


Fig. 31: The fitting results of different moments for $J/\psi \rightarrow \Sigma^+ \bar{\Sigma}^-$ in 2017 year.

571

The distributions of the different moments are shown in the Fig. 32 for J/ψ samples in 2018 year.

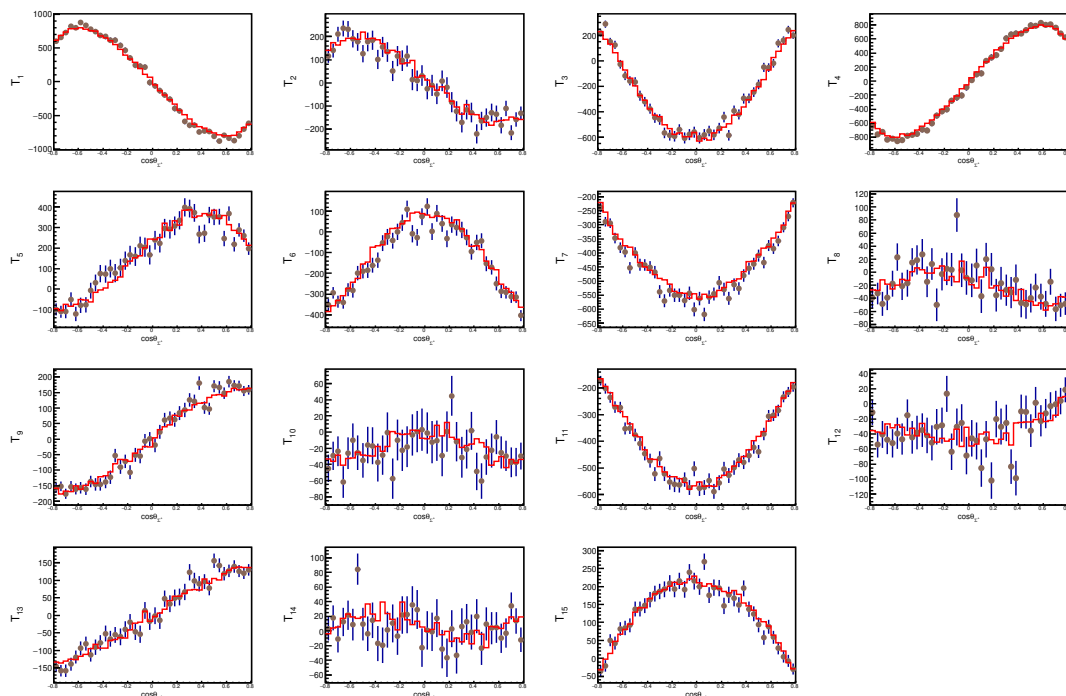


Fig. 32: The fitting results of different moments for $J/\psi \rightarrow \Sigma^+ \bar{\Sigma}^-$ in 2018 year.

572 **11.3 comparison of the different moments related to θ_{Σ^+} for $\psi(3686) \rightarrow \Sigma^+ \bar{\Sigma}^-$ decay chan-**
 573 **nel**

574 The distributions of the different moments are shown in the Fig. 33 for $\psi(3686)$ samples in 2009 and
 575 2012 years.

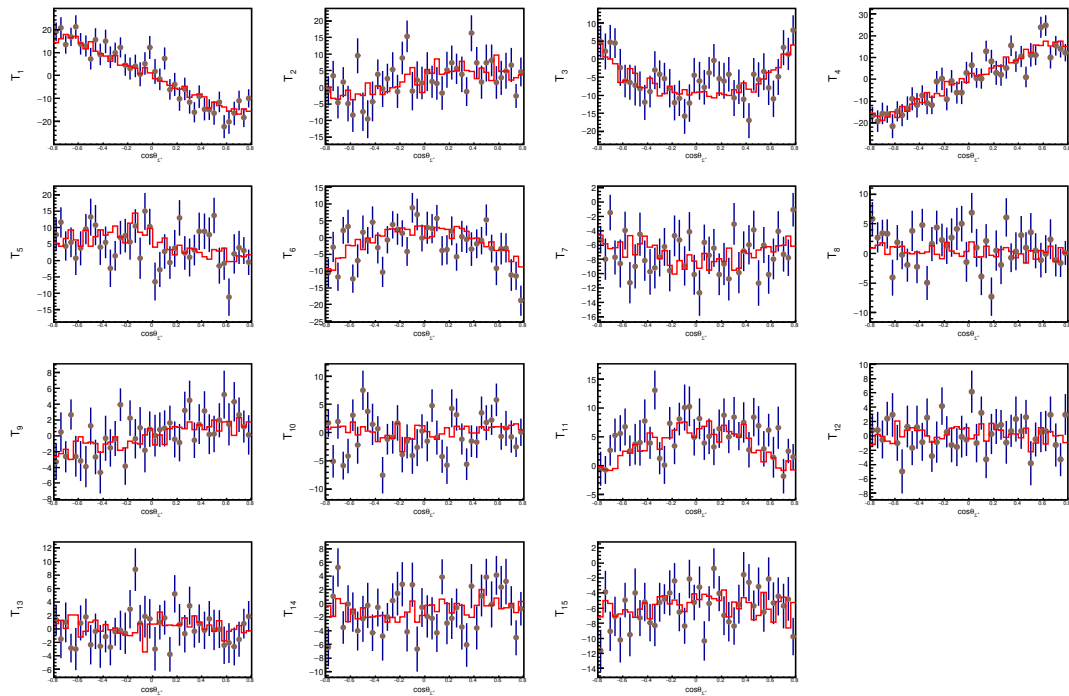
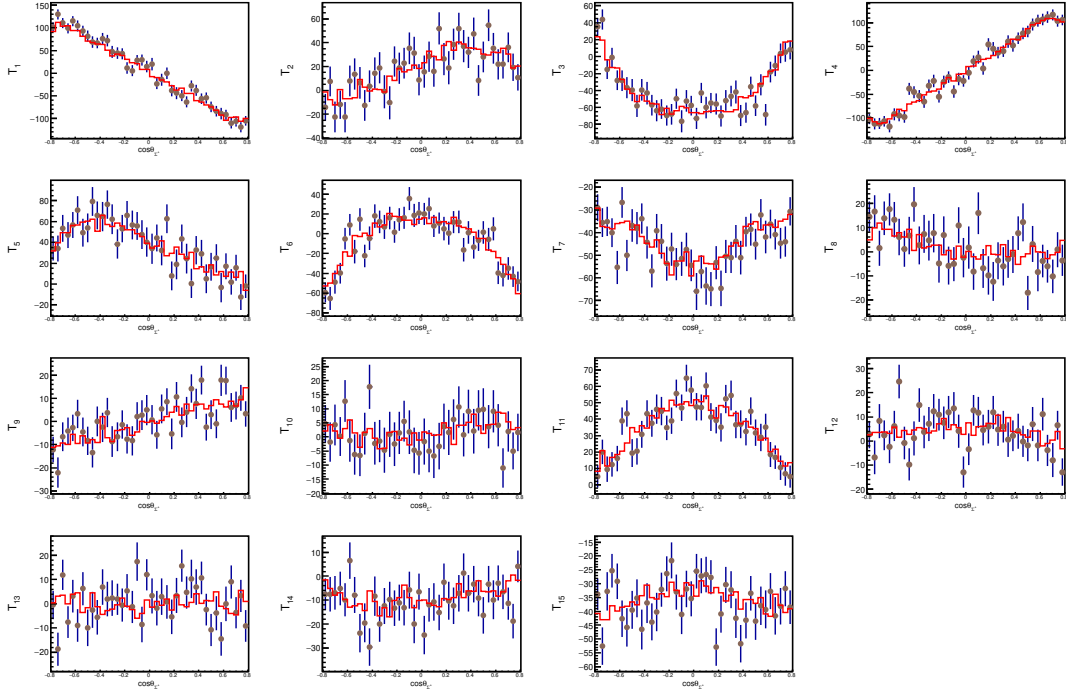


Fig. 33: The fitting results of different moments for $J/\psi \rightarrow \Sigma^+ \bar{\Sigma}^-$ in 2009 and 2012 years.

576 The distributions of the different moments are shown in the Fig. 34 for $\psi(3686)$ samples in 2021 year.

Fig. 34: The fitting results of different moments for $\psi(3686) \rightarrow \Sigma^+ \bar{\Sigma}^-$ in 2021 year.

Tab. 17: The comparison between our measurements with all data sets and the published results with old data sets

Decay parameters	Our measurements(all data sets)	Previous measurements(old data sets)	Difference
$\alpha_{J/\psi}$	$-0.5042 \pm 0.0018 \pm 0.0012$	$-0.508 \pm 0.006 \pm 0.004$ [12]	$<1\sigma$
$\Delta\Phi_{J/\psi}$	$-0.2743 \pm 0.0033 \pm 0.0011$	$-0.270 \pm 0.012 \pm 0.009$ [12]	$<1\sigma$
$\alpha_{(\Sigma^+ \rightarrow p\pi^0)}$	$-0.9753 \pm 0.0106 \pm 0.0018$	$-0.998 \pm 0.037 \pm 0.009$ [12]	$<1\sigma$
$\alpha_{(\bar{\Sigma}^- \rightarrow \bar{p}\pi^0)}$	$0.9986 \pm 0.0108 \pm 0.0040$	$0.990 \pm 0.037 \pm 0.011$ [12]	$<1\sigma$
$\alpha_{\psi(3686)}$	$0.7133 \pm 0.0094 \pm 0.0066$	$0.682 \pm 0.030 \pm 0.011$ [12]	$<1\sigma$
$\Delta\Phi_{\psi(3686)}$	$0.4267 \pm 0.0217 \pm 0.0038$	$0.379 \pm 0.070 \pm 0.014$ [12]	$<1\sigma$

Tab. 18: The comparison between our measurements with old data sets and the published results with old data sets

Decay parameters	Our measurements(old data sets)	Previous measurements(old data sets)	Difference
$\alpha_{J/\psi}$	-0.5140 ± 0.0047	$-0.508 \pm 0.006 \pm 0.004$ [12]	$<1\sigma$
$\Delta\Phi_{J/\psi}$	-0.2753 ± 0.0089	$-0.270 \pm 0.012 \pm 0.009$ [12]	$<1\sigma$
$\alpha_{(\Sigma^+ \rightarrow p\pi^0)}$	-0.9683 ± 0.0285	$-0.998 \pm 0.037 \pm 0.009$ [12]	$<1\sigma$
$\alpha_{(\bar{\Sigma}^- \rightarrow \bar{p}\pi^0)}$	1.0292 ± 0.0303	$0.990 \pm 0.037 \pm 0.011$ [12]	$<1\sigma$
$\alpha_{\psi(3686)}$	0.7064 ± 0.0227	$0.682 \pm 0.030 \pm 0.011$ [12]	$<1\sigma$
$\Delta\Phi_{\psi(3686)}$	0.3921 ± 0.0525	$0.379 \pm 0.070 \pm 0.014$ [12]	$<1\sigma$

Tab. 19: The comparison between our measurements with old data sets and new data sets

Decay parameters	Our measurements(old data sets)	Our measurements(new data sets)	Difference
$\alpha_{J/\psi}$	-0.5140 ± 0.0047	-0.5022 ± 0.0019	$<2.3\sigma$
$\Delta\Phi_{J/\psi}$	-0.2753 ± 0.0089	-0.2742 ± 0.0035	$<1\sigma$
$\alpha_{(\Sigma^+ \rightarrow p\pi^0)}$	-0.9683 ± 0.0285	-0.9769 ± 0.0114	$<1\sigma$
$\alpha_{(\bar{\Sigma}^- \rightarrow \bar{p}\pi^0)}$	1.0292 ± 0.0303	0.9964 ± 0.0116	$<1\sigma$
$\alpha_{\psi(3686)}$	0.7064 ± 0.0227	0.7129 ± 0.0102	$<1\sigma$
$\Delta\Phi_{\psi(3686)}$	0.3921 ± 0.0525	0.4322 ± 0.0238	$<1\sigma$

Tab. 20: The comparison between our measurements with all J/ψ data sets and all $\psi(3686)$ data sets

Decay parameters	Our measurements(all J/ψ data sets)	Our measurements(all $\psi(3686)$ data sets)	Difference
$\alpha_{J/\psi}$	-0.5042 ± 0.0018	–	–
$\Delta\Phi_{J/\psi}$	-0.2744 ± 0.0033	–	–
$\alpha_{(\Sigma^+ \rightarrow p\pi^0)}$	-0.9718 ± 0.0107	-1.1013 ± 0.0698	$<1.8\sigma$
$\alpha_{(\bar{\Sigma}^- \rightarrow \bar{p}\pi^0)}$	1.0016 ± 0.0110	0.8985 ± 0.0571	$<1.8\sigma$
$\alpha_{\psi(3686)}$	–	0.6917 ± 0.0107	–
$\Delta\Phi_{\psi(3686)}$	–	0.4007 ± 0.0212	–

577 References

- 578 [1] Z. T. Liang and X. N. Wang, Phys. Rev. Lett. **94**, 102301 (2005) [erratum: Phys. Rev. Lett. **96**,
579 039901 (2006)] doi:10.1103/PhysRevLett.94.102301 [arXiv:nucl-th/0410079 [nucl-th]].
- 580 [2] P. J. Mulders and R. D. Tangerman, Nucl. Phys. B **461**, 197-237 (1996).
- 581 [3] M. Anselmino, D. Boer, U. D'Alesio and F. Murgia, Phys. Rev. D **63**, 054029 (2001).
- 582 [4] H. Li, X. Wang, Y. Yang and Z. Lu, Eur. Phys. J. C **81**, no.4, 289 (2021).
- 583 [5] L. Gamberg, Z. B. Kang, D. Y. Shao, J. Terry and F. Zhao, Phys. Lett. B **818**, 136371 (2021).
- 584 [6] T. D. Lee, J. Steinberger, G. Feinberg, P. K. Kabir and C. N. Yang, Phys. Rev. **106**, 1367 (1957).
- 585 [7] S. Okubo, Phys. Rev. **109**, 984 (1958).
- 586 [8] A. Pais, Phys. Rev. Lett. **3**, 242 (1959).
- 587 [9] D. G. Ireland, M. Döring, D. I. Glazier, J. Haidenbauer, M. Mai, R. Murray-Smith and D. Rönchen,
588 Phys. Rev. Lett. **123**, no.18, 182301 (2019).
- 589 [10] M. Ablikim *et al.* (BESIII Collaboration), Nature **606**, no.7912, 64-69 (2022).
- 590 [11] M. Ablikim *et al.* (BESIII Collaboration), [arXiv:2206.10900 [hep-ex]].
- 591 [12] M. Ablikim *et al.* (BESIII Collaboration), Phys. Rev. Lett. **125**, no.5, 052004 (2020).
- 592 [13] M. Ablikim *et al.* (BESIII Collaboration), Nature Phys. **15**, 631-634 (2019).
- 593 [14] M. Ablikim *et al.* (BESIII Collaboration), [arXiv:2204.11058 [hep-ex]].
- 594 [15] E. Klempert, F. Bradamante, A. Martin and J. M. Richard, Phys. Rept. **368**, 119-316 (2002).
- 595 [16] G. Aad *et al.* (ATLAS Collaboration), Phys. Rev. D **91**, no.3, 032004 (2015).
- 596 [17] C. A. Paterson *et al.* (CLAS Collaboration), Phys. Rev. C **93**, no.6, 065201 (2016).
- 597 [18] L. Adamczyk *et al.* (STAR Collaboration), Nature **548**, 62-65 (2017).
- 598 [19] L. C. Lu *et al.* (HyperCP Collaboration), Phys. Lett. B **617**, 11-17 (2005).
- 599 [20] J. Adam *et al.* (STAR Collaboration), Phys. Rev. Lett. **126**, no.16, 162301 (2021).
- 600 [21] S. Acharya *et al.* (ALICE Collaboration), Phys. Rev. C **101**, no.4, 044611 (2020).

- 601 [22] Y. Guan *et al.* (Belle Collaboration), [Phys. Rev. Lett. **122**, no.4, 042001 \(2019\)](#).
- 602 [23] J. W. Cronin and O. E. Overseth, [Phys. Rev. **129**, 1795-1807 \(1963\)](#).
- 603 [24] M. Ablikim *et al.* (BESIII Collaboration), [Phys. Rev. Lett. **123**, no.12, 122003 \(2019\)](#).
- 604 [25] A. D. Sakharov, [Pisma Zh. Eksp. Teor. Fiz. **5**, 32 \(1967\)](#).
- 605 [26] M. E. Peskin, [Nature **419**, 24 \(2002\)](#).
- 606 [27] J. H. Christenson, J. W. Cronin, V. L. Fitch and R. Turlay, [Phys. Rev. Lett. **13**, 138 \(1964\)](#).
- 607 [28] A. Abashian *et al.* (Belle Collaboration), [Phys. Rev. Lett. **86**, 2509 \(2001\)](#).
- 608 [29] B. Aubert *et al.* (BaBar Collaboration), [Phys. Rev. Lett. **86**, 2515 \(2001\)](#).
- 609 [30] Y. Chao *et al.* (Belle Collaboration), [Phys. Rev. Lett. **93**, 191802 \(2004\)](#).
- 610 [31] B. Aubert *et al.* (BaBar Collaboration), [Phys. Rev. Lett. **93**, 131801 \(2004\)](#).
- 611 [32] R. Aaij *et al.* (LHCb Collaboration), [Phys. Rev. Lett. **122**, 211803 \(2019\)](#).
- 612 [33] J. H. Christenson et al., Phys. Rev. Lett. 13, 138 (1964); KTeV Collaboration, A. Alavi-Harati et
613 al., *ibid.* 83, 22 (1999); NA48 Collaboration, V. Fanti et al., Phys. Lett. B 465, 335 (1999); BABAR
614 Collaboration, B. Aubert et al., Phys. Rev. Lett. 87, 091801(2001); Belle Collaboration, K. Abe et
615 al., *ibid.* 87, 091802(2001)
- 616 [34] R. Handler, R. Grobel, L. Pondrom, M. Sheaff, C. Wilkinson, P. T. Cox, J. Dworkin, O. E. Overseth,
617 K. J. Heller and T. Devlin, *et al.* Phys. Rev. D **25** (1982), 639-651 doi:10.1103/PhysRevD.25.639
- 618 [35] T. Holmstrom *et al.* [HyperCP], Phys. Rev. Lett. **93** (2004), 262001
619 doi:10.1103/PhysRevLett.93.262001 [arXiv:hep-ex/0412038 [hep-ex]].
- 620 [36] P. Astbury, J. Gallivan, J. Jafar, M. Letheren, V. Steiner, J. A. Wilson, W. Beusch, M. Borghini,
621 D. Websdale and L. Fluri, *et al.* Nucl. Phys. B **99** (1975), 30-52 doi:10.1016/0550-3213(75)90054-
622 1
- 623 [37] P.A. Zyla *et al.* (Particle Data Group), [PTEP **2022**, 083C01 \(2022\)](#).
- 624 [38] G. Falldt (GF), Eur. Ph. J. A 52 141(2016); GF, A. Kupsc (AK), Phys. Lett. B 772 16(2017); GF,
625 Phys. Rev. D 97 053002 (2018); GF, AK, S. Leupold, E. Perotti, arXiv:1809.04038 (2018).

- 626 [39] M. Ablikim *et al.* (BESIII Collaboration), Phys. Rev. Lett. **123** (2019) no.12, 122003
627 doi:10.1103/PhysRevLett.123.122003 [arXiv:1903.09421 [hep-ex]].
- 628 [40] M. Ablikim et al. (BESIII Collaboration), Phys. Rev. D 81 (2010) 012003.
- 629 [41] S. J. Brodsky and G. P. Lepage, Phys. Rev. D 24, 2848 (1981).
- 630 [42] M. Claudson, S. L. Glashow and M. B. Wise, Phys. Rev. D 25, 1345 (1982). C. Carimalo, Int. J.
631 Mod. Phys. A2, 249 (1987).
- 632 [43] C. Carimalo, Int. J. Mod. Phys. A2, 249 (1987).
- 633 [44] T. Appelquist and H. Politzer, Phys. Rev. Lett. 34, 43 (1975).
- 634 [45] A. DeRujula and S. Glashow, Phys. Rev. Lett. 34, 46 (1975).
- 635 [46] M. E. B. Franklin et al. (MARKII Collaboration), Phys. Rev. Lett. 51, 963 (1983).
- 636 [47] M. Ablikim et al. (BESIII Collaboration), Phys. Lett. B 614 37 (2005).
- 637 [48] R. A. Briere *et al.* (CLEO Collaboration), Phys. Rev. Lett. **95**, 062001 (2005)
638 doi:10.1103/PhysRevLett.95.062001 [arXiv:hep-ex/0505101 [hep-ex]].
- 639 [49] N. Brambilla et al. (Quarkonium Working Group), Eur. Phys. J. C 71 1534 (2011).
- 640 [50] Q. Wang, G. Li and Q. Zhao, Phys. Rev. D 85, 074015 (2012).
- 641 [51] X. H. Mo, C. Z. Yuan and P. Wang, Chin. Phys. C **31**, 686 (2007).
- 642 [52] G. Li, Q. Zhao and C. H. Chang, J. Phys. G **35**, 055002 (2008).
- 643 [53] S. J. Brodsky and M. Karliner, Phys. Rev. Lett. **78**, 4682 (1997).
- 644 [54] G. Karl and W. Roberts, Phys. Lett. B **144**, 263 (1984).
- 645 [55] M. Chaichian and N. A. Tornqvist, Nucl. Phys. B **323**, 75 (1989).
- 646 [56] K. Y. Liu and K. T. Chao, Phys. Rev. D **70**, 094001 (2004).
- 647 [57] J. L. Rosner, Phys. Rev. D **64**, 094002 (2001).
- 648 [58] X. Q. Li, D. V. Bugg and B. S. Zou, Phys. Rev. D **55**, 1421 (1997).
- 649 [59] K. F. Liu and C. W. Wong, Phys. Rev. D 28, 170 (1983).

- 650 [60] M. Ablikim et al. (BESIII Collaboration), Nucl. Instrum. Meth. A 614, 345 (2010).
- 651 [61] C. H. Yu et al., Proceedings of IPAC2016, Busan, Korea, 2016, doi:10.18429/JACoW- IPAC2016-
652 TUYA01.
- 653 [62] M. Ablikim et al. (BESIII Collaboration), Chin. Phys. C 44, 040001 (2020).
- 654 [63] X. Li et al., Radiat. Detect. Technol. Methods 1, 13 (2017); Y. X. Guo et al., Radiat. Detect. Technol.
655 Methods 1, 15 (2017); P. Cao et al., Nucl. Instrum. Meth. A 953, 163053 (2020).
- 656 [64] M. Ablikim et al. (BESIII Collaboration), [arXiv:2111.07571 [hep-ex]].
- 657 [65] https://indico.ihep.ac.cn/event/16632/contributions/49274/attachments/23536/26672/number_of_psi2S.pdf
- 658 [66] S. Agostinelli et al. (geant4 Collaboration), Nucl. Instrum. Meth. A 506, 250 (2003).
- 659 [67] S. Jadach, B. F. L. Ward and Z. Was, Comp. Phys. Commu. 130, 260 (2000); Phys. Rev. D 63,
660 113009 (2001).
- 661 [68] D. J. Lange, Nucl. Instrum. Meth. A 462, 152 (2001); R. G. Ping, Chin. Phys. C 32, 599 (2008).
- 662 [69] J. C. Chen et al., Phys. Rev. D 62, 034003 (2000).
- 663 [70] <https://hnbes3.ihep.ac.cn/HyperNews/get/AUX/2020/12/24>(BAM-00476)
- 664 [71] <https://docbes3.ihep.ac.cn/DocDB/0002/000250/026/Asymmetry%20Parameters%20Measurement.pdf>
- 665 [72] M. Ablikim et al. (BESIII Collaboration), Phys. Rev. D **101**, no.9,092002(2020)
666 doi:10.1103/PhysRevD.101.092002 [arXiv:2004.01394 [hep-ex]].
- 667 [73] https://docbes3.ihep.ac.cn/DocDB/0005/000574/031/Sigma_memo_v6.0.pdf
- 668 [74] <https://hnbes3.ihep.ac.cn/HyperNews/get/paper504.html>
- 669 [75] <https://indico.ihep.ac.cn/event/10989/session/19/contribution/141/material/slides/0.pdf>
- 670 [76] <https://indico.ihep.ac.cn/event/11850/contribution/0/material/slides/0.pdf>
- 671 [77] M. Ablikim et al. (BESII Collaboration), Phys. Rev. D **78** (2008), 092005
672 doi:10.1103/PhysRevD.78.092005 [arXiv:0810.1896 [hep-ex]].
- 673 [78] Y. P. Guo and C. Z. Yuan, “Impact of the interference between the resonance and continuum am-
674 plitudes on vector quarkonia decay branching fraction measurements,” Phys. Rev. D **105**, no.11,
675 114001 (2022) doi:10.1103/PhysRevD.105.114001 [arXiv:2203.00244 [hep-ph]].

676 [79] <https://indico.ihep.ac.cn/event/17202/contributions/115011/attachments/62101/71630/Report.OCS.pdf>

677 Appendices

678 A π^0 control sample

679 To study the π^0 reconstruction efficiency, we choose the $J/\psi \rightarrow \Sigma^+ \bar{\Sigma}^- \rightarrow p\bar{p}\pi^0\pi^0$ and $\psi(3686) \rightarrow$
 680 $\Sigma^+ \bar{\Sigma}^- \rightarrow p\bar{p}\pi^0\pi^0$ as the control samples. The π^0 transverse momentum distributed in the region from 0.0
 681 to 0.6 GeV, which could cover our signal area.

682 Charged tracks reconstructed by main drift chamber(MDC) hit information must be fitted by Kalman
 683 method successfully and come from the interaction region in three dimensions. Due to changing beam
 684 conditions, the interaction point (IP) moves. Thus, a separate average IP (beam position) is determined
 685 for each run using the VertexDbSvc package. Relative to this run-dependent IP, each charged track must
 686 satisfy the following requirements:

- 687 • $V_{xy} < 2$ cm,
- 688 • $|V_z| < 10$ cm,
- 689 • $|\cos\theta| < 0.93$,
- 690 • Good tracks is required $N = 2$.

691 Here, θ is the polar angle of the charged track with respect to the beam axis, V_{xy} and $|V_z|$ are the closest
 692 approaches of a charged track to the interaction point in the Oxy plane and in the z position.

693 A.1 Particle identification

694 The charged protons are identified via ParticleID package by using the TOF and dE/dx measure-
 695 ments with which the combined confidence levels $\mathcal{L}(p)$ for protons hypotheses are calculated, respec-
 696 tively. The particle is taken as p if the $Prob_{PID}$ more than any other particle hypothesis. We require the
 697 proton and anti-proton candidates satisfy the following criteria:

- 698 • p : $\mathcal{L}(p) > \mathcal{L}(\pi)$ and $\mathcal{L}(p) > \mathcal{L}(K)$.
- 699 • \bar{p} : $\mathcal{L}(\bar{p}) > \mathcal{L}(\pi)$ and $\mathcal{L}(\bar{p}) > \mathcal{L}(K)$.
- 700 • the number of p and \bar{p} is equal to 1.

701 A.2 Good shower

- 702 • Photon candidates are identified using showers in the EMC. The deposited energy of each shower
 703 must be more than 25 MeV in the barrel region ($|\cos\theta| < 0.80$) and more than 50 MeV in the end
 704 cap region ($0.86 < |\cos\theta| < 0.92$).

- 705 • To suppress electronic noise and showers unrelated to the event, the difference between the EMC
time and the event start time is required to be within (0, 700) ns.
- 707 • To exclude showers that originate from charged tracks (if from anti-proton), the angle between the
708 position of each shower in the EMC and the closest extrapolated charged track must be greater
709 than 10 degrees (20 degrees).
- 710 • The number of good showers $N_\gamma \geq 2$.

711 A.3 π^0 reconstruction

712 The π^0 mesons are reconstructed by the decays $\pi^0 \rightarrow \gamma\gamma$. To reconstruct π^0 meson, we perform a
713 kinematic fit on $\pi^0 \rightarrow \gamma\gamma$. To suppress combinatorial background, we require that the χ^2 of the kinematic
714 fit is less than 25. π^0 candidates are reconstructed from pairs of photons whose invariant mass satisfies
715 $[M_{\pi^0} - 60] < M_{\gamma\gamma} < [M_{\pi^0} + 40] \text{ MeV}/c^2$, where M_{π^0} is the nominal mass of π^0 taken from the PDG and
716 the number of $\pi^0 \geq 1$.

717 A.4 Σ^+ reconstruction

- 718 • Looping all π^0 candidates, the smallest value $E(p\pi^0) - 3.097/2$ is considered as final state and
719 $|E(p\pi^0) - 3.097/2| \leq 0.01 \text{ GeV}$ is required.
- 720 • The $|M(p\pi^0) - 1.18937| \leq 0.02 \text{ GeV}/c^2$ is required.

721 A.5 π^0 reconstruction efficiency

- 722 • The number of $\pi^0 \geq 2$.
- 723 • Fitting range: $M_{\Sigma^+ \bar{p}} \text{ recoil} \in [0, 0.25] \text{ GeV}$
- 724 • π^0 reconstruction efficiency is defined as : $\frac{N_{M(\gamma\gamma)}^{\text{found}}}{N_{M(\gamma\gamma)}^{\text{found}} + N_{M(\gamma\gamma)}^{\text{un-found}}}$, where $N_{M(\gamma\gamma)}^{\text{found}}$ is the number of π^0 after
725 requiring selection of π^0 and $N_{M(\gamma\gamma)}^{\text{un-found}}$ is the number of π^0 which means that π^0 can not be found
726 from the selected sample. Here, the values of $N_{M(\gamma\gamma)}^{\text{found}}$ and $N_{M(\gamma\gamma)}^{\text{un-found}}$ can be determined by fitting
727 the recoil mass of $M_{\Sigma^+ \bar{p}}$.

728 Detailed informations are shown in following figures(The red dashed line is the signal contribution,
729 and the blue dotted line is the background contribution.). The total fit function PDFs(probability density
730 function) are described as: $N_{\text{sig}} \times (\text{PDF}_{\text{SignalShape}} \otimes \text{Gauss}(\text{Mean}, \sigma)) + N_{\text{bkg}} \times \text{PDF}_{\text{1st-OrderPolynomialFunction}}$,
731 where N_{sig} represents signal events and N_{bkg} represents background events.

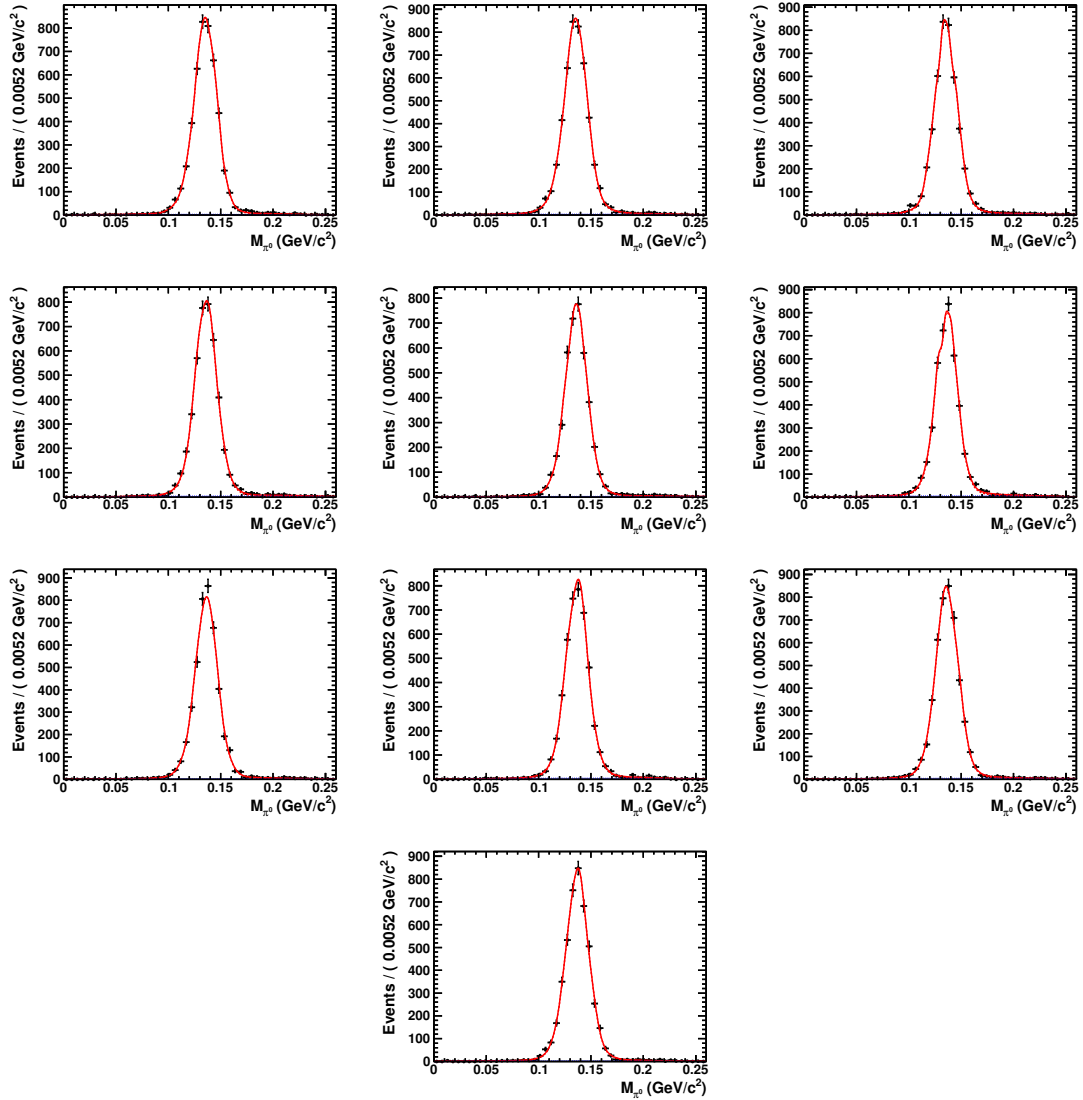
732 A.5.1 Found π^0 

Fig. 35: Momentum: 0.0-0.15 GeV for selecting π^0 in different $\cos \theta$ range. Front to back angles: [- 1.0, - 0.8], [- 0.8, - 0.6], [- 0.6, - 0.4], [- 0.4, - 0.2], [0.0, 0.2], [0.2, 0.4], [0.4, 0.6], [0.6, 0.8], [0.8, 1.0]

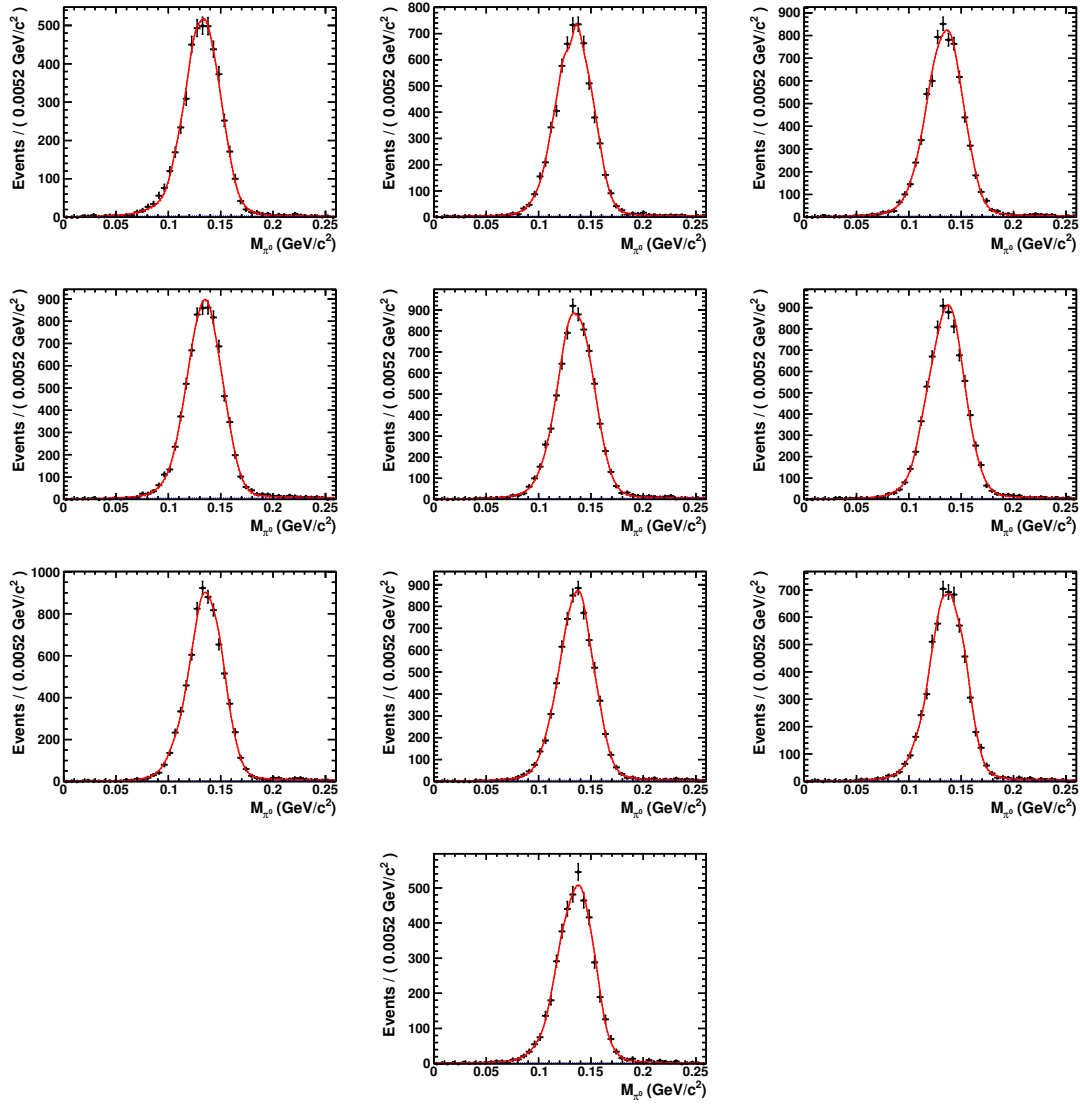


Fig. 36: Momentum: 0.15-0.25 GeV for selecting π^0 in different $\cos \theta$ range. Front to back angles: [-1.0, -0.8], [-0.8, -0.6], [-0.6, -0.4], [-0.4, -0.2], [0.0, 0.2], [0.2, 0.4], [0.4, 0.6], [0.6, 0.8], [0.8, 1.0]

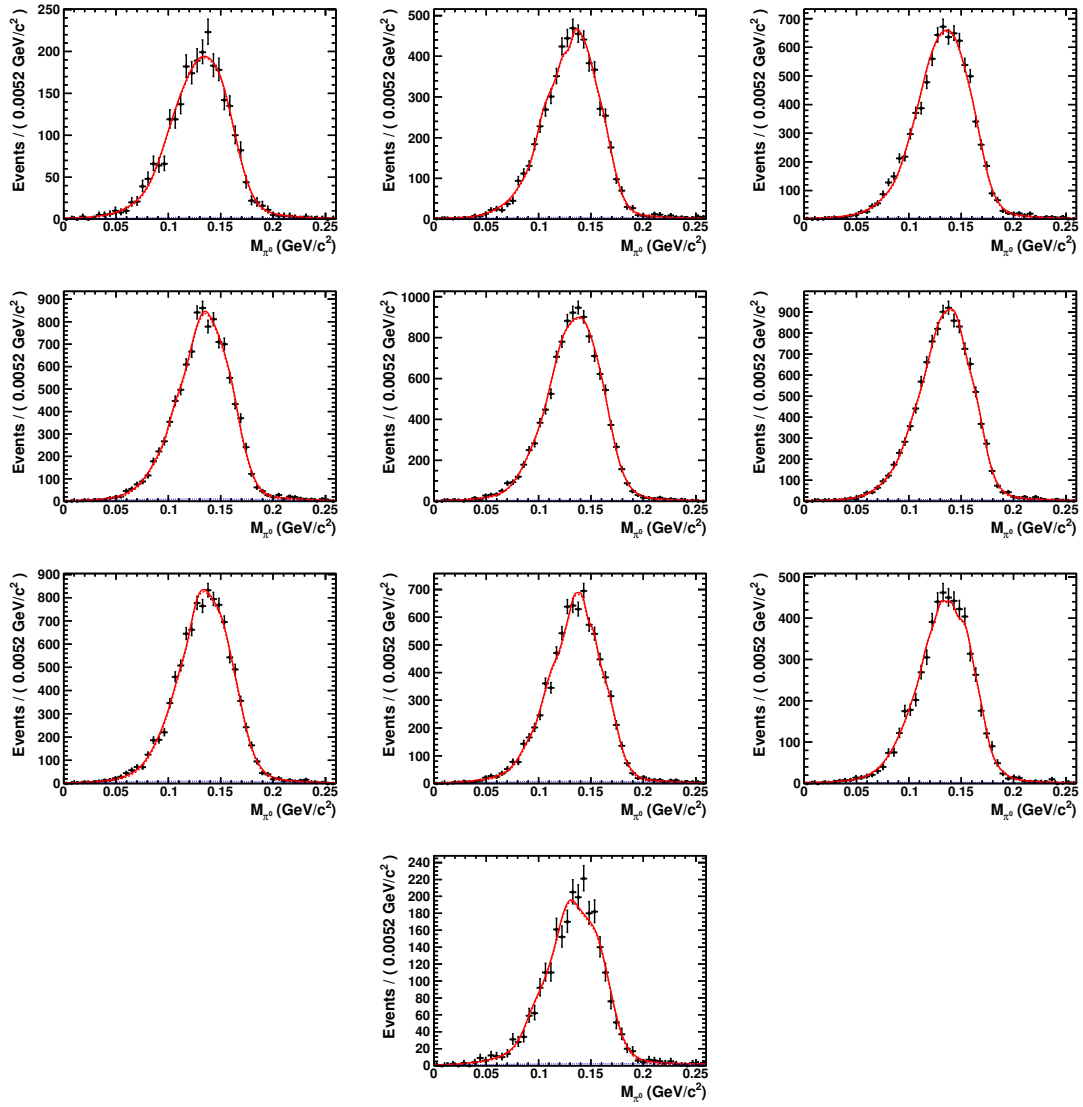


Fig. 37: Momentum: 0.25-0.35 GeV for selecting π^0 in different $\cos \theta$ range. Front to back angles: [-1.0, -0.8], [-0.8, -0.6], [-0.6, -0.4], [-0.4, -0.2], [0.0, 0.2], [0.2, 0.4], [0.4, 0.6], [0.6, 0.8], [0.8, 1.0]

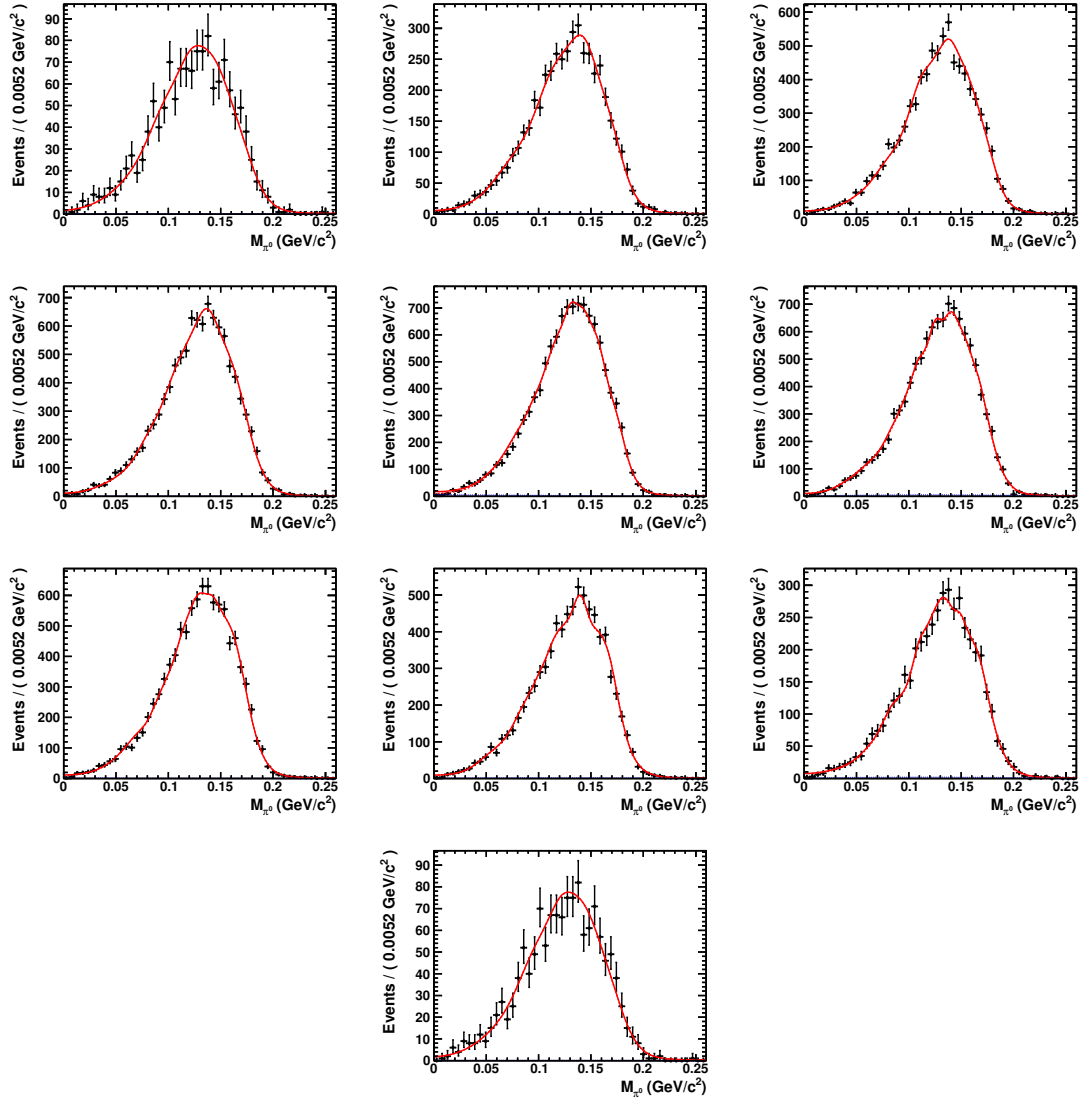


Fig. 38: Momentum: 0.35-0.55 GeV for selecting π^0 in different $\cos \theta$ range. Front to back angles: [-1.0, -0.8], [-0.8, -0.6], [-0.6, -0.4], [-0.4, -0.2], [0.0, 0.2], [0.2, 0.4], [0.4, 0.6], [0.6, 0.8], [0.8, 1.0]

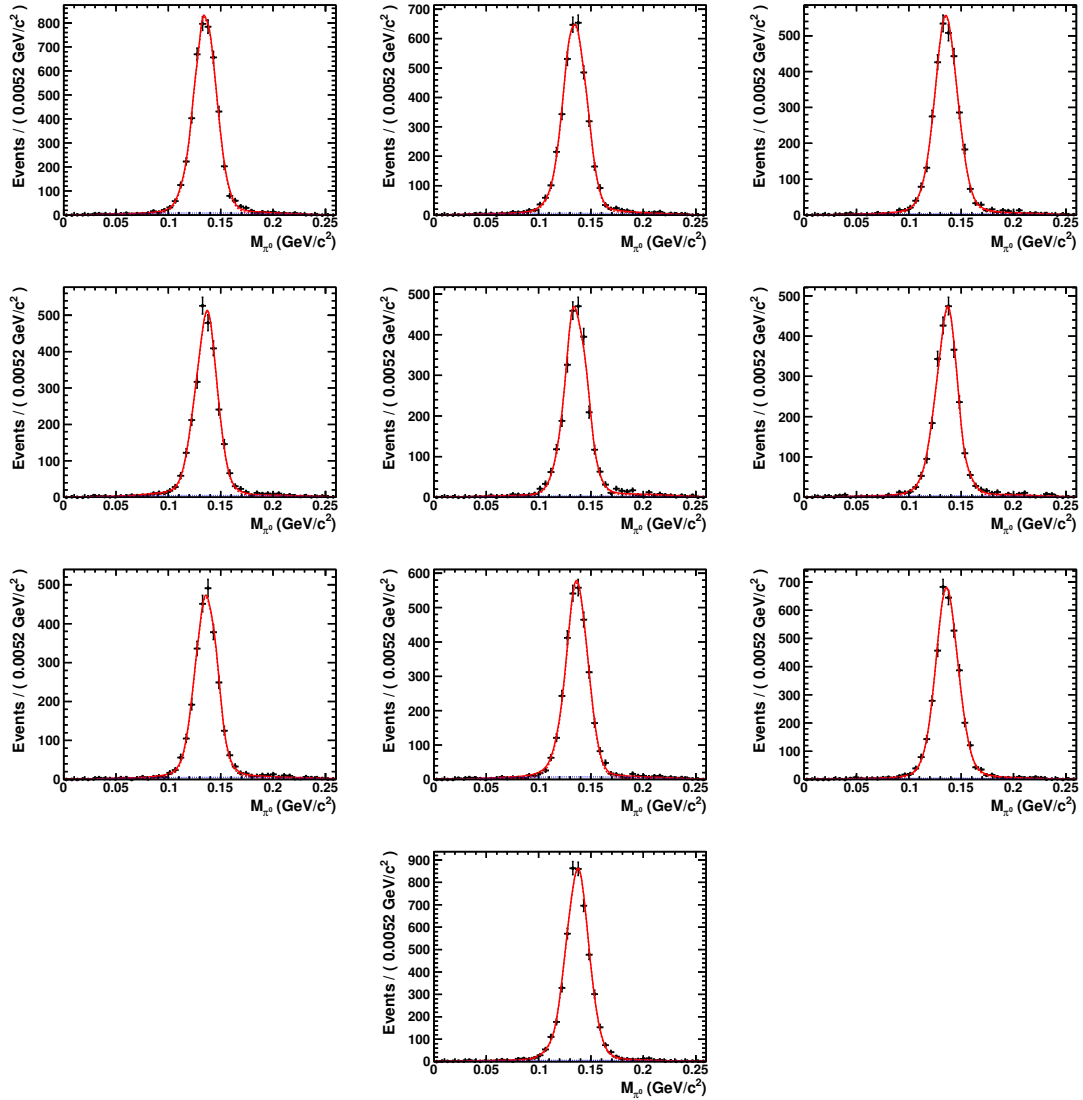
733 A.5.2 Not found π^0 

Fig. 39: Momentum: 0.0-0.15 GeV for no π^0 is selected in different $\cos \theta$ range. Front to back angles: [-1.0, -0.8], [-0.8, -0.6], [-0.6, -0.4], [-0.4, -0.2], [0.0, 0.2], [0.2, 0.4], [0.4, 0.6], [0.6, 0.8], [0.8, 1.0]

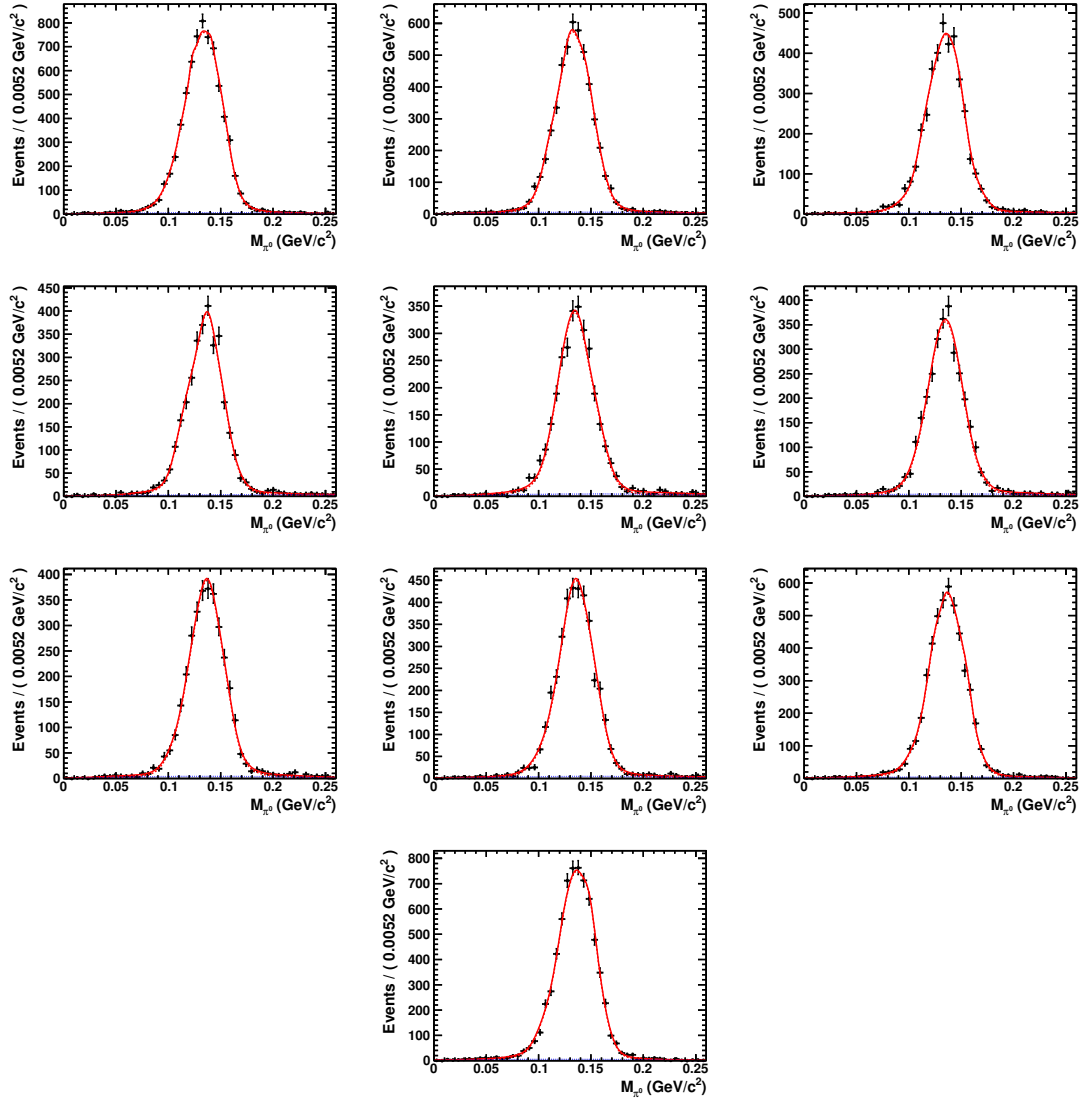


Fig. 40: Momentum: 0.15-0.25 GeV for no π^0 is selected in different $\cos \theta$ range. Front to back angles: [- 1.0, - 0.8], [- 0.8, - 0.6], [- 0.6, - 0.4], [- 0.4, - 0.2], [0.0, 0.2], [0.2, 0.4], [0.4, 0.6], [0.6, 0.8], [0.8, 1.0]

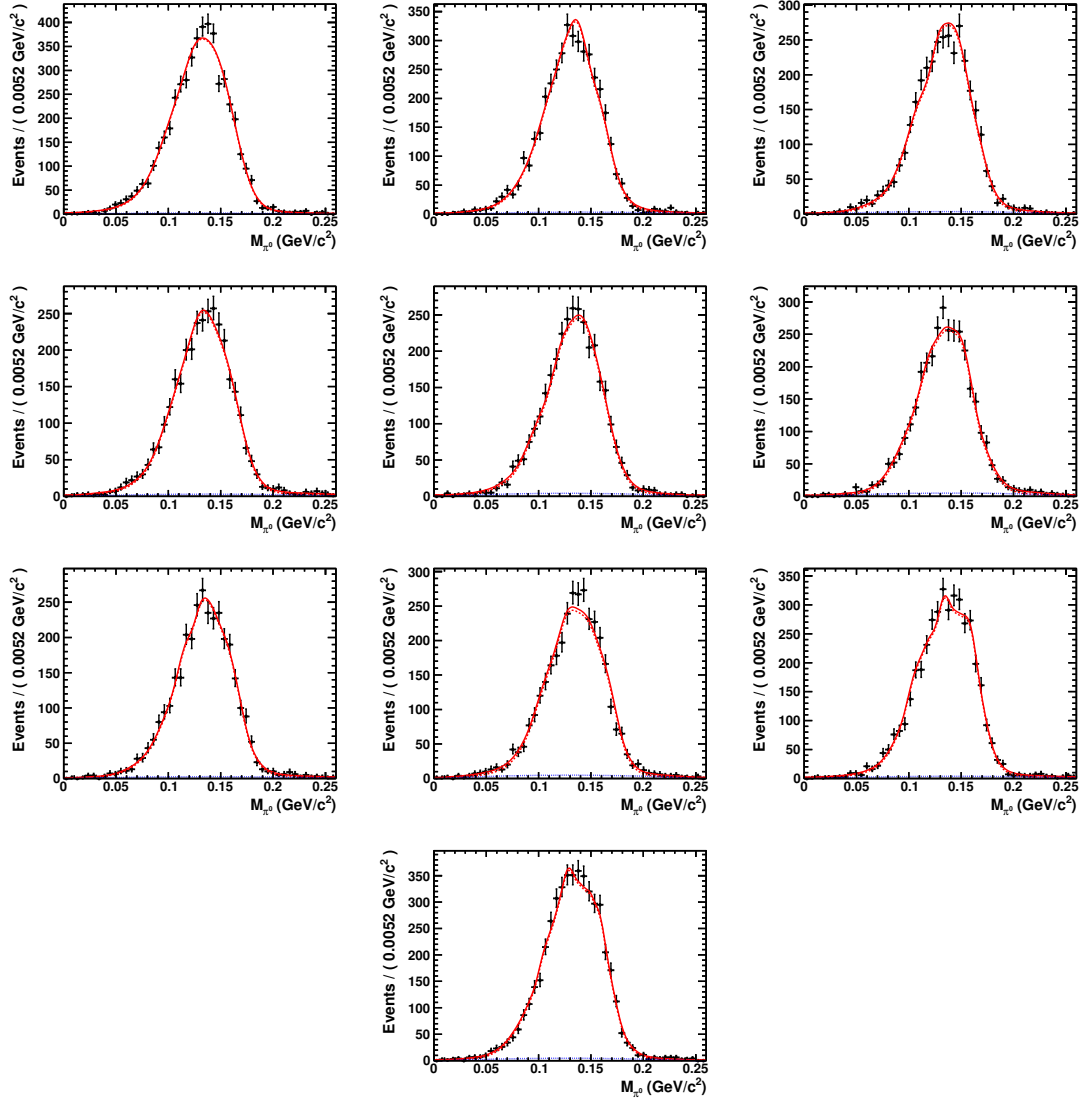


Fig. 41: Momentum: 0.25-0.35 GeV for no π^0 is selected in different $\cos \theta$ range. Front to back angles: [- 1.0, - 0.8], [- 0.8, - 0.6], [- 0.6, - 0.4], [- 0.4, - 0.2], [0.0, 0.2], [0.2, 0.4], [0.4, 0.6], [0.6, 0.8], [0.8, 1.0]

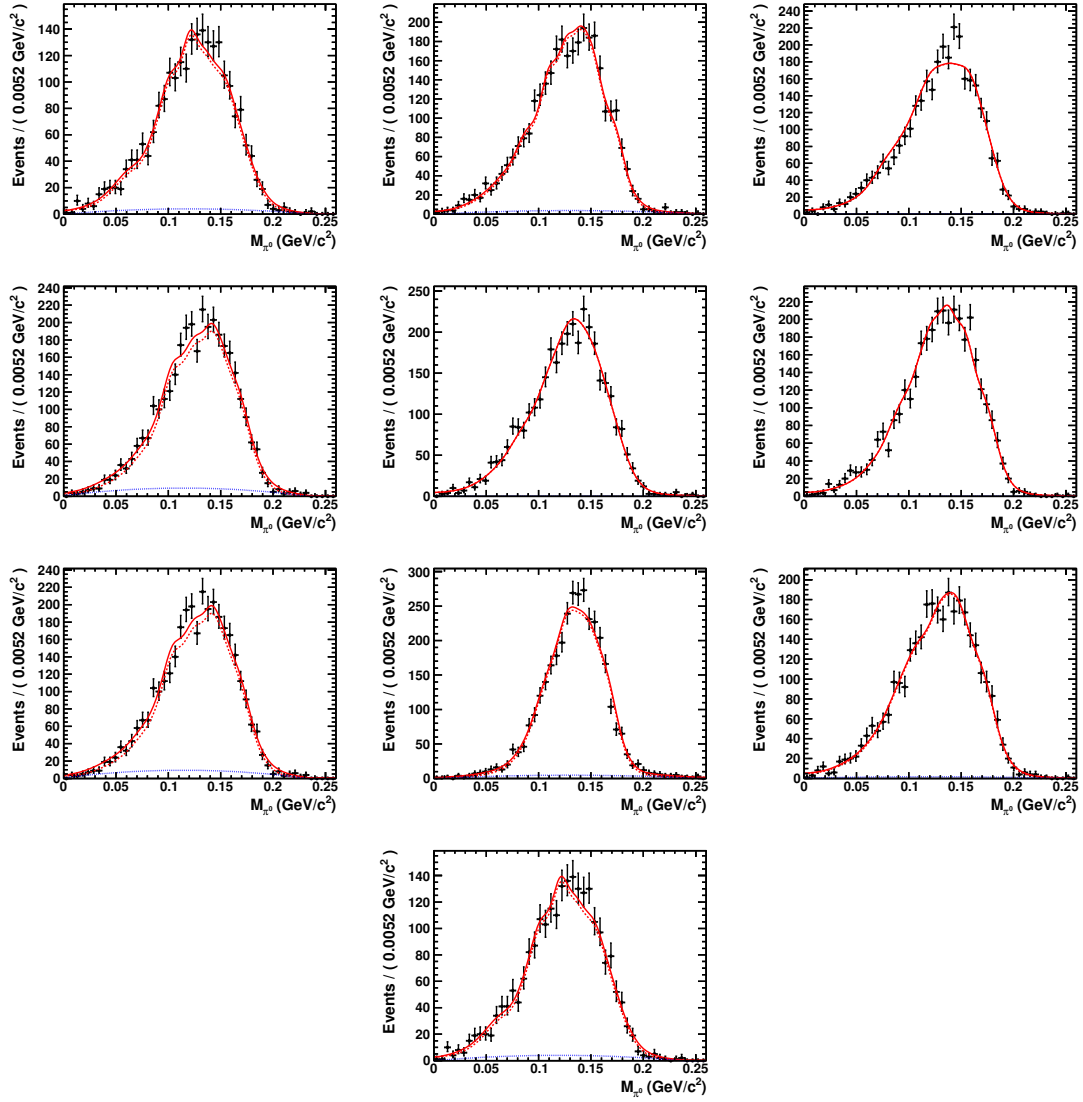


Fig. 42: Momentum: 0.35-0.55 GeV for no π^0 is selected in different $\cos \theta$ range. Front to back angles: [- 1.0, - 0.8], [- 0.8, - 0.6], [- 0.6, - 0.4], [- 0.4, - 0.2], [0.0, 0.2], [0.2, 0.4], [0.4, 0.6], [0.6, 0.8], [0.8, 1.0]

734 Appendices

735 B p (\bar{p}) control sample

736 To study the p (\bar{p}) reconstruction efficiency, we choose the $J/\psi \rightarrow \Sigma^+ \bar{\Sigma}^- \rightarrow p\bar{p}\pi^0\pi^0$ and $\psi(3686) \rightarrow$
 737 $\Sigma^+ \bar{\Sigma}^- \rightarrow p\bar{p}\pi^0\pi^0$ as the control samples. The p (\bar{p}) transverse momentum distributed in the region from
 738 0.55 to 1.1 GeV, which could cover our signal area.

739 Charged tracks reconstructed by main drift chamber(MDC) hit information must be fitted by Kalman
 740 method successfully and come from the interaction region in three dimensions. Due to changing beam
 741 conditions, the interaction point (IP) moves. Thus, a separate average IP (beam position) is determined
 742 for each run using the VertexDbSvc package. Relative to this run-dependent IP, each charged track must
 743 satisfy the following requirements:

- 744 • $V_{xy} < 2$ cm,
- 745 • $|V_z| < 10$ cm,
- 746 • $|\cos\theta| < 0.93$,
- 747 • Good tracks is required $N \geq 1$.

748 Here, θ is the polar angle of the charged track with respect to the beam axis, V_{xy} and $|V_z|$ are the closest
 749 approaches of a charged track to the interaction point in the Oxy plane and in the z position.

750 B.1 Particle identification

751 The charged pions and protons are identified via ParticleID package by using the TOF and dE/dx
 752 measurements with which the combined confidence levels $\mathcal{L}(\pi^-)$ and $\mathcal{L}(p)$ for pion and proton hy-
 753 potheses are calculated, respectively. The particle is taken as $p(\bar{p})$ if the $Prob_{PID}$ more than any other
 754 particle hypothesis. We require the proton and anti-proton candidates satisfy the following criteria:

- 755 • \bar{p} (p): $\mathcal{L}(p) > \mathcal{L}(\pi)$ and $\mathcal{L}(p) > \mathcal{L}(k)$.
- 756 • The number of \bar{p} (p) is equal to 1.

757 B.2 Good shower

- 758 • Photon candidates are identified using showers in the EMC. The deposited energy of each shower
 759 must be more than 25 MeV in the barrel region ($|\cos\theta| < 0.80$) and more than 50 MeV in the end
 760 cap region ($0.86 < |\cos\theta| < 0.92$).

- 761 • To suppress electronic noise and showers unrelated to the event, the difference between the EMC
762 time and the event start time is required to be within (0, 700) ns.
- 763 • To exclude showers that originate from charged tracks if (from anti-proton), the angle between the
764 position of each shower in the EMC and the closest extrapolated charged track must be greater
765 than 10 degrees (10 degrees).
- 766 • The number of good showers $N_\gamma \geq 4$.

767 **B.3 π^0 reconstruction**

768 The π^0 mesons are reconstructed by the decays $\pi^0 \rightarrow \gamma\gamma$. To reconstruct π^0 meson, we perform a
769 kinematic fit on $\pi^0 \rightarrow \gamma\gamma$. To suppress combinatorial background, we require that the χ^2 of the kinematic
770 fit is less than 25. π^0 candidates are reconstructed from pairs of photons whose invariant mass satisfies
771 $[M_{\pi^0} - 60] < M_{\gamma\gamma} < [M_{\pi^0} + 40] \text{ MeV}/c^2$, where M_{π^0} is the nominal mass of π^0 taken from the PDG. The
772 candidates of π^0 is required to be $N_{\pi^0} \geq 2$.

773 **B.4 kinematic fit**

774 To further remove potential backgrounds and to improve the mass resolution, a two-constraint-
775 energy-momentum conservation kinematic fit is performed by looping all π^0 candidates (2C kinemat-
776 ic fit: The resonance $\Sigma^+(\bar{\Sigma}^-)$ is reconstructed from π^0 and miss p mass (or π^0 and miss \bar{p} mass). A
777 requirement on the quality of the 2C kinematic fit $\chi^2_{2C} \leq 50$ is imposed. If the number of π^0 candidates
778 in an event is more than one, the combination with the lowest χ^2_{2C} is selected as the final event candidate.

779 **B.5 selection of p (\bar{p})**

780 Charged tracks reconstructed by main drift chamber(MDC) hit information must be fitted by Kalman
781 method successfully and come from the interaction region in three dimensions. Due to changing beam
782 conditions, the interaction point (IP) moves. Thus, a separate average IP (beam position) is determined
783 for each run using the VertexDbSvc package. Relative to this run-dependent IP, each charged track must
784 satisfy the following requirements:

- 785 • $V_{xy} < 2 \text{ cm}$,
- 786 • $|V_z| < 10 \text{ cm}$,
- 787 • $|\cos\theta| < 0.93$,
- 788 • Good tracks is required $N \geq 1$.

789 Here, θ is the polar angle of the charged track with respect to the beam axis, V_{xy} and $|V_z|$ are the closest
 790 approaches of a charged track to the interaction point in the Oxy plane and in the z position.

791 The charged pions and protons are identified via ParticleID package by using the TOF and dE/dx
 792 measurements with which the combined confidence levels $\mathcal{L}(\pi^-)$ and $\mathcal{L}(p)$ for pion and proton hy-
 793 potheses are calculated, respectively. The particle is taken as $\bar{p}(p)$ if the $Prob_{PID}$ more than any other
 794 particle hypothesis. We require the pion and proton candidates satisfy the following criteria:

- 795 • $p (\bar{p})$: $\mathcal{L}(p) > \mathcal{L}(\pi)$ and $\mathcal{L}(p) > \mathcal{L}(K)$.
- 796 • The number of $p (\bar{p})$ is equal to 1.
- 797 • R_{xy} , the closest approaches of vertex point to the interaction point. Here, vertex point can be
 798 obtained by performing vertex fit for p and \bar{p} and R_{xy} is required to be larger than 0.34.

799 **B.6 $p (\bar{p})$ reconstruction efficiency**

- 800 • fitting range: $M(p\pi^-) \in [1.08, 1.28]$ GeV

- 801 • $p (\bar{p})$ reconstruction efficiency is defined as : $\frac{N_{M(p\pi^0)}^{found}}{N_{M(p\pi^0)}^{found} + N_{M(p\pi^0)}^{un-found}}$, where $N_{M(p\pi^0)}^{found}$ is the number of p
 802 (\bar{p}) after requiring selection of $p (\bar{p})$ and $N_{M(p\pi^0)}^{un-found}$ is the number of $p (\bar{p})$ which means that p
 803 (\bar{p}) can not be found from the selected sample. Here, the values of $N_{M(p\pi^0)}^{found}$ and $N_{M(p\pi^0)}^{un-found}$ can be
 804 determined by fitting the recoil mass $\bar{p}\pi^0$.

805 Detailed informations are shown in following figures(The red dashed line is the signal contribution,
 806 and the blue dotted line is the background contribution.). The total fit function PDFs(probability density
 807 function) are described as: $N_{sig} \times (PDF_{SignalShape} \otimes Gauss(Mean, \sigma)) + N_{bkg} \times PDF_{1st-OrderPolynomialFunction}$,
 808 where N_{sig} represents signal events and N_{bkg} represents background events.

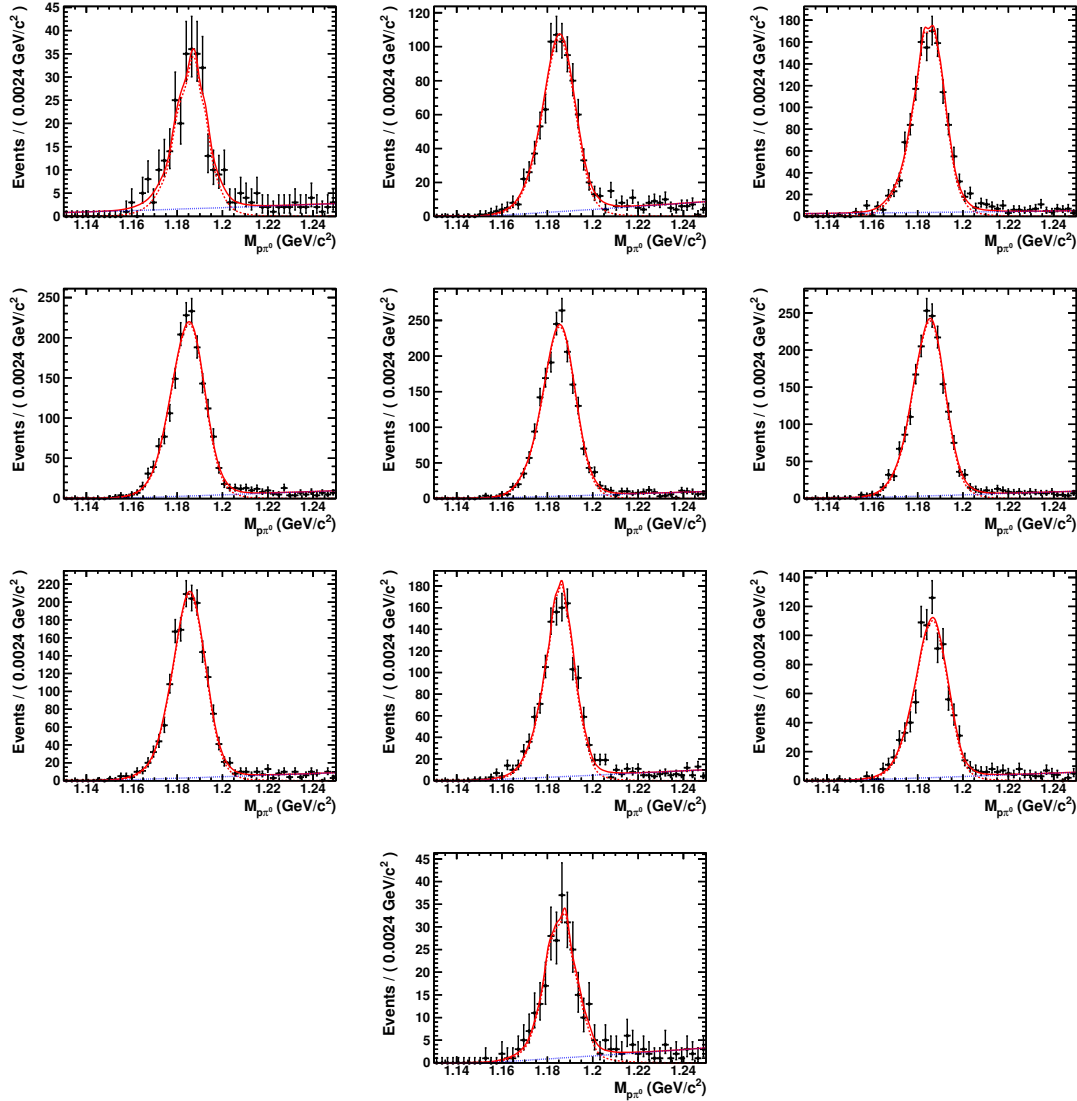
809 **B.7 p reconstruction efficiency**810 **B.7.1 Found p** 

Fig. 43: Momentum: 0.55-0.65 GeV for selecting proton in different $\cos \theta$ range. Front to back angles: [- 1.0, - 0.8], [- 0.8, - 0.6], [- 0.6, - 0.4], [- 0.4, - 0.2], [0.0, 0.2], [0.2, 0.4], [0.4, 0.6], [0.6, 0.8], [0.8, 1.0]

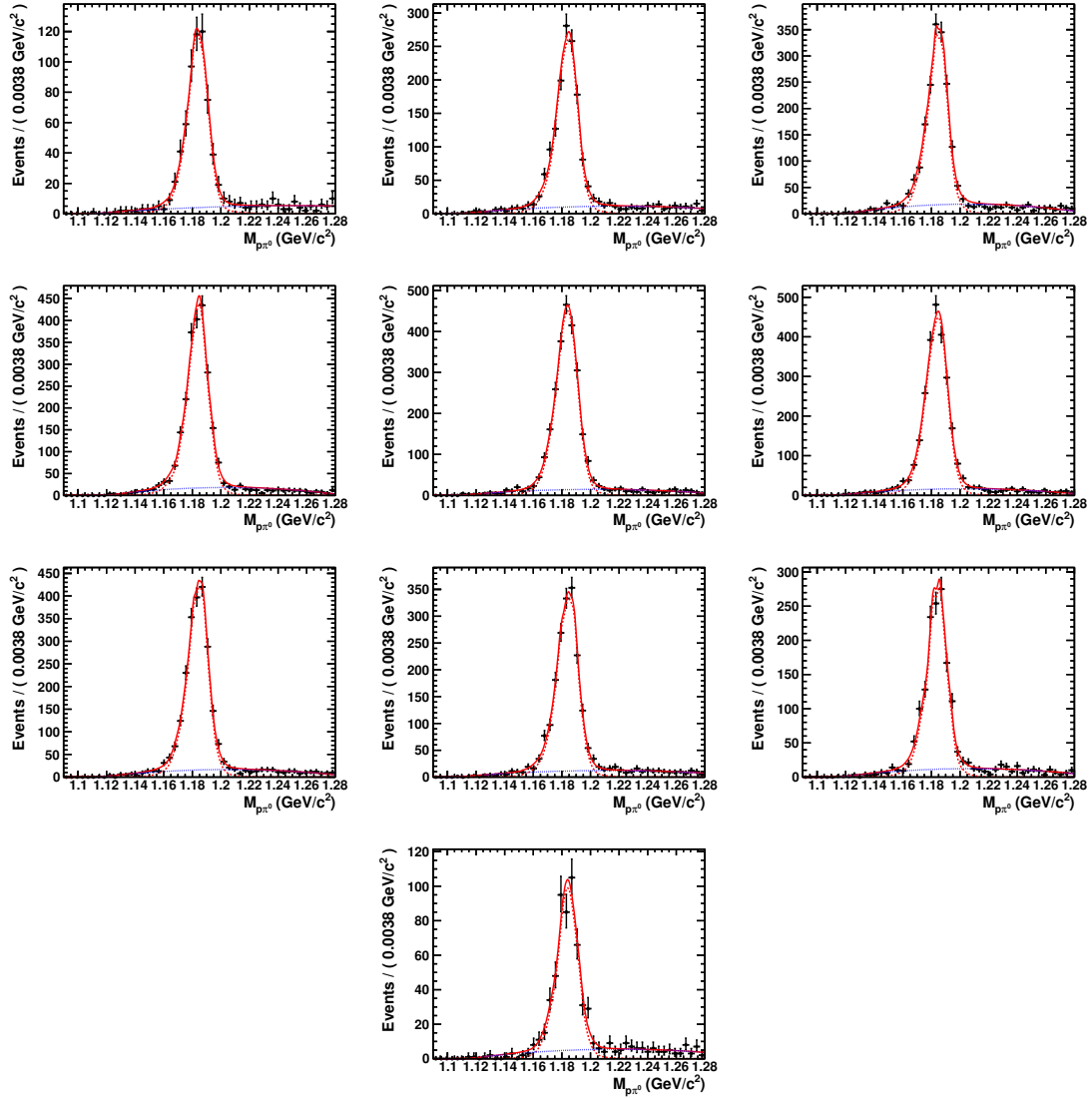


Fig. 44: Momentum: 0.65-0.75 GeV for selecting proton in different $\cos \theta$ range. Front to back angles: [- 1.0, - 0.8], [- 0.8, - 0.6], [- 0.6, - 0.4], [- 0.4, - 0.2], [0.0, 0.2], [0.2, 0.4], [0.4, 0.6], [0.6, 0.8], [0.8, 1.0]

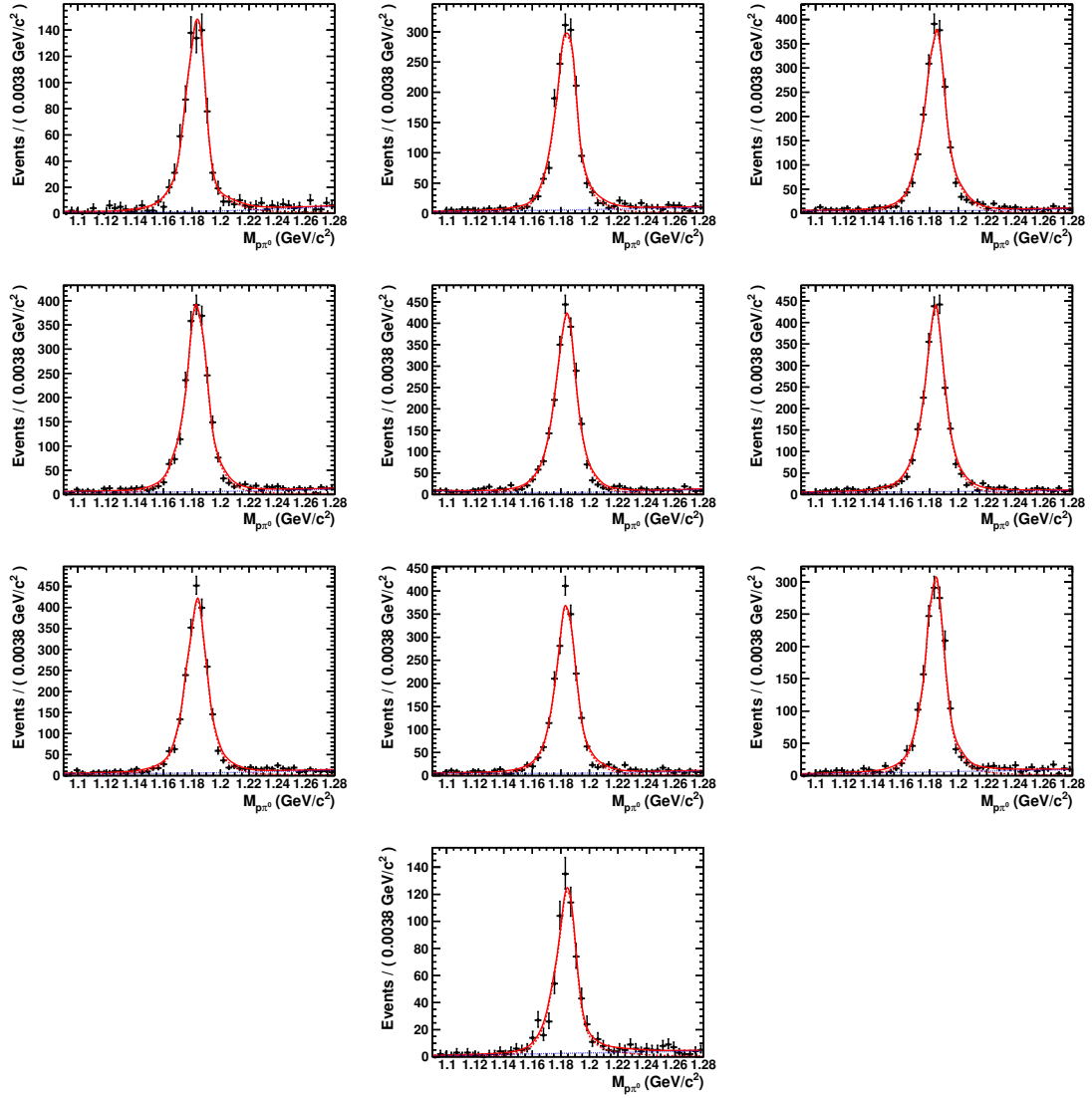


Fig. 45: Momentum: 0.75-0.85 GeV for selecting proton in different $\cos \theta$ range. Front to back angles: [- 1.0, - 0.8], [- 0.8, - 0.6], [- 0.6, - 0.4], [- 0.4, - 0.2], [0.0, 0.2], [0.2, 0.4], [0.4, 0.6], [0.6, 0.8], [0.8, 1.0]

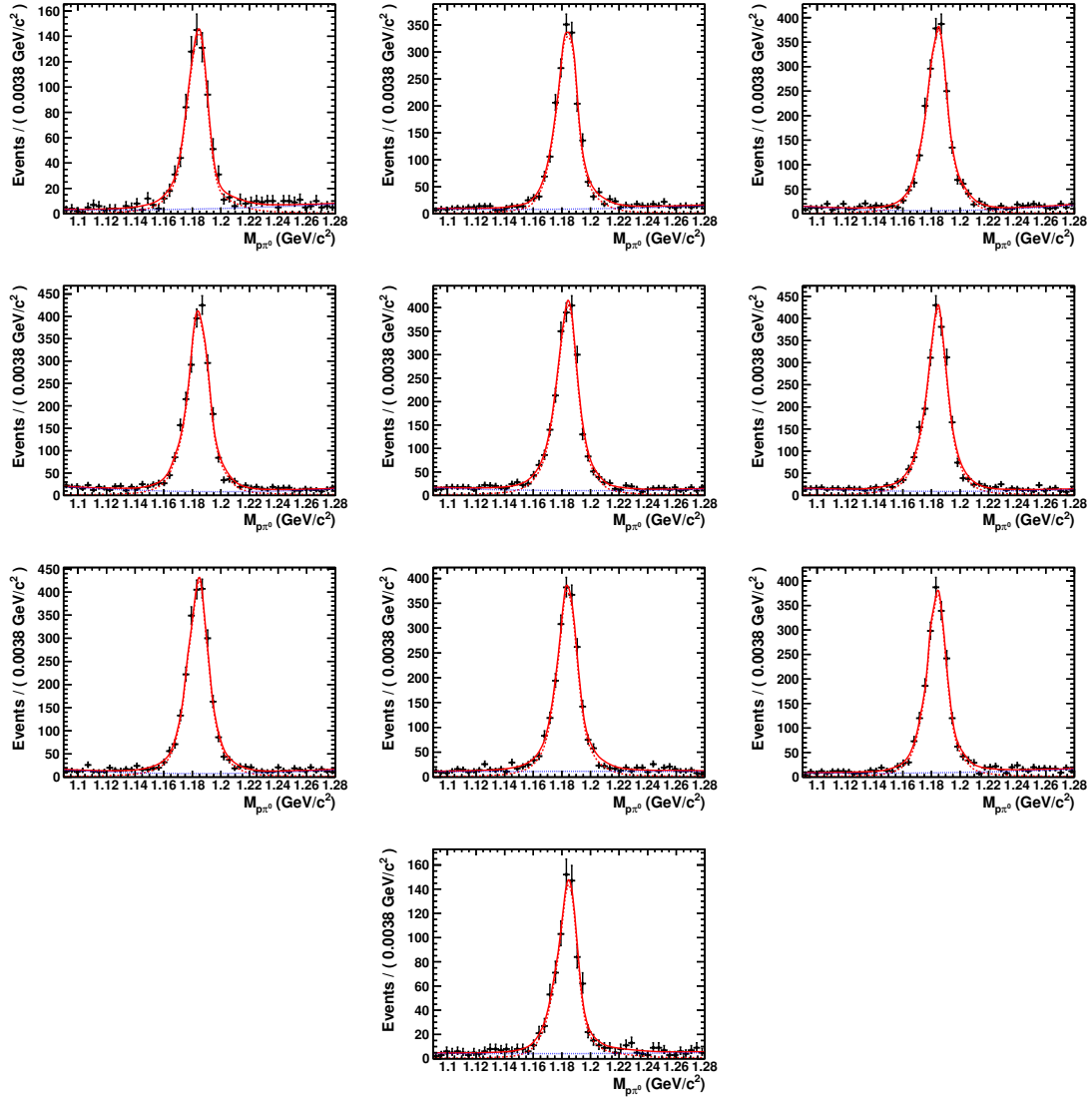


Fig. 46: Momentum: 0.85-0.95 GeV for selecting proton in different $\cos \theta$ range. Front to back angles: [- 1.0, - 0.8], [- 0.8, - 0.6], [- 0.6, - 0.4], [- 0.4, - 0.2], [0.0, 0.2], [0.2, 0.4], [0.4, 0.6], [0.6, 0.8], [0.8, 1.0]

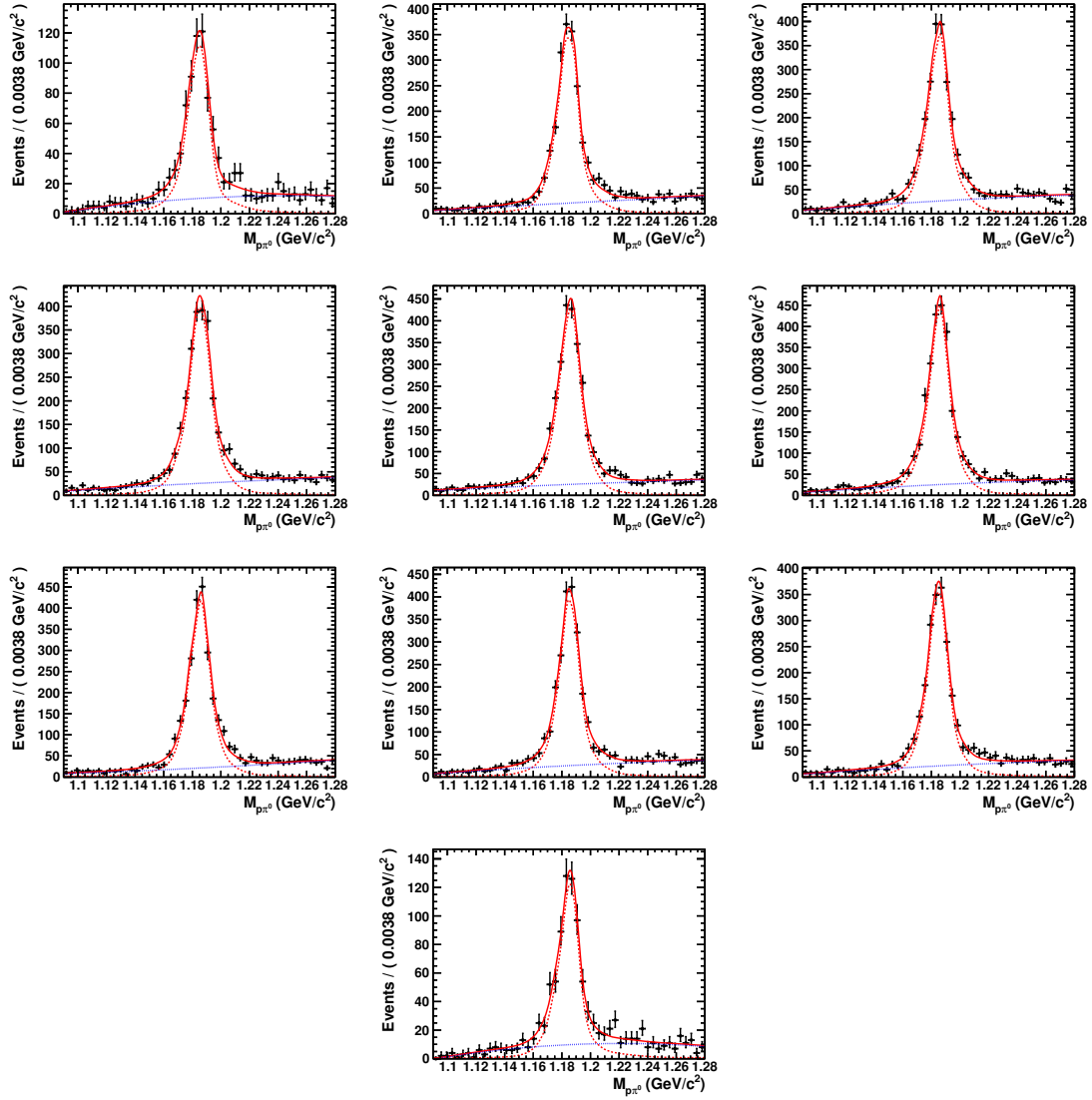


Fig. 47: Momentum: 0.95-1.15 GeV for selecting proton in different $\cos \theta$ range. Front to back angles: [- 1.0, - 0.8], [- 0.8, - 0.6], [- 0.6, - 0.4], [- 0.4, - 0.2], [0.0, 0.2], [0.2, 0.4], [0.4, 0.6], [0.6, 0.8], [0.8, 1.0]

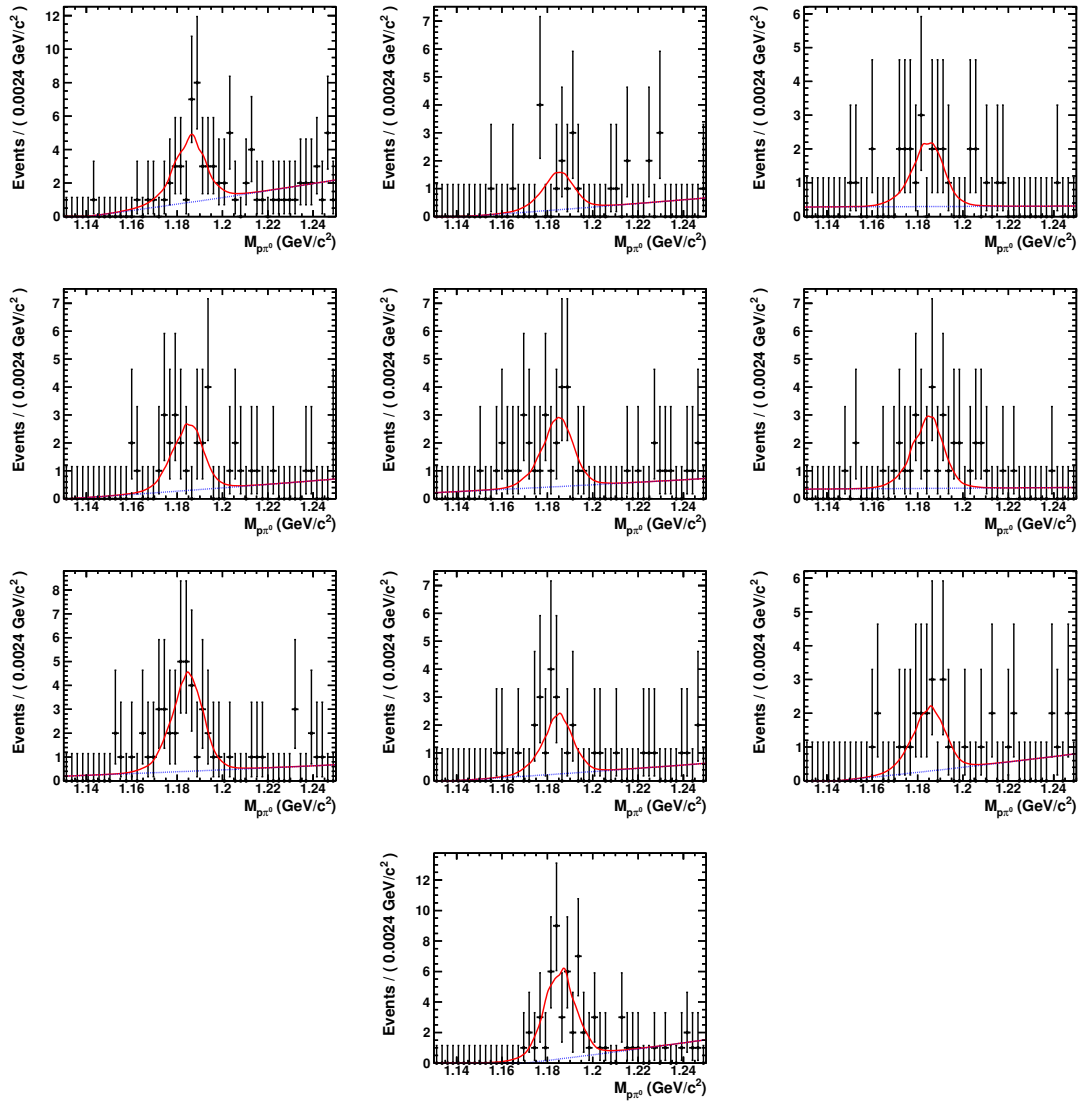
811 B.7.2 Not found p 

Fig. 48: Momentum: 0.55-0.65 GeV for no proton is selected in different $\cos \theta$ range. Front to back angles: [- 1.0, - 0.8], [- 0.8, - 0.6], [- 0.6, - 0.4], [- 0.4, - 0.2], [0.0, 0.2], [0.2, 0.4], [0.4, 0.6], [0.6, 0.8], [0.8, 1.0]

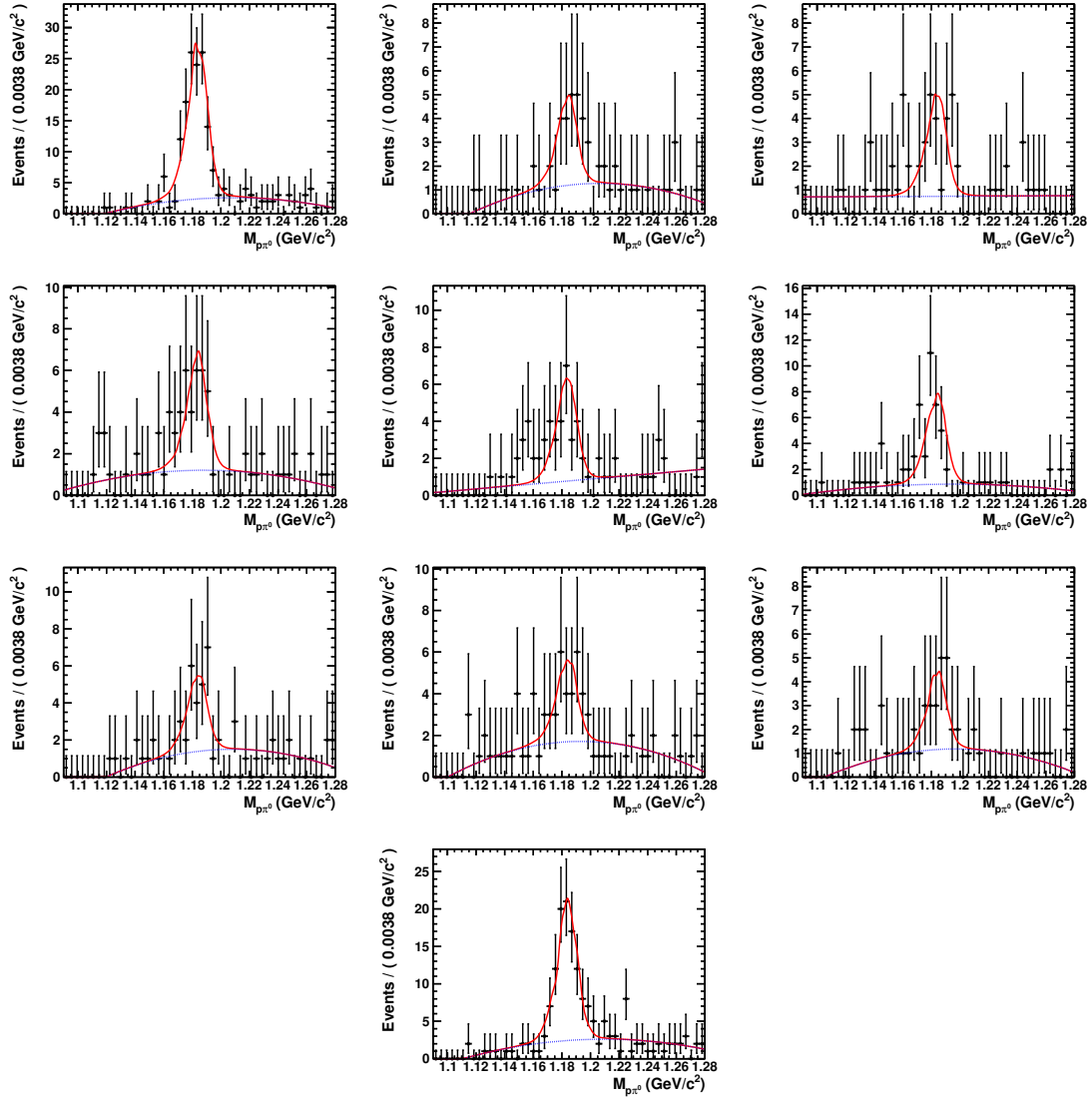


Fig. 49: Momentum: 0.65-0.75 GeV for no proton is selected in different $\cos \theta$ range. Front to back angles: [- 1.0, - 0.8], [- 0.8, - 0.6], [- 0.6, - 0.4], [- 0.4, - 0.2], [0.0, 0.2], [0.2, 0.4], [0.4, 0.6], [0.6, 0.8], [0.8, 1.0]

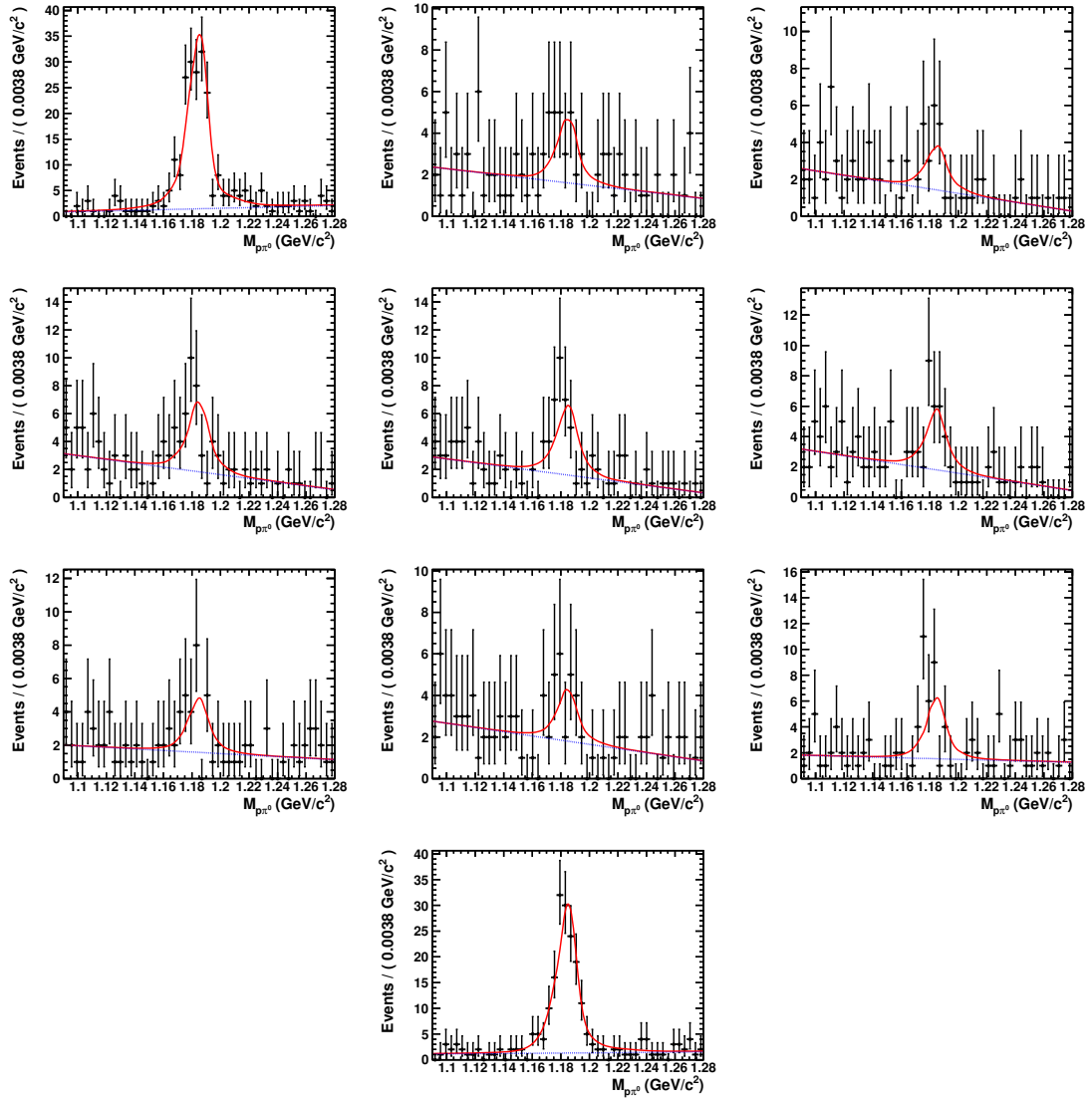


Fig. 50: Momentum: 0.75-0.85 GeV for no proton is selected in different $\cos \theta$ range. Front to back angles: [- 1.0, - 0.8], [- 0.8, - 0.6], [- 0.6, - 0.4], [- 0.4, - 0.2], [0.0, 0.2], [0.2, 0.4], [0.4, 0.6], [0.6, 0.8], [0.8, 1.0]

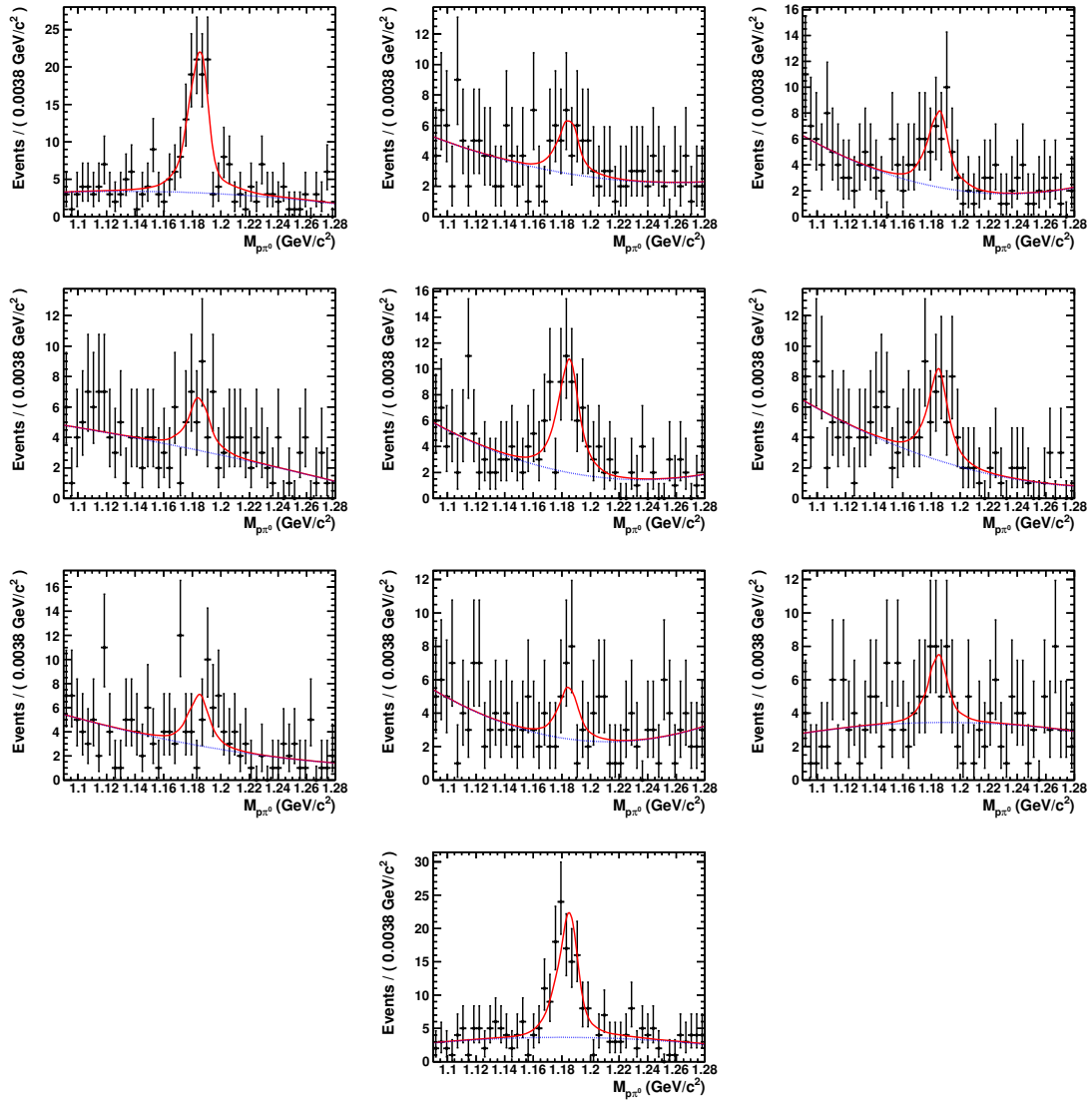


Fig. 51: Momentum: 0.85-0.95 GeV for no proton is selected in different $\cos \theta$ range. Front to back angles: [- 1.0, - 0.8], [- 0.8, - 0.6], [- 0.6, - 0.4], [- 0.4, - 0.2], [0.0, 0.2], [0.2, 0.4], [0.4, 0.6], [0.6, 0.8], [0.8, 1.0]

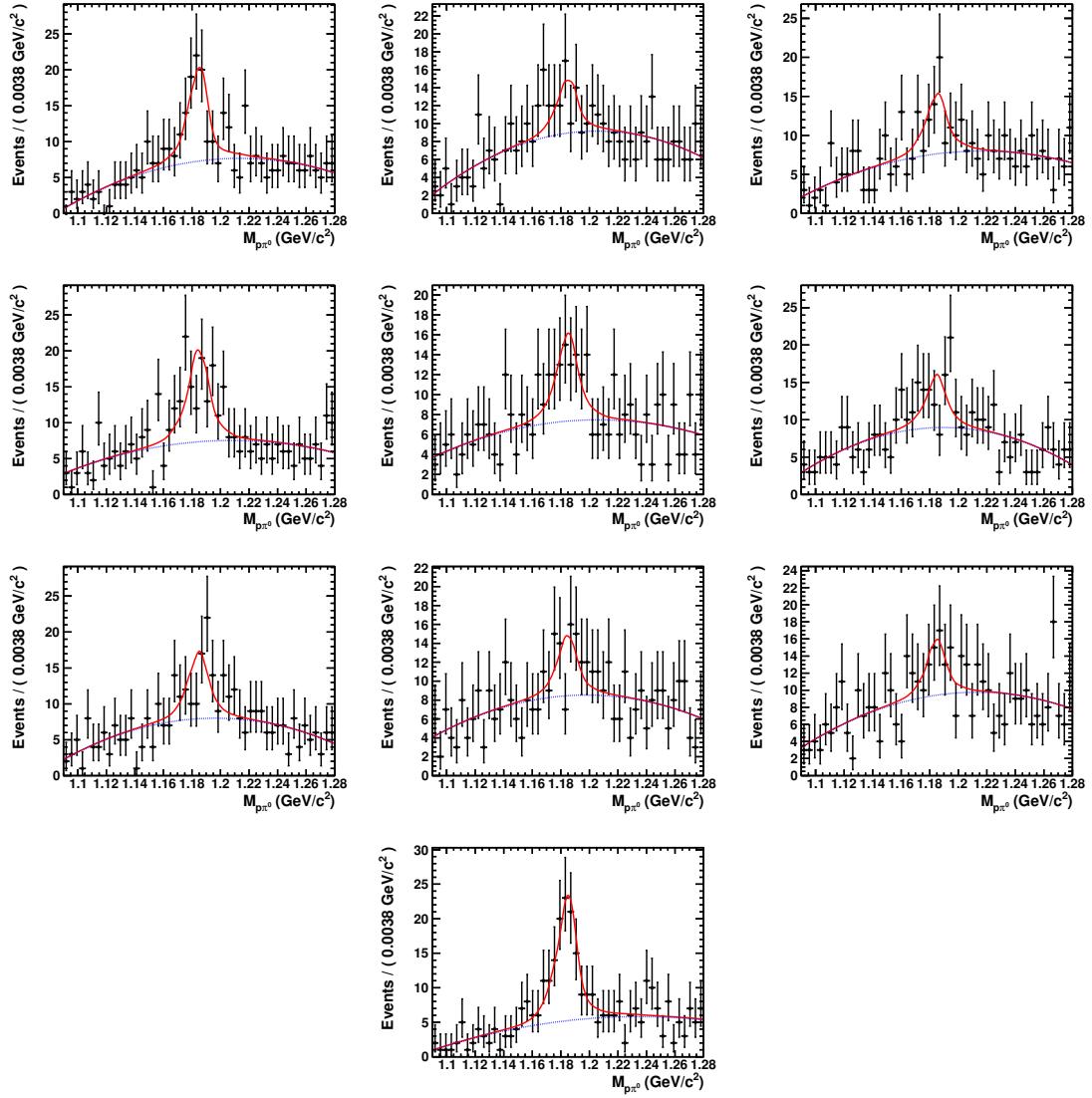


Fig. 52: Momentum: 0.95-1.15 GeV for no proton is selected in different $\cos \theta$ range. Front to back angles: [- 1.0, - 0.8], [- 0.8, - 0.6], [- 0.6, - 0.4], [- 0.4, - 0.2], [0.0, 0.2], [0.2, 0.4], [0.4, 0.6], [0.6, 0.8], [0.8, 1.0]

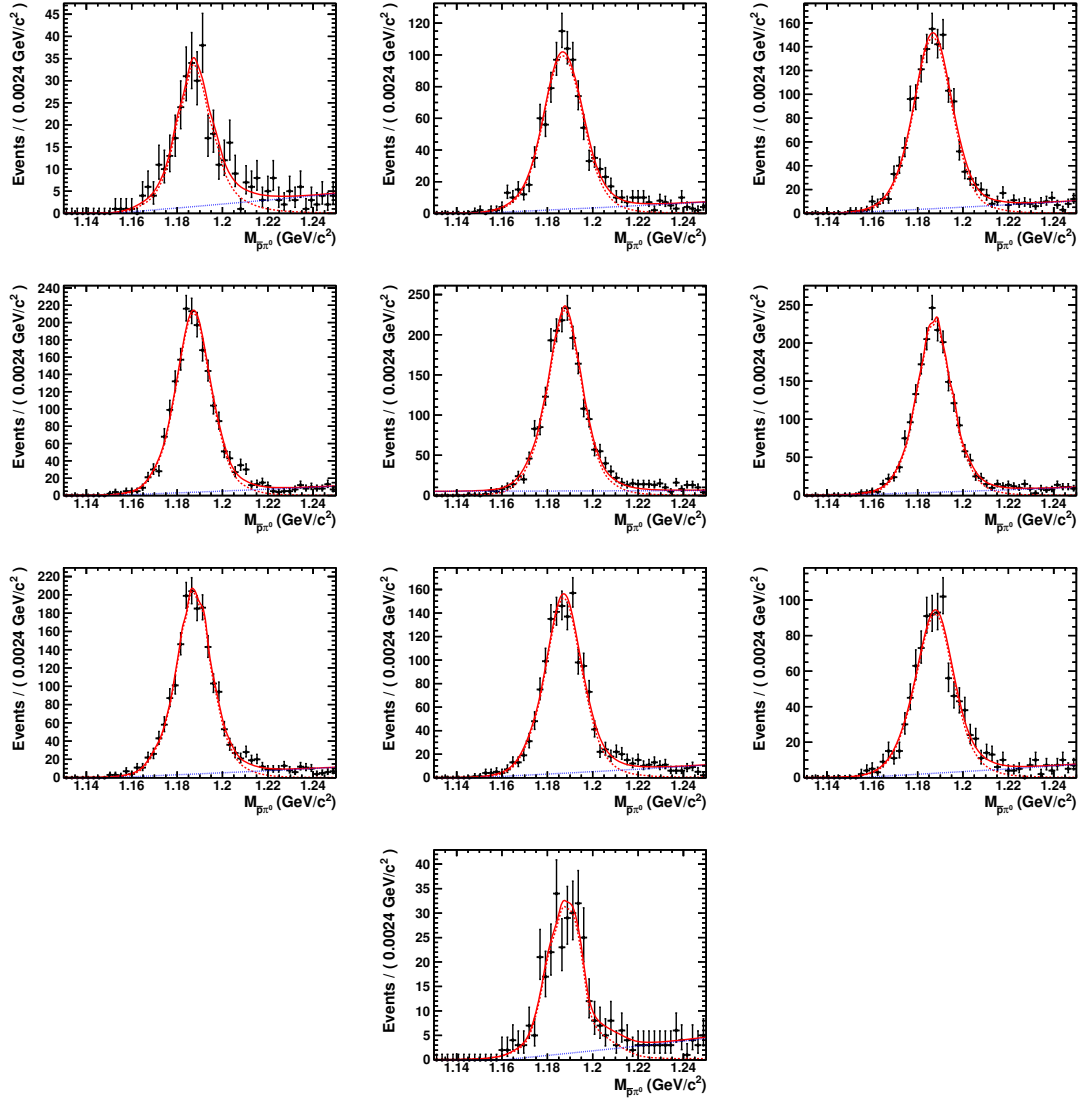
812 **B.8 \bar{p} reconstruction efficiency**813 **B.8.1 Found \bar{p}** 

Fig. 53: Momentum: 0.55-0.65 GeV for selecting anti-proton in different $\cos \theta$ range. Front to back angles: [- 1.0, - 0.8], [- 0.8, - 0.6], [- 0.6, - 0.4], [- 0.4, - 0.2], [0.0, 0.2], [0.2, 0.4], [0.4, 0.6], [0.6, 0.8], [0.8, 1.0]

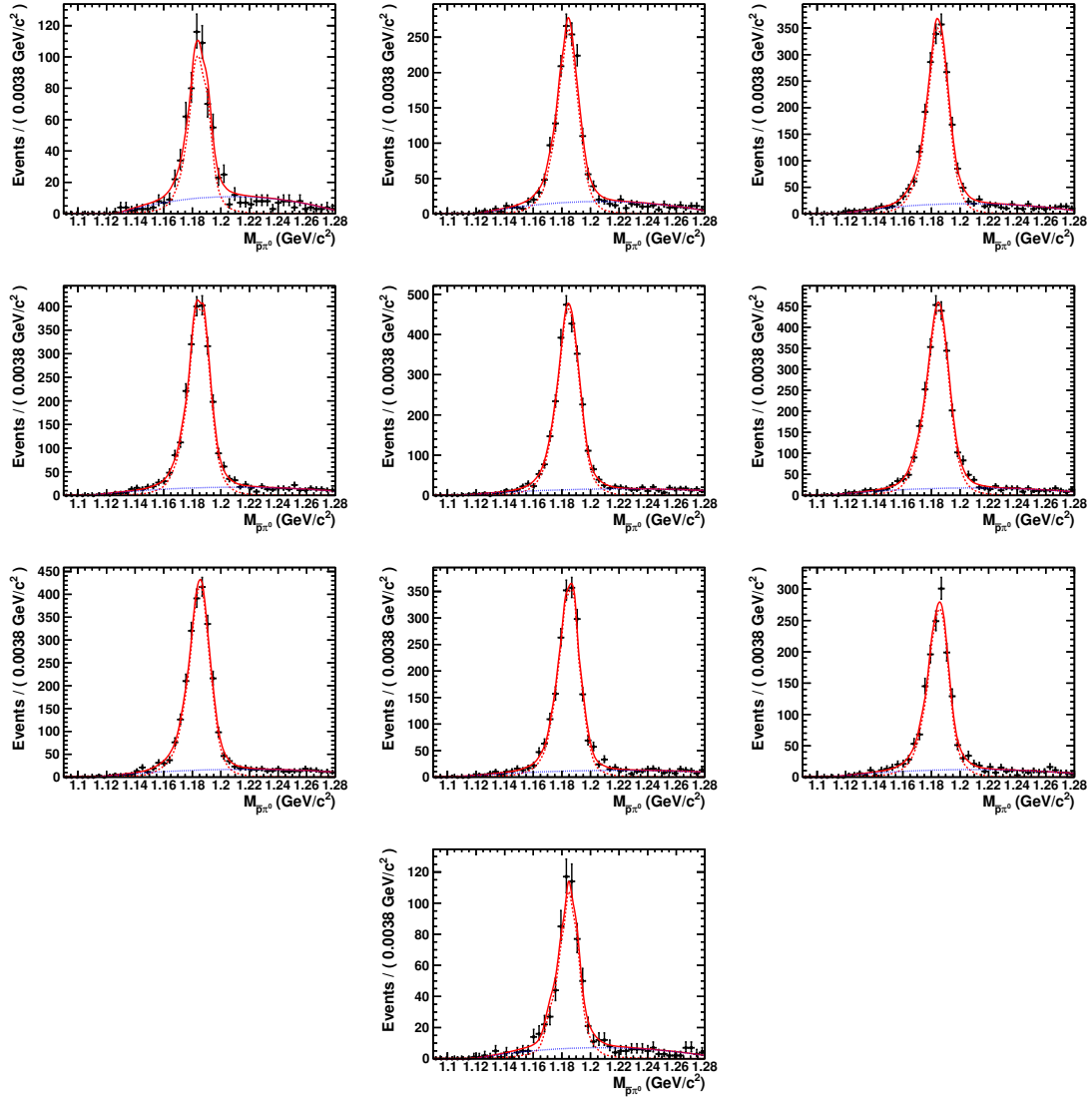


Fig. 54: Momentum: 0.65-0.75 GeV for selecting anti-proton in different $\cos \theta$ range. Front to back angles: [- 1.0, - 0.8], [- 0.8, - 0.6], [- 0.6, - 0.4], [- 0.4, - 0.2], [0.0, 0.2], [0.2, 0.4], [0.4, 0.6], [0.6, 0.8], [0.8, 1.0]

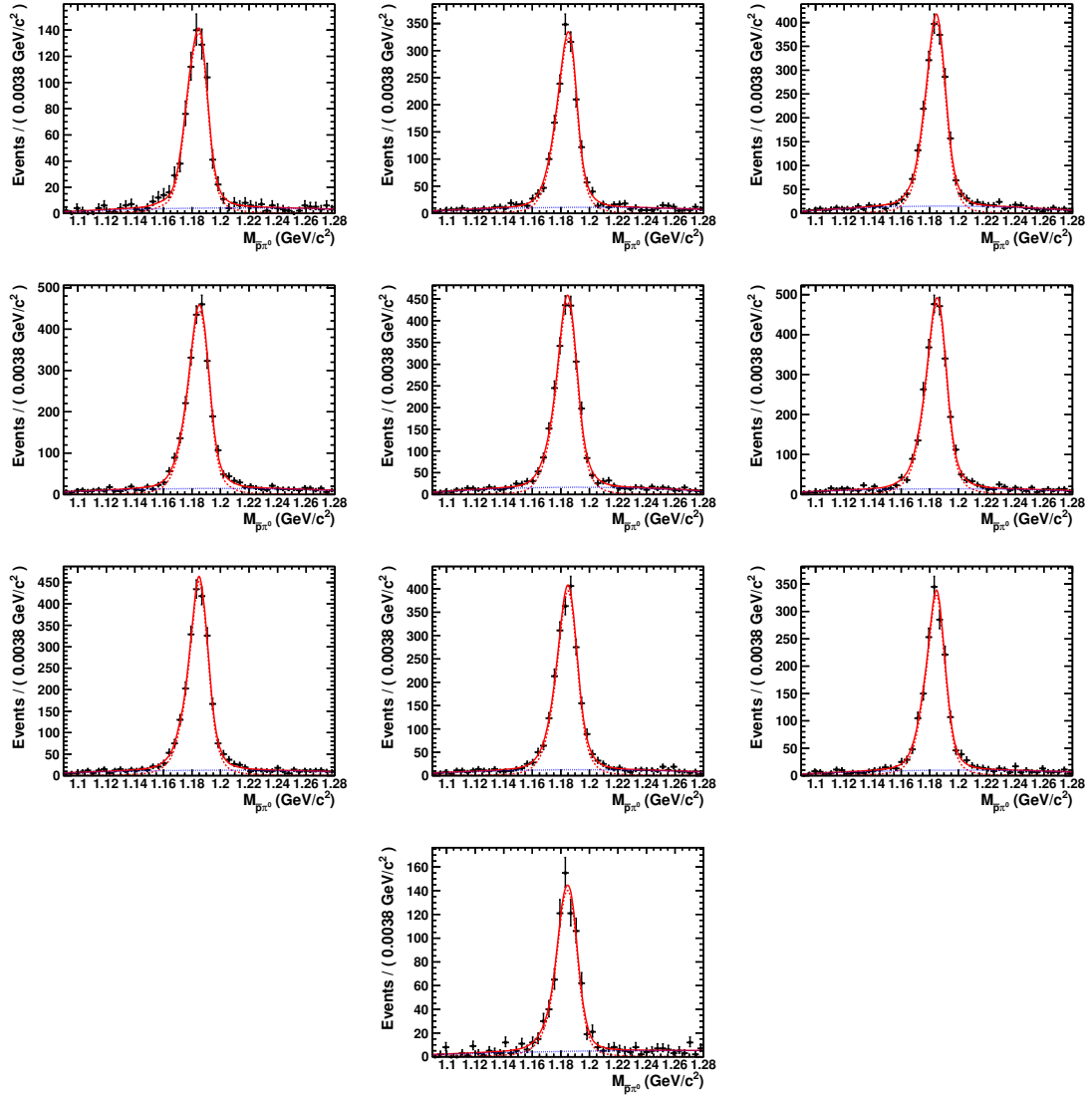


Fig. 55: Momentum: 0.75-0.85 GeV for selecting anti-proton in different $\cos \theta$ range. Front to back angles: [- 1.0, - 0.8], [- 0.8, - 0.6], [- 0.6, - 0.4], [- 0.4, - 0.2], [0.0, 0.2], [0.2, 0.4], [0.4, 0.6], [0.6, 0.8], [0.8, 1.0]

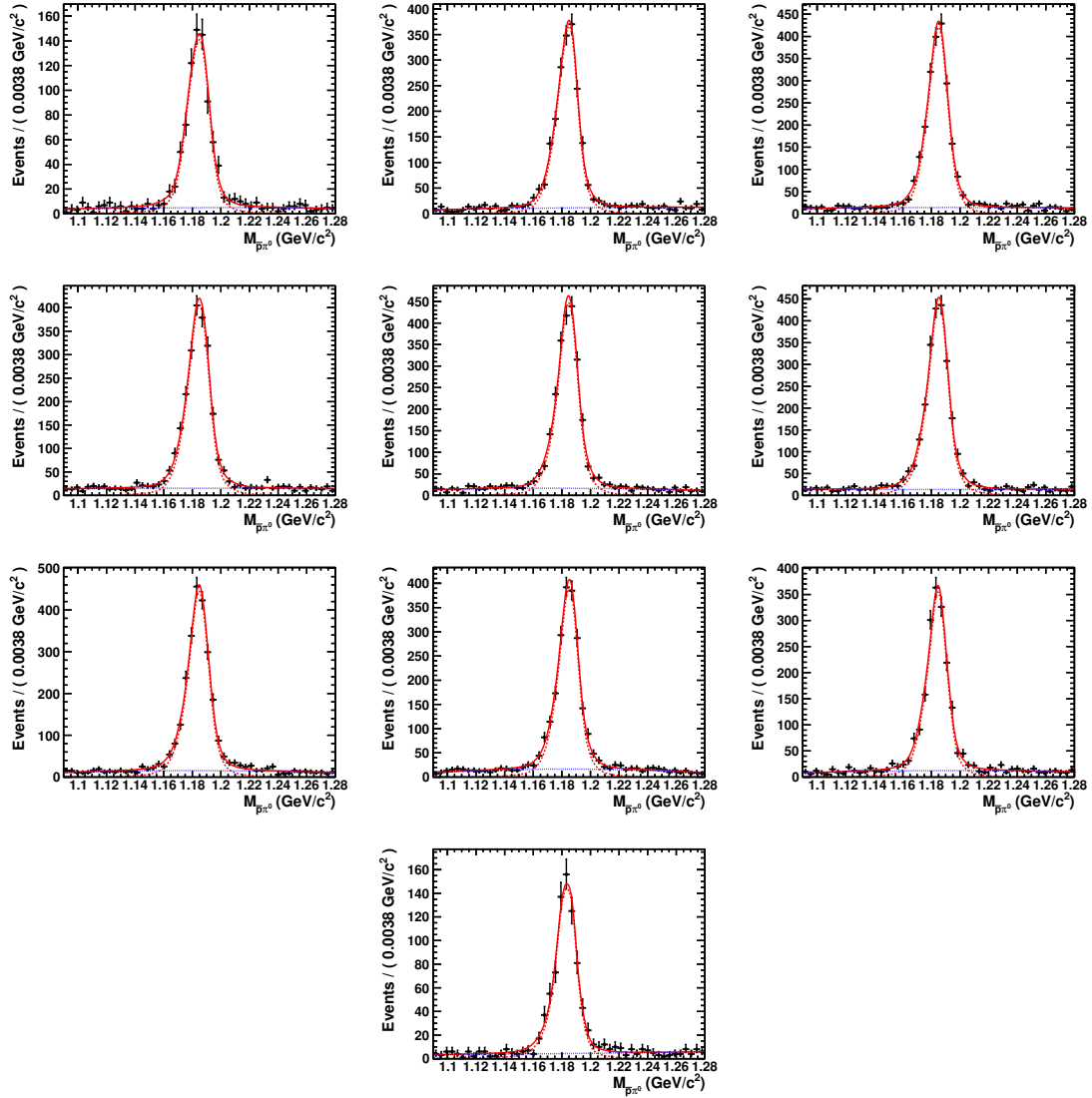


Fig. 56: Momentum: 0.85-0.95 GeV for selecting anti-proton in different $\cos \theta$ range. Front to back angles: [- 1.0, - 0.8], [- 0.8, - 0.6], [- 0.6, - 0.4], [- 0.4, - 0.2], [0.0, 0.2], [0.2, 0.4], [0.4, 0.6], [0.6, 0.8], [0.8, 1.0]

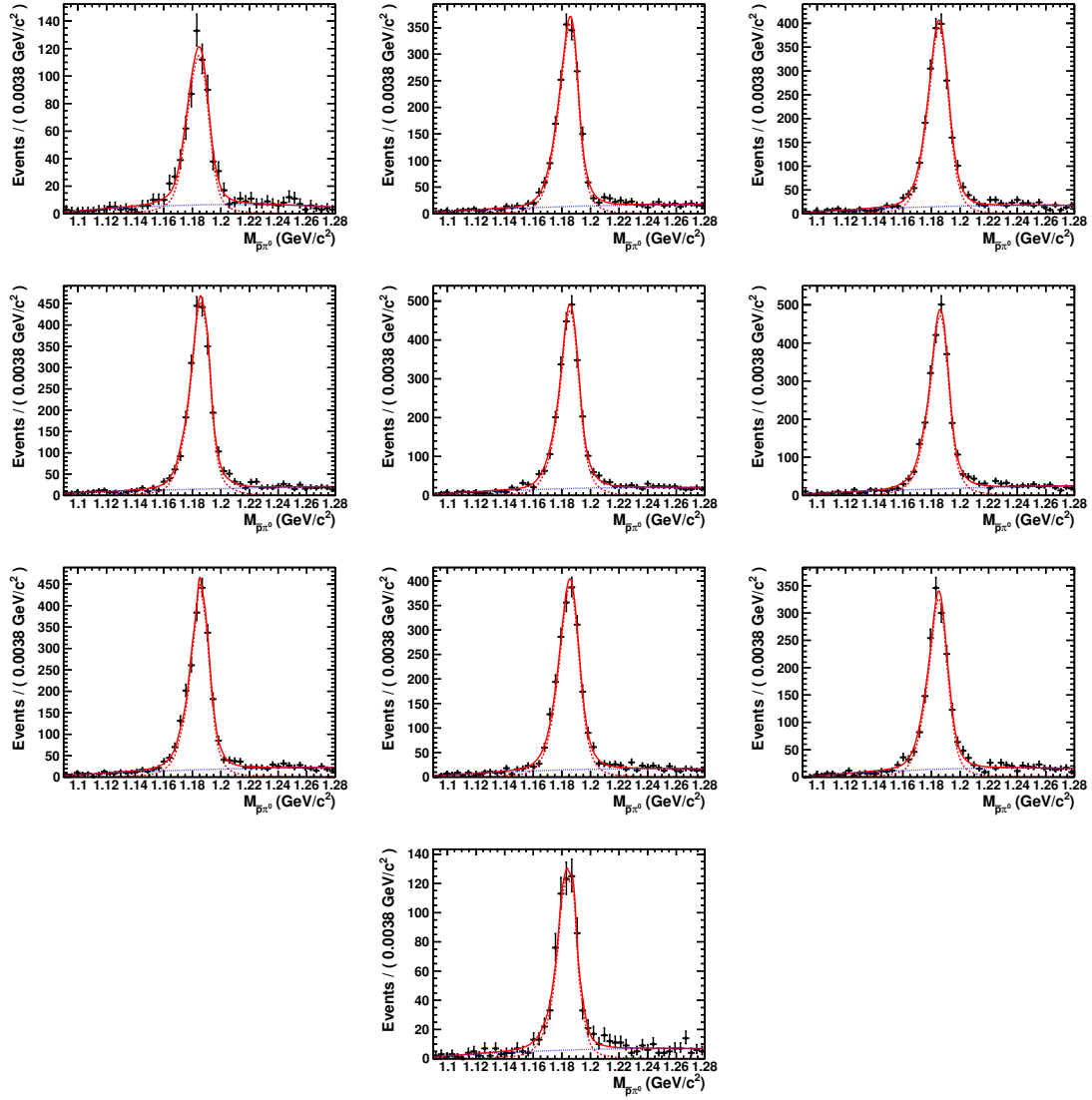


Fig. 57: Momentum: 0.95-1.15 GeV for selecting anti-proton in different $\cos \theta$ range. Front to back angles: [- 1.0, - 0.8], [- 0.8, - 0.6], [- 0.6, - 0.4], [- 0.4, - 0.2], [0.0, 0.2], [0.2, 0.4], [0.4, 0.6], [0.6, 0.8], [0.8, 1.0]

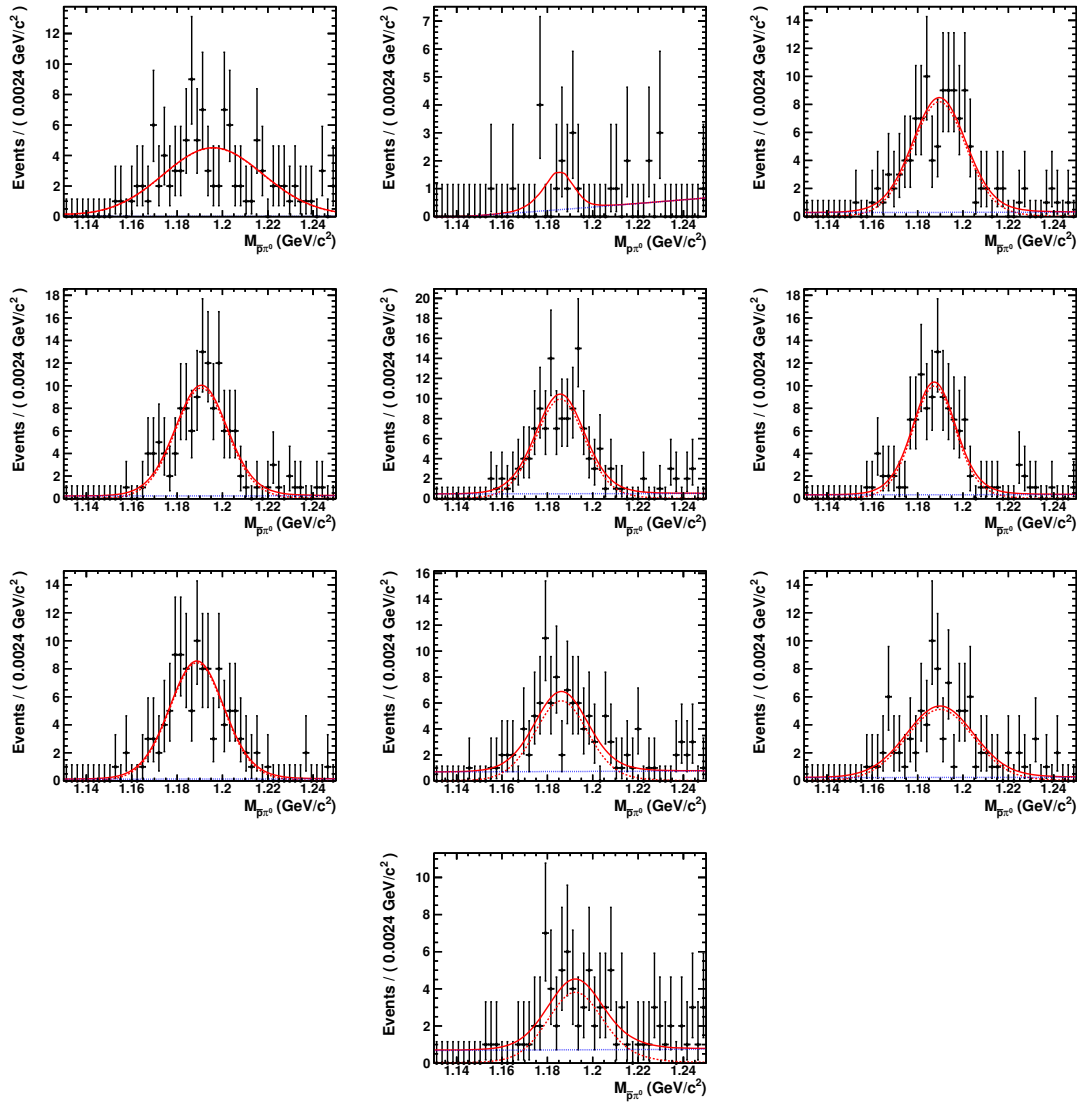
814 B.8.2 Not found \bar{p} 

Fig. 58: Momentum: 0.55-0.65 GeV for no anti-proton is selected in different $\cos \theta$ range. Front to back angles: [- 1.0, - 0.8], [- 0.8, - 0.6], [- 0.6, - 0.4], [- 0.4, - 0.2], [0.0, 0.2], [0.2, 0.4], [0.4, 0.6], [0.6, 0.8], [0.8, 1.0]

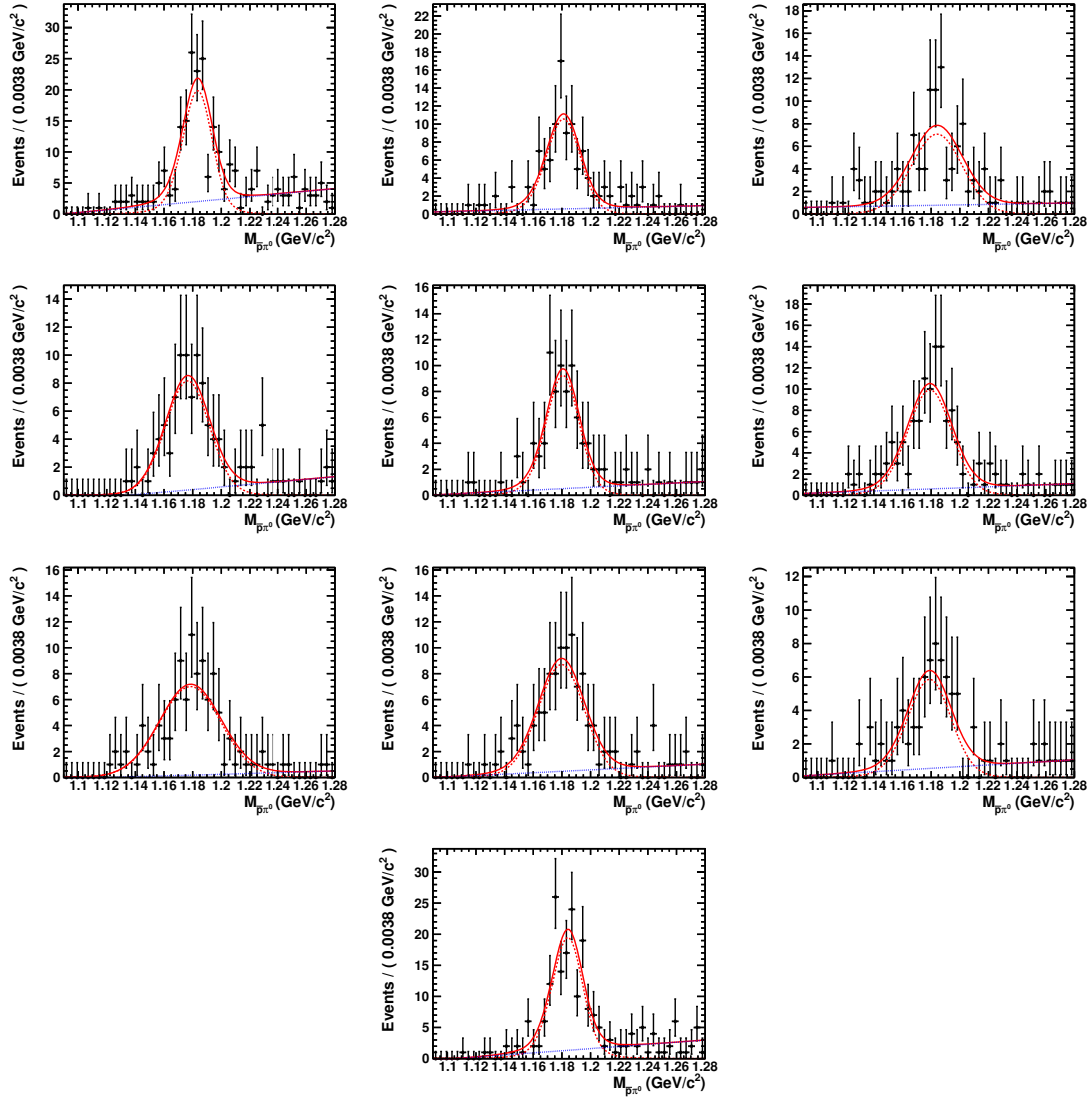


Fig. 59: Momentum: 0.65-0.75 GeV for no anti-proton is selected in different $\cos \theta$ range. Front to back angles: [- 1.0, - 0.8], [- 0.8, - 0.6], [- 0.6, - 0.4], [- 0.4, - 0.2], [0.0, 0.2], [0.2, 0.4], [0.4, 0.6], [0.6, 0.8], [0.8, 1.0]

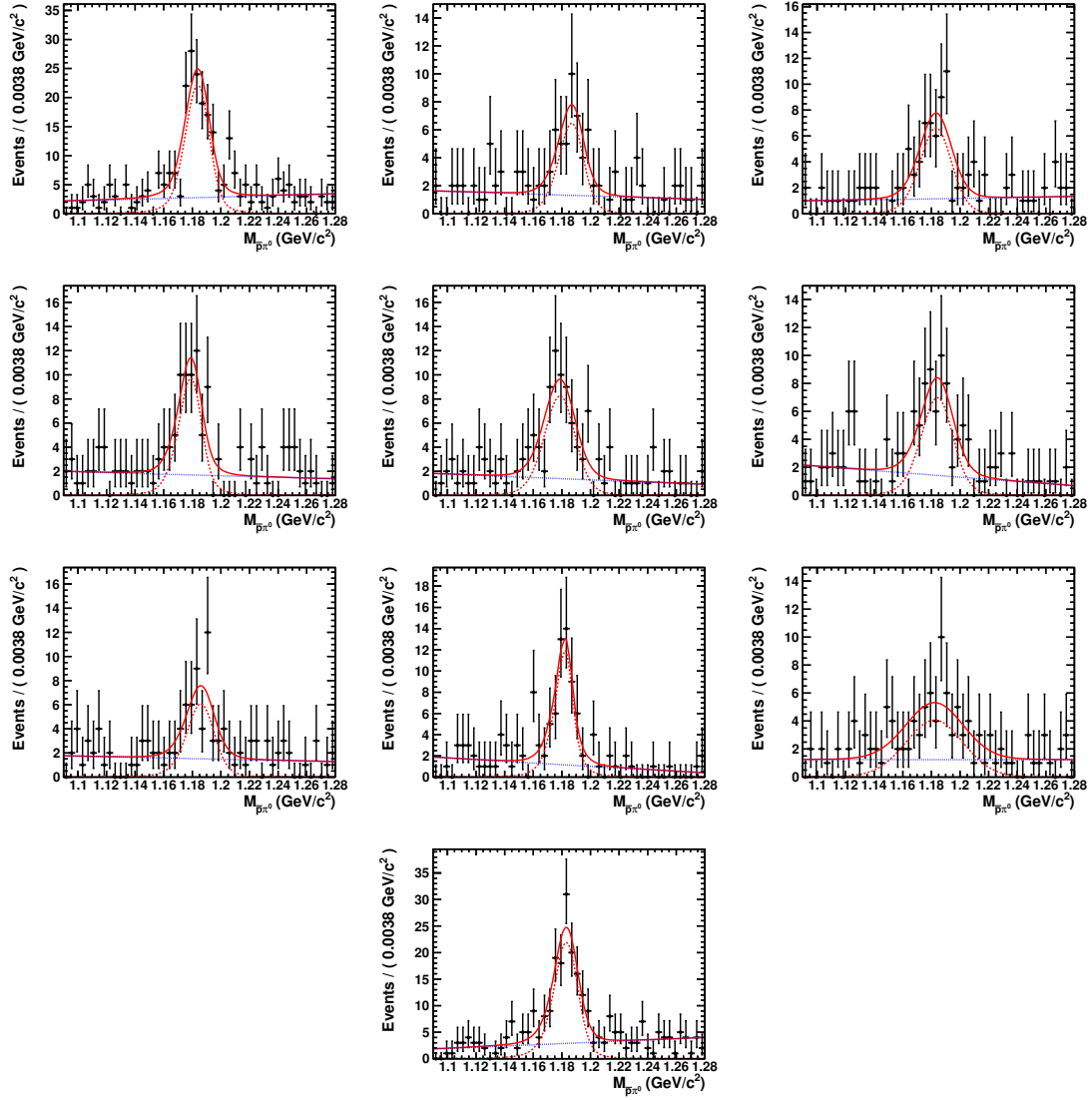


Fig. 60: Momentum: 0.75-0.85 GeV for no anti-proton is selected in different $\cos \theta$ range. Front to back angles: [- 1.0, - 0.8], [- 0.8, - 0.6], [- 0.6, - 0.4], [- 0.4, - 0.2], [0.0, 0.2], [0.2, 0.4], [0.4, 0.6], [0.6, 0.8], [0.8, 1.0]

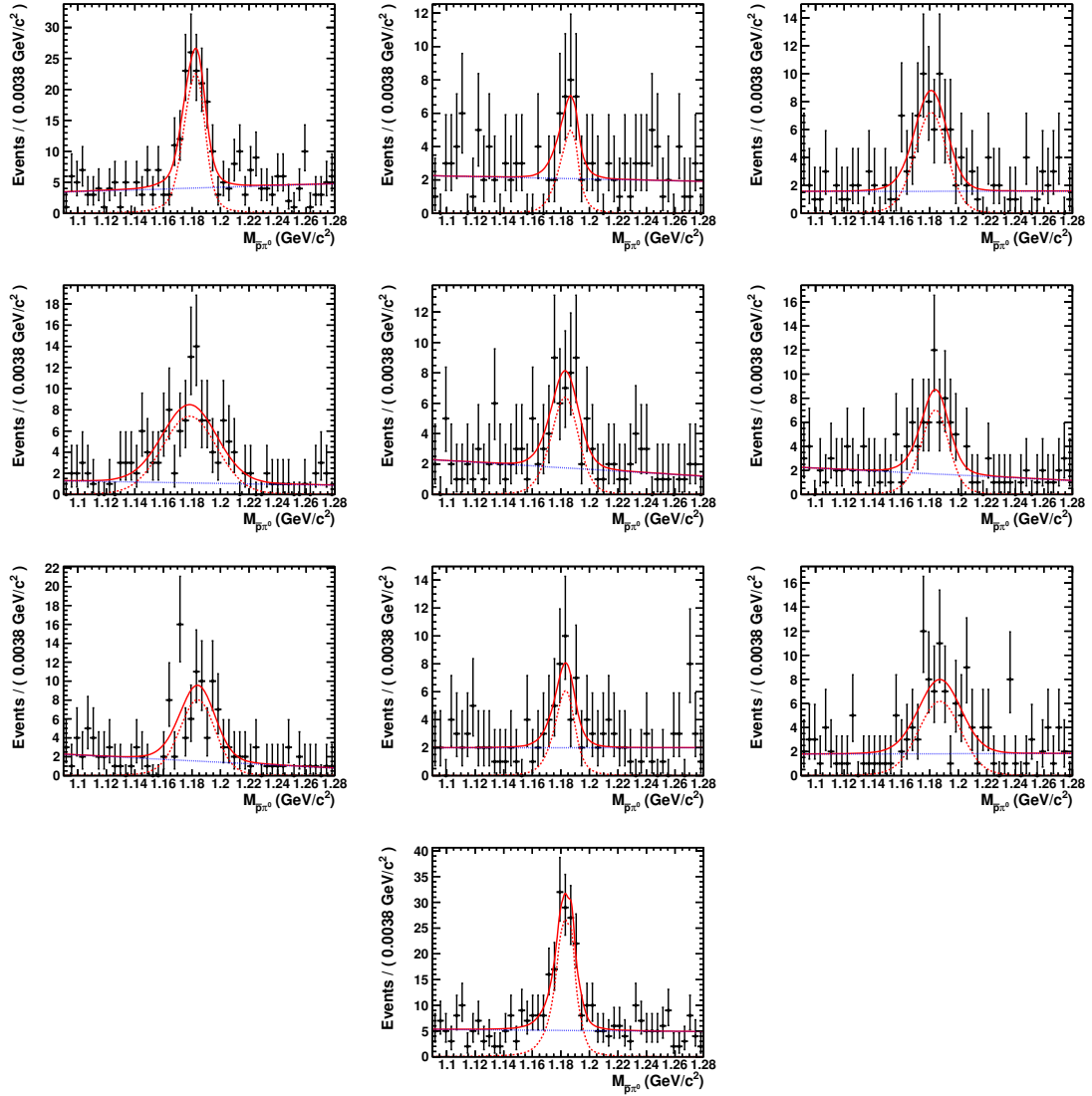


Fig. 61: Momentum: 0.85-0.95 GeV for no anti-proton is selected in different $\cos \theta$ range. Front to back angles: [- 1.0, - 0.8], [- 0.8, - 0.6], [- 0.6, - 0.4], [- 0.4, - 0.2], [0.0, 0.2], [0.2, 0.4], [0.4, 0.6], [0.6, 0.8], [0.8, 1.0]

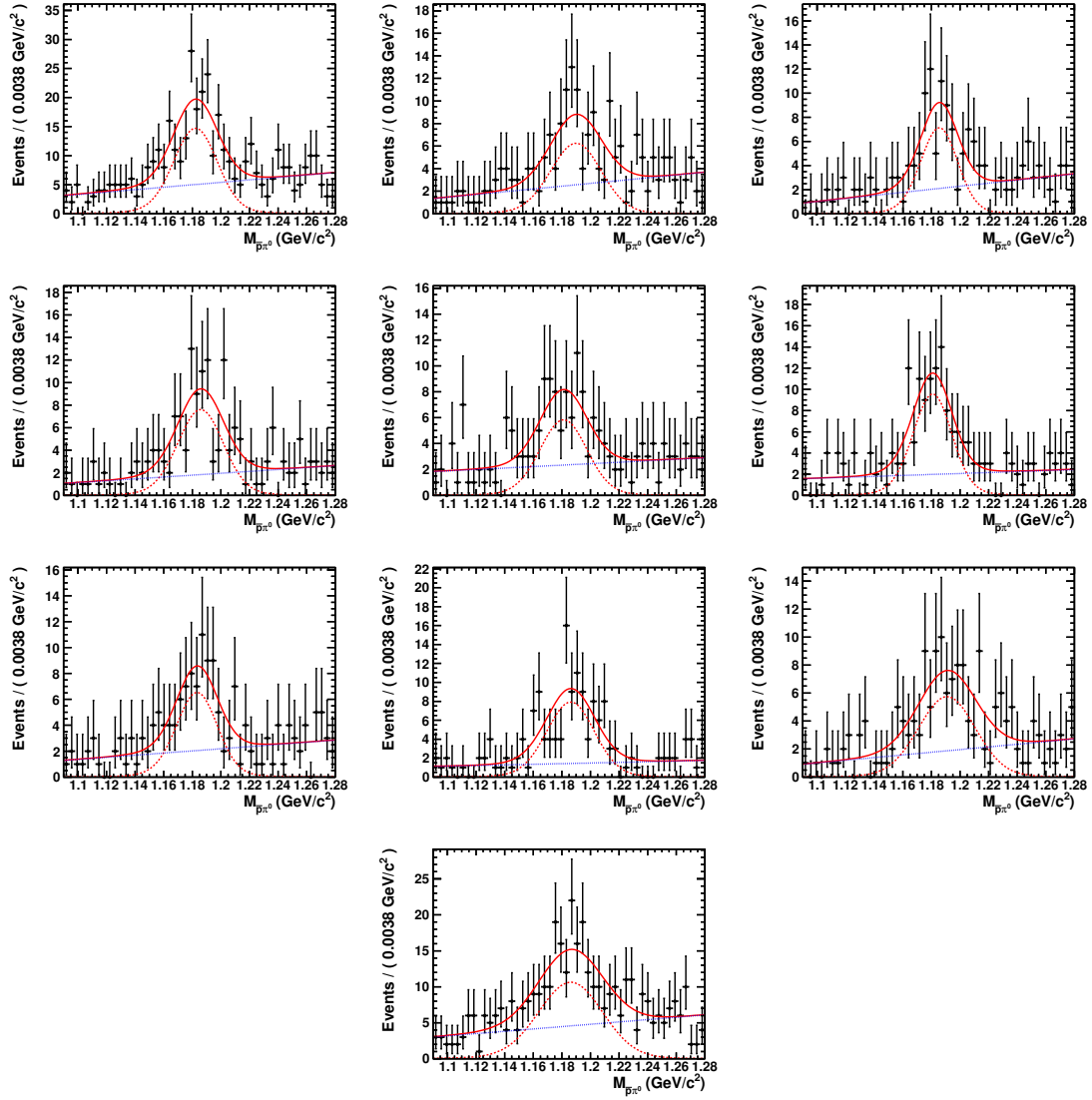


Fig. 62: Momentum: 0.95-1.15 GeV for no anti-proton is selected in different $\cos \theta$ range. Front to back angles: [- 1.0, - 0.8], [- 0.8, - 0.6], [- 0.6, - 0.4], [- 0.4, - 0.2], [0.0, 0.2], [0.2, 0.4], [0.4, 0.6], [0.6, 0.8], [0.8, 1.0]

815 Appendices

816 C The ratio of selection efficiency between data and MC

817 C.1 from our results

Tab. 21: The correction factor $\epsilon_p^{data}/\epsilon_p^{MC}$ in terms of $\cos\theta$ in different momentum range by using control sample $J/\psi(\psi(3686)) \rightarrow \Sigma^+\bar{\Sigma}^- \rightarrow p\bar{p}\pi^0\pi^0$.

Cosθ	[0.45, 0.65] GeV	[0.65, 0.75] GeV	[0.75, 0.85] GeV	[0.85, 0.95] GeV	[0.95, 1.15] GeV
[-1.0, -0.8]	1.0615 ± 0.0376	1.0143 ± 0.0092	1.0058 ± 0.0031	1.0736 ± 0.0036	1.0471 ± 0.0013
[-0.8, -0.6]	1.0016 ± 0.0073	0.9983 ± 0.0036	0.9878 ± 0.0009	0.9975 ± 0.0003	0.9894 ± 0.0009
[-0.6, -0.4]	1.0078 ± 0.0042	0.9937 ± 0.0009	1.0046 ± 0.0002	0.9905 ± 0.0003	0.9896 ± 0.0005
[-0.4, -0.2]	0.9993 ± 0.0065	0.9797 ± 0.0004	0.9909 ± 0.0004	1.0007 ± 0.0001	0.9708 ± 0.0006
[-0.2, 0.0]	0.9987 ± 0.0053	1.0011 ± 0.0004	0.9965 ± 0.0004	0.9829 ± 0.0003	0.9857 ± 0.0003
[0.0, 0.2]	0.9961 ± 0.0104	0.9789 ± 0.0005	1.0004 ± 0.0002	0.9937 ± 0.0006	0.9830 ± 0.0003
[0.2, 0.4]	0.9906 ± 0.0029	1.0021 ± 0.0009	0.9967 ± 0.0002	0.9894 ± 0.0003	0.9827 ± 0.0003
[0.4, 0.6]	0.9842 ± 0.0030	1.0026 ± 0.0005	1.0016 ± 0.0005	0.9997 ± 0.0001	0.9893 ± 0.0002
[0.6, 0.8]	0.9971 ± 0.0011	1.0051 ± 0.0039	0.9917 ± 0.0025	1.0014 ± 0.0005	0.9939 ± 0.0004
[0.8, 1.0]	0.9767 ± 0.0286	1.0311 ± 0.0077	0.9820 ± 0.0031	1.0535 ± 0.0036	1.0056 ± 0.0023

Tab. 22: The correction factor $\epsilon_{\bar{p}}^{data}/\epsilon_{\bar{p}}^{MC}$ in terms of $\cos\theta$ in different momentum range by using control sample $J/\psi(\psi(3686)) \rightarrow \Sigma^+\bar{\Sigma}^- \rightarrow p\bar{p}\pi^0\pi^0$.

Cosθ	[0.45, 0.65] GeV	[0.65, 0.75] GeV	[0.75, 0.85] GeV	[0.85, 0.95] GeV	[0.95, 1.15] GeV
[-1.0, -0.8]	0.9005 ± 0.0376	1.0168 ± 0.0092	1.0000 ± 0.0031	1.0000 ± 0.0036	1.0000 ± 0.0013
[-0.8, -0.6]	0.9900 ± 0.0073	1.0000 ± 0.0036	1.0000 ± 0.0009	1.0000 ± 0.0003	1.0000 ± 0.0009
[-0.6, -0.4]	0.9869 ± 0.0042	1.0000 ± 0.0009	1.0000 ± 0.0002	1.0000 ± 0.0003	1.0000 ± 0.0005
[-0.4, -0.2]	0.9756 ± 0.0065	1.0000 ± 0.0004	1.0000 ± 0.0004	1.0000 ± 0.0001	1.0000 ± 0.0006
[-0.2, 0.0]	0.9426 ± 0.0053	1.0000 ± 0.0004	1.0000 ± 0.0004	1.0000 ± 0.0003	1.0000 ± 0.0003
[0.0, 0.2]	0.9389 ± 0.0104	1.0000 ± 0.0005	1.0000 ± 0.0002	1.0000 ± 0.0006	1.0000 ± 0.0003
[0.2, 0.4]	0.9851 ± 0.0029	1.0000 ± 0.0009	1.0000 ± 0.0002	1.0000 ± 0.0003	1.0000 ± 0.0003
[0.4, 0.6]	0.9918 ± 0.0030	1.0000 ± 0.0005	1.0000 ± 0.0005	1.0000 ± 0.0001	1.0000 ± 0.0002
[0.6, 0.8]	0.9877 ± 0.0039	1.0000 ± 0.0025	1.0000 ± 0.0005	1.0000 ± 0.0004	1.0000 ± 0.0011
[0.8, 1.0]	0.9506 ± 0.0286	1.0191 ± 0.0077	1.0070 ± 0.0031	1.0000 ± 0.0036	1.0000 ± 0.0023

Tab. 23: The correction factor $\epsilon_{\pi^0}^{data}/\epsilon_{\pi^0}^{MC}$ in terms of $\cos\theta$ in different momentum range using control sample $J/\psi(\psi(3686)) \rightarrow \Sigma^+\bar{\Sigma}^- \rightarrow p\bar{p}\pi^0\pi^0$

Cosθ	[0.05, 0.15] GeV	[0.15, 0.25] GeV	[0.25, 0.35] GeV	[0.35, 0.45] GeV
[-1.0, -0.8]	0.9960 ± 0.0167	1.0003 ± 0.0156	0.9641 ± 0.0214	0.9758 ± 0.0372
[-0.8, -0.6]	0.9859 ± 0.0163	0.9908 ± 0.0145	0.9793 ± 0.0153	0.9772 ± 0.0216
[-0.6, -0.4]	0.9698 ± 0.0176	0.9897 ± 0.0136	0.9808 ± 0.0105	0.9664 ± 0.0138
[-0.4, -0.2]	1.0063 ± 0.0170	0.9990 ± 0.0145	0.9899 ± 0.0113	1.0049 ± 0.0026
[-0.2, 0.0]	0.9899 ± 0.0177	0.9950 ± 0.0099	0.9933 ± 0.0123	0.9887 ± 0.0015
[0.0, 0.2]	0.9966 ± 0.0178	0.9808 ± 0.0098	0.9914 ± 0.0118	0.9757 ± 0.0057
[0.2, 0.4]	1.0373 ± 0.0198	0.9890 ± 0.0046	0.9994 ± 0.0135	0.9797 ± 0.0097
[0.4, 0.6]	0.9875 ± 0.0167	0.9909 ± 0.0062	0.9803 ± 0.0152	0.9832 ± 0.0069
[0.6, 0.8]	0.9906 ± 0.0163	0.9878 ± 0.0156	0.9975 ± 0.0188	1.0347 ± 0.0123
[0.8, 1.0]	0.9889 ± 0.0163	0.9882 ± 0.0166	0.9743 ± 0.0219	0.9604 ± 0.0131

818 **C.2 from other results**

Tab. 24: The correction factor $\epsilon_{\bar{p}}^{data}/\epsilon_{\bar{p}}^{MC}$ in terms of $\cos\theta$ in different momentum range by using control sample $J/\psi \rightarrow p\bar{p}\pi^+\pi^-$.

$\cos\theta$	[0.2, 0.3] GeV	[0.3, 0.4] GeV	[0.4, 0.5] GeV	[0.5, 0.6] GeV	[0.6, 0.7] GeV	[0.7, 0.8] GeV	[0.8, 0.9] GeV	[0.9, 1.0] GeV
[-1.0, -0.8]	0.9005 \pm 0.0376	1.0168 \pm 0.0092	1.0000 \pm 0.0031	1.0000 \pm 0.0036	1.0000 \pm 0.0013	1.0000 \pm 0.0019	0.9919 \pm 0.0028	0.9900 \pm 0.0038
[-0.8, -0.6]	0.9900 \pm 0.0073	1.0000 \pm 0.0036	1.0000 \pm 0.0009	1.0000 \pm 0.0003	1.0000 \pm 0.0009	1.0000 \pm 0.0010	1.0000 \pm 0.0013	1.0000 \pm 0.0010
[-0.6, -0.4]	0.9869 \pm 0.0042	1.0000 \pm 0.0009	1.0000 \pm 0.0002	1.0000 \pm 0.0003	1.0000 \pm 0.0005	1.0000 \pm 0.0007	1.0000 \pm 0.0006	1.0000 \pm 0.0009
[-0.4, -0.2]	0.9756 \pm 0.0065	1.0000 \pm 0.0004	1.0000 \pm 0.0004	1.0000 \pm 0.0001	1.0000 \pm 0.0006	1.0000 \pm 0.0005	1.0000 \pm 0.0006	1.0000 \pm 0.0010
[-0.2, 0.0]	0.9426 \pm 0.0053	1.0000 \pm 0.0004	1.0000 \pm 0.0004	1.0000 \pm 0.0003	1.0000 \pm 0.0003	1.0000 \pm 0.0007	1.0000 \pm 0.0007	1.0000 \pm 0.0006
[0.0, 0.2]	0.9389 \pm 0.0104	1.0000 \pm 0.0005	1.0000 \pm 0.0002	1.0000 \pm 0.0006	1.0000 \pm 0.0003	1.0000 \pm 0.0005	1.0000 \pm 0.0005	1.0000 \pm 0.0018
[0.2, 0.4]	0.9851 \pm 0.0029	1.0000 \pm 0.0009	1.0000 \pm 0.0002	1.0000 \pm 0.0003	1.0000 \pm 0.0003	1.0000 \pm 0.0005	1.0000 \pm 0.0006	1.0000 \pm 0.0013
[0.4, 0.6]	0.9918 \pm 0.0030	1.0000 \pm 0.0005	1.0000 \pm 0.0005	1.0000 \pm 0.0001	1.0000 \pm 0.0002	1.0000 \pm 0.0004	1.0000 \pm 0.0009	1.0000 \pm 0.0013
[0.6, 0.8]	0.9877 \pm 0.0039	1.0000 \pm 0.0025	1.0000 \pm 0.0005	1.0000 \pm 0.0004	1.0000 \pm 0.0011	1.0000 \pm 0.0010	1.0000 \pm 0.0011	1.0000 \pm 0.0012
[0.8, 1.0]	0.9506 \pm 0.0286	1.0191 \pm 0.0077	1.0070 \pm 0.0031	1.0000 \pm 0.0036	1.0000 \pm 0.0023	1.0000 \pm 0.0014	1.0000 \pm 0.0046	1.0000 \pm 0.0056

Tab. 25: The correction factor $\epsilon_{\bar{p}}^{data}/\epsilon_{\bar{p}}^{MC}$ in terms of $\cos\theta$ in different momentum range by using control sample $J/\psi \rightarrow p\bar{p}\pi^+\pi^-$ (2012 year).

$\cos\theta$	[0.2, 0.3] GeV	[0.3, 0.4] GeV	[0.4, 0.5] GeV	[0.5, 0.6] GeV	[0.6, 0.7] GeV	[0.7, 0.8] GeV	[0.8, 0.9] GeV	[0.9, 1.0] GeV
[-1.0, -0.8]	2.3589 \pm 0.2068	1.0587 \pm 0.0175	1.0000 \pm 0.0065	0.9918 \pm 0.0019	1.0000 \pm 0.0019	1.0000 \pm 0.0042	0.9935 \pm 0.0014	1.0000 \pm 0.0029
[-0.8, -0.6]	1.0142 \pm 0.0114	1.0000 \pm 0.0025	1.0000 \pm 0.0006	1.0000 \pm 0.0004	1.0000 \pm 0.0003	1.0000 \pm 0.0004	1.0000 \pm 0.0009	1.0000 \pm 0.0010
[-0.6, -0.4]	0.9707 \pm 0.0031	1.0000 \pm 0.0004	1.0000 \pm 0.0004	1.0000 \pm 0.0003	1.0000 \pm 0.0004	1.0000 \pm 0.0005	1.0000 \pm 0.0012	1.0000 \pm 0.0009
[-0.4, -0.2]	0.9704 \pm 0.0033	1.0000 \pm 0.0003	1.0000 \pm 0.0004	1.0000 \pm 0.0002	1.0000 \pm 0.0003	1.0000 \pm 0.0004	1.0000 \pm 0.0005	1.0000 \pm 0.0016
[-0.2, 0.0]	0.9238 \pm 0.0046	1.0000 \pm 0.0019	1.0000 \pm 0.0006	1.0000 \pm 0.0003	1.0000 \pm 0.0004	1.0000 \pm 0.0004	1.0000 \pm 0.0005	1.0000 \pm 0.0008
[0.0, 0.2]	0.9238 \pm 0.0047	1.0000 \pm 0.0020	1.0000 \pm 0.0004	1.0000 \pm 0.0004	1.0000 \pm 0.0003	1.0000 \pm 0.0003	1.0000 \pm 0.0006	1.0000 \pm 0.0014
[0.2, 0.4]	0.9830 \pm 0.0036	1.0000 \pm 0.0003	1.0000 \pm 0.0002	1.0000 \pm 0.0002	1.0000 \pm 0.0003	1.0000 \pm 0.0004	1.0000 \pm 0.0007	1.0000 \pm 0.0012
[0.4, 0.6]	0.9815 \pm 0.0031	1.0000 \pm 0.0008	1.0000 \pm 0.0004	1.0000 \pm 0.0002	1.0000 \pm 0.0002	1.0000 \pm 0.0005	1.0000 \pm 0.0011	1.0000 \pm 0.0015
[0.6, 0.8]	1.0326 \pm 0.0097	1.0000 \pm 0.0025	1.0000 \pm 0.0012	1.0000 \pm 0.0002	1.0000 \pm 0.0003	1.0000 \pm 0.0005	1.0000 \pm 0.0006	1.0000 \pm 0.0012
[0.8, 1.0]	2.0037 \pm 0.1134	1.0687 \pm 0.0225	1.0073 \pm 0.0062	0.9894 \pm 0.0022	1.0000 \pm 0.0019	0.9943 \pm 0.0007	0.9903 \pm 0.0012	1.0000 \pm 0.0039

Tab. 26: The correction factor $\epsilon_{\bar{p}}^{data}/\epsilon_{\bar{p}}^{MC}$ in terms of $\cos\theta$ in different momentum range by using control sample $J/\psi \rightarrow p\bar{p}\pi^+\pi^-$ (2018 year).

$\cos\theta$	[0.2, 0.3] GeV	[0.3, 0.4] GeV	[0.4, 0.5] GeV	[0.5, 0.6] GeV	[0.6, 0.7] GeV	[0.7, 0.8] GeV	[0.8, 0.9] GeV	[0.9, 1.0] GeV
[-1.0, -0.8]	0.9279 \pm 0.0112	1.0156 \pm 0.0063	1.0000 \pm 0.0049	1.0000 \pm 0.0010	1.0000 \pm 0.0004	1.0000 \pm 0.0005	1.0000 \pm 0.0007	1.0000 \pm 0.0018
[-0.8, -0.6]	0.9874 \pm 0.0022	1.0000 \pm 0.0019	1.0000 \pm 0.0002	1.0000 \pm 0.0001	1.0000 \pm 0.0004	1.0000 \pm 0.0003	1.0000 \pm 0.0007	1.0000 \pm 0.0012
[-0.6, -0.4]	1.0000 \pm 0.0045	1.0000 \pm 0.0008	1.0000 \pm 0.0002	1.0000 \pm 0.0001	1.0000 \pm 0.0006	1.0000 \pm 0.0003	1.0000 \pm 0.0011	1.0000 \pm 0.0014
[-0.4, -0.2]	0.9875 \pm 0.0035	1.0000 \pm 0.0003	1.0000 \pm 0.0002	1.0000 \pm 0.0001	1.0000 \pm 0.0004	1.0000 \pm 0.0004	1.0000 \pm 0.0005	1.0000 \pm 0.0012
[-0.2, 0.0]	0.8910 \pm 0.0042	1.0000 \pm 0.0024	1.0000 \pm 0.0005	1.0000 \pm 0.0002	1.0000 \pm 0.0002	1.0000 \pm 0.0004	1.0000 \pm 0.0006	1.0000 \pm 0.0010
[0.0, 0.2]	0.8860 \pm 0.0057	1.0000 \pm 0.0021	1.0000 \pm 0.0003	1.0000 \pm 0.0001	1.0000 \pm 0.0005	1.0000 \pm 0.0003	1.0000 \pm 0.0006	1.0000 \pm 0.0008
[0.2, 0.4]	0.9863 \pm 0.0045	1.0000 \pm 0.0002	1.0000 \pm 0.0001	1.0000 \pm 0.0001	1.0000 \pm 0.0006	1.0000 \pm 0.0007	1.0000 \pm 0.0007	1.0000 \pm 0.0012
[0.4, 0.6]	1.0000 \pm 0.0028	1.0000 \pm 0.0007	1.0000 \pm 0.0001	1.0000 \pm 0.0000	1.0000 \pm 0.0005	1.0000 \pm 0.0003	1.0000 \pm 0.0009	1.0000 \pm 0.0016
[0.6, 0.8]	0.9907 \pm 0.0028	1.0000 \pm 0.0036	1.0000 \pm 0.0002	1.0000 \pm 0.0002	1.0000 \pm 0.0003	1.0000 \pm 0.0003	1.0000 \pm 0.0007	1.0000 \pm 0.0016
[0.8, 1.0]	0.9394 \pm 0.0106	1.0260 \pm 0.0081	1.0000 \pm 0.0044	1.0000 \pm 0.0013	1.0000 \pm 0.0016	1.0000 \pm 0.0009	1.0000 \pm 0.0007	1.0000 \pm 0.0043

Tab. 27: The correction factor $\epsilon_{\bar{p}}^{data}/\epsilon_{\bar{p}}^{MC}$ in terms of $\cos\theta$ in different momentum range by using control sample $J/\psi \rightarrow p\bar{p}\pi^+\pi^-$ (2019 year).

$\cos\theta$	[0.2, 0.3] GeV	[0.3, 0.4] GeV	[0.4, 0.5] GeV	[0.5, 0.6] GeV	[0.6, 0.7] GeV	[0.7, 0.8] GeV	[0.8, 0.9] GeV	[0.9, 1.0] GeV
[-1.0, -0.8]	0.8734 \pm 0.0133	1.0157 \pm 0.0057	1.0000 \pm 0.0020	1.0000 \pm 0.0006	1.0000 \pm 0.0007	1.0000 \pm 0.0010	1.0000 \pm 0.0006	1.0000 \pm 0.0006
[-0.8, -0.6]	0.9440 \pm 0.0030	1.0000 \pm 0.0025	1.0000 \pm 0.0003	1.0000 \pm 0.0002	1.0000 \pm 0.0005	1.0000 \pm 0.0006	1.0000 \pm 0.0011	1.0000 \pm 0.0010
[-0.6, -0.4]	0.9700 \pm 0.0017	1.0000 \pm 0.0003	1.0000 \pm 0.0001	1.0000 \pm 0.0001	1.0000 \pm 0.0002	1.0000 \pm 0.0003	1.0000 \pm 0.0006	1.0000 \pm 0.0015
[-0.4, -0.2]	0.9718 \pm 0.0036	1.0000 \pm 0.0002	1.0000 \pm 0.0002	1.0000 \pm 0.0003	1.0000 \pm 0.0004	1.0000 \pm 0.0003	1.0000 \pm 0.0010	1.0000 \pm 0.0007
[-0.2, 0.0]	0.8952 \pm 0.0069	1.0000 \pm 0.0026	1.0000 \pm 0.0003	1.0000 \pm 0.0001	1.0000 \pm 0.0003	1.0000 \pm 0.0005	1.0000 \pm 0.0004	1.0000 \pm 0.0009
[0.0, 0.2]	0.9031 \pm 0.0053	1.0000 \pm 0.0016	1.0000 \pm 0.0003	1.0000 \pm 0.0001	1.0000 \pm 0.0003	1.0000 \pm 0.0004	1.0000 \pm 0.0004	1.0000 \pm 0.0011
[0.2, 0.4]	0.9816 \pm 0.0033	1.0000 \pm 0.0002	1.0000 \pm 0.0001	1.0000 \pm 0.0001	1.0000 \pm 0.0001	1.0000 \pm 0.0003	1.0000 \pm 0.0006	1.0000 \pm 0.0007
[0.4, 0.6]	0.9808 \pm 0.0020	1.0000 \pm 0.0007	1.0000 \pm 0.0001	1.0000 \pm 0.0001	1.0000 \pm 0.0003	1.0000 \pm 0.0004	1.0000 \pm 0.0013	1.0000 \pm 0.0010
[0.6, 0.8]	0.9563 \pm 0.0025	1.0000 \pm 0.0026	1.0000 \pm 0.0002	1.0000 \pm 0.0001	1.0000 \pm 0.0002	1.0000 \pm 0.0003	1.0000 \pm 0.0005	1.0000 \pm 0.0017
[0.8, 1.0]	0.9038 $\pm</math$							

Tab. 28: The correction factor $\epsilon_p^{data}/\epsilon_p^{MC}$ in terms of $\cos\theta$ in different momentum range by using control sample $J/\psi \rightarrow p\bar{p}\pi^+\pi^-$ (2009 year).

$\cos\theta$	[0.2, 0.3] GeV	[0.3, 0.4] GeV	[0.4, 0.5] GeV	[0.5, 0.6] GeV	[0.6, 0.7] GeV	[0.7, 0.8] GeV	[0.8, 0.9] GeV	[0.9, 1.0] GeV
[-1.0, -0.8]	0.9631 \pm 0.0204	1.0228 \pm 0.0085	1.0122 \pm 0.0068	1.0000 \pm 0.0022	1.0000 \pm 0.0013	1.0000 \pm 0.0010	0.9919 \pm 0.0019	1.0000 \pm 0.0044
[-0.8, -0.6]	0.9885 \pm 0.0050	1.0000 \pm 0.0037	1.0000 \pm 0.0015	1.0000 \pm 0.0006	1.0000 \pm 0.0009	1.0000 \pm 0.0014	1.0000 \pm 0.0012	1.0000 \pm 0.0018
[-0.6, -0.4]	0.9895 \pm 0.0031	1.0000 \pm 0.0035	1.0000 \pm 0.0027	1.0000 \pm 0.0033	1.0000 \pm 0.0013	1.0000 \pm 0.0009	1.0000 \pm 0.0010	1.0000 \pm 0.0010
[-0.4, -0.2]	0.9820 \pm 0.0046	1.0000 \pm 0.0027	1.0000 \pm 0.0021	1.0000 \pm 0.0010	1.0000 \pm 0.0017	1.0000 \pm 0.0007	1.0000 \pm 0.0010	1.0000 \pm 0.0005
[-0.2, 0.0]	0.9087 \pm 0.0104	1.0000 \pm 0.0034	1.0000 \pm 0.0030	1.0000 \pm 0.0011	1.0000 \pm 0.0007	1.0000 \pm 0.0006	1.0000 \pm 0.0008	1.0000 \pm 0.0007
[0.0, 0.2]	0.8990 \pm 0.0075	1.0000 \pm 0.0018	1.0000 \pm 0.0029	1.0000 \pm 0.0013	1.0000 \pm 0.0007	1.0000 \pm 0.0009	1.0000 \pm 0.0008	1.0000 \pm 0.0007
[0.2, 0.4]	0.9720 \pm 0.0049	1.0000 \pm 0.0041	1.0000 \pm 0.0028	1.0000 \pm 0.0016	1.0000 \pm 0.0021	1.0000 \pm 0.0010	1.0000 \pm 0.0008	1.0000 \pm 0.0011
[0.4, 0.6]	0.9882 \pm 0.0046	1.0000 \pm 0.0034	1.0000 \pm 0.0025	1.0000 \pm 0.0016	1.0000 \pm 0.0008	1.0000 \pm 0.0009	1.0000 \pm 0.0011	1.0000 \pm 0.0014
[0.6, 0.8]	0.9867 \pm 0.0049	1.0000 \pm 0.0037	1.0000 \pm 0.0013	1.0000 \pm 0.0007	1.0000 \pm 0.0009	1.0000 \pm 0.0027	1.0000 \pm 0.0011	1.0000 \pm 0.0012
[0.8, 1.0]	0.9497 \pm 0.0192	1.0176 \pm 0.0062	1.0099 \pm 0.0045	1.0000 \pm 0.0017	1.0000 \pm 0.0020	1.0000 \pm 0.0011	1.0000 \pm 0.0017	1.0000 \pm 0.0033

Tab. 29: The correction factor $\epsilon_p^{data}/\epsilon_p^{MC}$ in terms of $\cos\theta$ in different momentum range by using control sample $J/\psi \rightarrow p\bar{p}\pi^+\pi^-$ (2012 year).

$\cos\theta$	[0.2, 0.3] GeV	[0.3, 0.4] GeV	[0.4, 0.5] GeV	[0.5, 0.6] GeV	[0.6, 0.7] GeV	[0.7, 0.8] GeV	[0.8, 0.9] GeV	[0.9, 1.0] GeV
[-1.0, -0.8]	2.1201 \pm 0.1244	1.0658 \pm 0.0188	1.0165 \pm 0.0055	1.0085 \pm 0.0029	1.0000 \pm 0.0034	1.0000 \pm 0.0010	1.0000 \pm 0.0016	1.0000 \pm 0.0044
[-0.8, -0.6]	1.0327 \pm 0.0100	1.0000 \pm 0.0034	1.0000 \pm 0.0022	1.0000 \pm 0.0005	1.0000 \pm 0.0006	1.0000 \pm 0.0008	1.0000 \pm 0.0008	1.0000 \pm 0.0011
[-0.6, -0.4]	0.9755 \pm 0.0030	1.0000 \pm 0.0031	1.0000 \pm 0.0019	1.0000 \pm 0.0017	1.0000 \pm 0.0013	1.0000 \pm 0.0016	1.0000 \pm 0.0012	1.0000 \pm 0.0008
[-0.4, -0.2]	0.9839 \pm 0.0041	1.0000 \pm 0.0021	1.0000 \pm 0.0041	1.0000 \pm 0.0026	1.0000 \pm 0.0006	1.0000 \pm 0.0007	1.0000 \pm 0.0005	1.0000 \pm 0.0004
[-0.2, 0.0]	0.8662 \pm 0.0038	1.0000 \pm 0.0016	1.0000 \pm 0.0027	1.0000 \pm 0.0013	1.0000 \pm 0.0006	1.0000 \pm 0.0005	1.0000 \pm 0.0008	1.0000 \pm 0.0006
[0.0, 0.2]	0.8843 \pm 0.0037	1.0000 \pm 0.0013	1.0000 \pm 0.0029	1.0000 \pm 0.0012	1.0000 \pm 0.0009	1.0000 \pm 0.0005	1.0000 \pm 0.0005	1.0000 \pm 0.0005
[0.2, 0.4]	0.9692 \pm 0.0047	1.0000 \pm 0.0032	1.0000 \pm 0.0039	1.0000 \pm 0.0015	1.0000 \pm 0.0005	1.0000 \pm 0.0006	1.0000 \pm 0.0011	1.0000 \pm 0.0006
[0.4, 0.6]	0.9686 \pm 0.0042	1.0000 \pm 0.0030	1.0000 \pm 0.0036	1.0000 \pm 0.0018	1.0000 \pm 0.0010	1.0000 \pm 0.0015	1.0000 \pm 0.0010	1.0000 \pm 0.0012
[0.6, 0.8]	1.0000 \pm 0.0089	1.0000 \pm 0.0047	1.0000 \pm 0.0017	1.0000 \pm 0.0009	1.0000 \pm 0.0006	1.0000 \pm 0.0006	1.0000 \pm 0.0024	1.0000 \pm 0.0008
[0.8, 1.0]	2.4815 \pm 0.0940	1.0633 \pm 0.0133	1.0170 \pm 0.0067	1.0077 \pm 0.0019	1.0000 \pm 0.0025	1.0000 \pm 0.0008	1.0000 \pm 0.0014	1.0000 \pm 0.0026

Tab. 30: The correction factor $\epsilon_p^{data}/\epsilon_p^{MC}$ in terms of $\cos\theta$ in different momentum range by using control sample $J/\psi \rightarrow p\bar{p}\pi^+\pi^-$ (2018 year).

$\cos\theta$	[0.2, 0.3] GeV	[0.3, 0.4] GeV	[0.4, 0.5] GeV	[0.5, 0.6] GeV	[0.6, 0.7] GeV	[0.7, 0.8] GeV	[0.8, 0.9] GeV	[0.9, 1.0] GeV
[-1.0, -0.8]	0.9265 \pm 0.0116	1.0255 \pm 0.0118	1.0000 \pm 0.0047	1.0000 \pm 0.0007	1.0000 \pm 0.0005	1.0000 \pm 0.0005	1.0000 \pm 0.0005	1.0000 \pm 0.0009
[-0.8, -0.6]	0.9851 \pm 0.0012	1.0066 \pm 0.0013	1.0000 \pm 0.0004	1.0000 \pm 0.0005	1.0000 \pm 0.0006	1.0000 \pm 0.0024	1.0000 \pm 0.0011	1.0000 \pm 0.0031
[-0.6, -0.4]	1.0000 \pm 0.0049	1.0052 \pm 0.0009	1.0000 \pm 0.0013	1.0000 \pm 0.0017	1.0000 \pm 0.0010	1.0000 \pm 0.0010	1.0000 \pm 0.0012	1.0000 \pm 0.0013
[-0.4, -0.2]	0.9760 \pm 0.0092	1.0000 \pm 0.0018	1.0000 \pm 0.0027	1.0000 \pm 0.0020	1.0000 \pm 0.0004	1.0000 \pm 0.0005	1.0000 \pm 0.0005	1.0000 \pm 0.0015
[-0.2, 0.0]	0.7128 \pm 0.0052	0.9774 \pm 0.0014	1.0000 \pm 0.0010	1.0000 \pm 0.0015	1.0000 \pm 0.0005	1.0000 \pm 0.0005	1.0000 \pm 0.0010	1.0000 \pm 0.0006
[0.0, 0.2]	0.7997 \pm 0.0110	0.9864 \pm 0.0010	1.0000 \pm 0.0010	1.0000 \pm 0.0006	1.0000 \pm 0.0008	1.0000 \pm 0.0005	1.0000 \pm 0.0006	1.0000 \pm 0.0009
[0.2, 0.4]	0.9824 \pm 0.0046	1.0000 \pm 0.0027	1.0000 \pm 0.0020	1.0000 \pm 0.0010	1.0000 \pm 0.0005	1.0000 \pm 0.0008	1.0000 \pm 0.0005	1.0000 \pm 0.0007
[0.4, 0.6]	1.0000 \pm 0.0050	1.0000 \pm 0.0050	1.0000 \pm 0.0012	1.0000 \pm 0.0011	1.0000 \pm 0.0012	1.0000 \pm 0.0006	1.0000 \pm 0.0018	1.0000 \pm 0.0013
[0.6, 0.8]	0.9892 \pm 0.0017	1.0000 \pm 0.0012	1.0000 \pm 0.0004	1.0000 \pm 0.0003	1.0000 \pm 0.0006	1.0000 \pm 0.0013	1.0000 \pm 0.0015	1.0000 \pm 0.0014
[0.8, 1.0]	0.9382 \pm 0.0075	1.0214 \pm 0.0083	1.0070 \pm 0.0022	1.0000 \pm 0.0006	1.0000 \pm 0.0009	1.0000 \pm 0.0009	1.0000 \pm 0.0011	1.0000 \pm 0.0012

Tab. 31: The correction factor $\epsilon_p^{data}/\epsilon_p^{MC}$ in terms of $\cos\theta$ in different momentum range by using control sample $J/\psi \rightarrow p\bar{p}\pi^+\pi^-$ (2019 year).

$\cos\theta$	[0.2, 0.3] GeV	[0.3, 0.4] GeV	[0.4, 0.5] GeV	[0.5, 0.6] GeV	[0.6, 0.7] GeV	[0.7, 0.8] GeV	[0.8, 0.9] GeV	[0.9, 1.0] GeV
[-1.0, -0.8]	0.8857 \pm 0.0094	1.0271 \pm 0.0107	1.0055 \pm 0.0037	1.0000 \pm 0.0015	1.0000 \pm 0.0006	1.0000 \pm 0.0007	1.0000 \pm 0.0009	1.0000 \pm 0.0022
[-0.8, -0.6]	0.9453 \pm 0.0033	1.0083 \pm 0.0011	1.0000 \pm 0.0004	1.0000 \pm 0.0007	1.0000 \pm 0.0005	1.0000 \pm 0.0010	1.0000 \pm 0.0010	1.0000 \pm 0.0018
[-0.6, -0.4]	0.9733 \pm 0.0019	1.0000 \pm 0.0045	1.0000 \pm 0.0016	1.0000 \pm 0.0018	1.0000 \pm 0.0007	1.0000 \pm 0.0007	1.0000 \pm 0.0009	1.0000 \pm 0.0006
[-0.4, -0.2]	0.9752 \pm 0.0072	1.0000 \pm 0.0023	1.0000 \pm 0.0020	1.0000 \pm 0.0014	1.0000 \pm 0.0006	1.0000 \pm 0.0006	1.0000 \pm 0.0007	1.0000 \pm 0.0009
[-0.2, 0.0]	0.7486 \pm 0.0103	1.9798 \pm 0.0017	1.0000 \pm 0.0014	1.0000 \pm 0.0006	1.0000 \pm 0.0011	1.0000 \pm 0.0006	1.0000 \pm 0.0004	1.0000 \pm 0.0005
[0.0, 0.2]	0.8265 \pm 0.0116	0.9884 \pm 0.0013	1.0000 \pm 0.0011	1.0000 \pm 0.0016	1.0000 \pm 0.0004	1.0000 \pm 0.0004	1.0000 \pm 0.0005	1.0000 \pm 0.0005
[0.2, 0.4]	0.9725 \pm 0.0035	1.0000 \pm 0.0012	1.0000 \pm 0.0022	1.0000 \pm 0.0011	1.0000 \pm 0.0006	1.0000 \pm 0.0006	1.0000 \pm 0.0005	1.0000 \pm 0.0007
[0.4, 0.6]	0.9672 \pm 0.0013	1.0000 \pm 0.0043	1.0000 \pm 0.0009	1.0000 \pm 0.0013	1.0000 \pm 0.0005	1.0000 \pm 0.0015	1.0000 \pm 0.0026	1.0000 \pm 0.0010
[0.6, 0.8]	0.9458 \pm 0.0031	1.0073 \pm 0.0013	1.0000 \pm 0.0003	1.0000 \pm 0.0003	1.0000 \pm 0.0004	1.0000 \pm 0.0006	1.0000 \pm 0.0015	1.0000 \pm 0.0023
[0.8, 1.0]	0.9021 \pm 0.0149	1.0173 \pm 0.0081	1.0000 \pm 0.0018	1.0000 \pm 0.0				

Tab. 32: The correction factor $\epsilon_{\pi^0}^{data}/\epsilon_{\pi^0}^{MC}$ in terms of $\cos\theta$ in different momentum range

Cosθ	[0.05, 0.15] GeV	[0.15, 0.25] GeV	[0.25, 0.35] GeV	[0.35, 0.45] GeV
[-1.0, -0.8]	0.9960 ± 0.0167	1.0003 ± 0.0156	0.9641 ± 0.0214	0.9758 ± 0.0372
[-0.8, -0.6]	0.9859 ± 0.0163	0.9908 ± 0.0145	0.9793 ± 0.0153	0.9772 ± 0.0216
[-0.6, -0.4]	0.9698 ± 0.0176	0.9897 ± 0.0136	0.9808 ± 0.0105	0.9664 ± 0.0138
[-0.4, -0.2]	1.0063 ± 0.0170	0.9990 ± 0.0145	0.9899 ± 0.0113	1.0049 ± 0.0026
[-0.2, 0.0]	0.9899 ± 0.0177	0.9950 ± 0.0099	0.9933 ± 0.0123	0.9887 ± 0.0015
[0.0, 0.2]	0.9966 ± 0.0178	0.9808 ± 0.0098	0.9914 ± 0.0118	0.9757 ± 0.0057
[0.2, 0.4]	1.0373 ± 0.0198	0.9890 ± 0.0046	0.9994 ± 0.0135	0.9797 ± 0.0097
[0.4, 0.6]	0.9875 ± 0.0167	0.9909 ± 0.0062	0.9803 ± 0.0152	0.9832 ± 0.0069
[0.6, 0.8]	0.9906 ± 0.0163	0.9878 ± 0.0156	0.9975 ± 0.0188	1.0347 ± 0.0123
[0.8, 1.0]	0.9889 ± 0.0163	0.9882 ± 0.0166	0.9743 ± 0.0219	0.9604 ± 0.0131